Design and Analysis of Methods to Eliminate Oscillatory Behavior in Bioreactors for Viral Vaccine Manufacturing

by

Kaylee Christine Schickel

B.S. Chemical Engineering, University of Iowa (2014)
M.S. Chemical Engineering Practice, Massachusetts Institute of Technology (2019)

Submitted to the Department of Chemical Engineering
in partial fulfillment of the requirements for the degree of

Doctor of Philosophy in Chemical Engineering

at the

MASSACHUSETTS INSTITUTE OF TECHNOLOGY

May 2022

Author . . . .
Department of Chemical Engineering
April 11, 2022

Certified by . . . .
Richard D. Braatz
Edwin R. Gilliland Professor of Chemical Engineering
Thesis Supervisor

Accepted by . . . .
Patrick S. Doyle
Robert T. Haslam Professor of Chemical Engineering
Singapore Research Professor
Chairman, Committee for Graduate Students

Design and Analysis of Methods to Eliminate Oscillatory Behavior in Bioreactors for Viral Vaccine Manufacturing

by

Kaylee Christine Schickel

Submitted to the Department of Chemical Engineering
on April 11, 2022, in partial fulfillment of the
requirements for the degree of
Doctor of Philosophy in Chemical Engineering

Abstract

Continuous stirred tank reactors, or CSTRs, are one of the most commonly used reactors in the biomanufacturing sector. This is because CSTRs offer a relatively simple design, operate by maintaining a constant and predictable outlet concentration, and have been utilized and studied long enough for the field to have developed a great familiarity. One major drawback of single-CSTR applications arises with certain cell-virus systems that exhibit the von Magnus effect. Through the von Magnus effect, oscillations in cellular and viral states arise with individual states sometimes spanning orders of magnitude within a single run. This work demonstrates two successful methods for reducing and eliminating this periodicity including designing and applying a proportional feedback controller for setpoint tracking as well as staging multiple CSTRs in series. Additionally, oscillatory behavior can be avoided through novel reactor designs. One such design, a novel hollow fiber bioreactor, is explored in this work. This design constrains larger cellular and viral species within a hollow fiber lumen where viral infection of the cells can take place along the length of the reactor. Fresh media is provided to the system through the extracapillary space with smaller waste and nutrient molecules able to pass through the membrane to maintain the health of the cells. With this design, we are able to achieve stable outlet concentrations that can be optimized. Finally, as an extension to these ideas, population balance models were analyzed to allow the tracking of individual populations of cells within a reactor - particularly those of a certain age group. As cells age, they may become less productive or more likely to exhibit genetic decomposition. Thus, tracking cell ages provides avenues to design new systems that may be able to filter such aging cell populations out, thereby potentially increasing the overall productivity of the system. The groundwork for this is providing solution strategies for population balance models including numerical approaches as well as direct analytical solutions. Both approaches are analyzed here in great depth.

Thesis Supervisor: Richard D. Braatz
Edwin R. Gilliland Professor of Chemical Engineering

Acknowledgments

As many readers will know, obtaining a PhD is no small feat. It is an extremely intense and life-changing process that I believe would be impossible to tackle alone. I will always be thankful for each and every person that has assisted me through this process.

During my academic career at MIT, I was fortunate enough to have had great mentors. First, thanks go to my research advisor, Richard Braatz. Richard has been a great teacher through my time at MIT, and he has never failed to surprise me with his patience and flexibility. A few of my early projects were delayed for a variety of reasons, but Richard helped me plan around this with some creativity to keep my PhD on track. I have grown in many ways through my time at MIT, both personally and professionally, and Richard has been instrumental in me realizing that growth. Thanks also go to my committee members, Chris Love and Tony Sinksey, whose guidance and inquisitive natures have broadened my view of even my own thesis work. They have continually offered their support for whatever I might need, and for that I will always be gracious.

Next I would like to thank the Braatz research group, both past and present members that I have been fortunate enough to meet and work alongside, for never failing to create an inviting and accepting environment. Thanks especially to Anastasia, Moo Sun, Tam, and Andy who have helped me on innumerable occasions. From debugging Matlab codes to dealing with life's uncertainties, these four always made time to bounce ideas with me or talk me through things.

Since day 1 at MIT, I have been surrounded by an incredible group of friends that has only continued to grow. The first year in MIT ChemE is a tough one, and I am so thankful that I was able to share that time with Lisa, Mike, Laura, Connor, Caroline, Kassi, Justin, Catie, Craig, and Ryan and Meg all of whom made the experience not only tolerable, but something I will cherish for years to come. I would especially like to thank Lisa for countless workouts, jumbles, and deep talks and Mike for being one of the best roommates I have ever had. Thank you also to Steven, John, Leia, Michael and to everyone else who took part in poker nights, pickup basketball games and intramural teams. It was these people and their contributions to my personal and social life that kept me sane throughout this process. Lastly, I would like to thank my partner, Lily. Although you only experienced the last couple years of my PhD, you were there when I needed you most. The final stretches

of the degree proved without a doubt to be the most mentally taxing, and you were always there to offer comfort and dry tears. I could not have reached this point without you.

Finally, I want to thank my family who have been a constant source of love and support. No matter what, they have always been there to celebrate me and the things I have accomplished. It has been a long road, and my family has seen to it that I was as well-prepared as possible for each stop along the way. Through their phone calls, video chats, hand-written letters and boxes of homemade baked goods, they have kept themselves ever close to me despite the physical distance between Massachusetts and Iowa. I love you all so much, and I cannot begin to tell you how much you all mean to me.

Contents

Chapter 1

Introduction

1.1   Importance of Viral Vaccines

Since their inception, viral vaccines have played an integral role in our society. These vital drugs are formulated to combat some of the deadliest and most prevalent diseases humankind has been faced with. To date, there are over 200 known species of virus [69]. Some of the most common, in terms of new cases per year, include Influenza (3-5 million severe cases per year, with mild case counts reaching even higher), HIV (1.5-2 milllion cases per year), Dengue (200-300 million cases per year) and Rotavirus (about 100 million cases per year) according to the respective World Health Organization Fact Sheets. Certain viruses affect particular areas of the world more prevalently, and some only present with mild symptoms. However, regardless of severity of the associated disease, it is imperative that we are prepared to create vaccines for any virus, at any time, and in any needed amount. This is particularly true during pandemic states, when demand for vaccines surges with little to no warning. The solution to this preparedness lies in continuous viral vaccine manufacturing.

1.2   A Brief Overview of Viral Vaccine Production

Viral vaccine manufacturing remains an important aspect of the pharmaceutical industry, particularly as global demand for certain vaccines continues to rise. The current platform with which many of these viral vaccines are produced is embryonated chicken eggs, by which

the eggs are infected with the virus of choice and then incubated to produce the antigenic material used in creating the vaccine. Although this method is well-established, the use of continuous cell lines as the hosts for viral replication has shown promise in recent decades. This is particularly true when considering that designer cell lines offer faster turnaround in the case of pandemics, are scalable to very high worldwide demands, and are impervious to avian virus outbreaks which can decimate the flocks that provide embryonated eggs.

To take the use of continuous cell lines a step further, many researchers have considered their use in continuous bioreactor systems. Continuous bioreactors are designed such that media is constantly flowed through them, and because of this setup, compared to their batch counterparts, continuous reactors offer increased flexibility in design, more robust controllability, higher productivity and reduced operating costs [27]. The continuous bioreactor, or chemostat, was designed in the 1950s as a method for constantly producing bacteria in culture for extended periods of time [43]. This work was adapted in the 1960s for the continuous cultivation of viruses ranging from polio to adenoviruses in two-stage reactor systems [18,24].

Perhaps the most influential work in the area of continuous reactors for viral infection was not undertaken until the late 1980s when Kompier, Tramper and Vlak developed a two-reactor system designed to grow and infect insect cell populations with baculovirus [26]. The goal of their study was increased yields and productivity in terms of percentage of cell population infected and amount of virus produced per feed materials, and they were able to show successfully that, by these metrics, the continuous system was more effective than batch. Their work was continued into the 1990s where different reactor configurations, as well as recombinant viruses were explored [61–63]. Parallel to much of this experimental work, some researchers took to modeling these continuous, multi-stage reactor systems, using first-order kinetics to represent the viral infection process [7, 8, 61].

More recently the focus on continuous bioreactors for viral infection has shifted toward broadening the field through the use of newly designed cell lines of a variety of types, as well as optimizing these systems through reactor design. Frensing et al. used a two-stage system to grow and infect duck cell populations with Influenza A [13], while Tapia et al. have focused on producing modified vaccinia ankara (MVA) virus in similar avian lines [55,57]. Tangentially, other researchers have sought ways to increase cell density in these continuous systems so

as to significantly increase virus yields. The primary work in this area is from Genzel et al. who have explored the use of hollow fiber reactors and alternating and tangential flow filtration to grow avian and human cell lines to densities an order of magnitude greater than is typically achieved in batch culture [16, 58].

A major finding connecting much of the work in viral vaccine production is the presence of defective interfering particles (DIPs) and the negative effect they have on virus yields. This was particularly evident in the work in the 80s and 90s where modeling efforts were undertaken in order to understand a marked decline in virus production after running a continuous system for a month, as well as periodic trends in relevant species concentrations [7]. What was then called the "passage effect" was later attributed to the von Magnus effect. Simply put, this phenomenon is described as an increase in defective viruses that are nearly indistinguishable from their standard counterparts except that they tend to have a degraded genome [64]. The defective viruses generally have a lower infectivity and tend to interfere with the production of the standard particles [13, 14]. Cells that become infected with DIPs exhibit behavior that resembles uninfected cells in terms of growth and development, and because of this, periodic build-ups of the defective species occur in continuous systems.

1.3   Frensing Model

To date, one of the most developed and accurate viral infectivity models is that of Frensing et al. who described the infection of a duck cell line with Influenza A. The model consists of six ordinary differential equations,

$$\frac{dT}{dt} = \mu T - k_1 \left(V_s + V_d \right) T + D \left(T_{\text{in}} - T \right), \tag{1.1}$$

$$\frac{dI_d}{dt} = k_1 V_d T - \left(k_1 V_s - \mu \right) I_d - D I_d, \tag{1.2}$$

$$\frac{dI_s}{dt} = k_1 V_s T - \left(k_1 V_d + k_2 \right) I_s - D I_s, \tag{1.3}$$

$$\frac{dI_c}{dt} = k1 \left(V_s I_d + V_d I_s \right) - k_2 I_c - D I_c, \tag{1.4}$$

Table 1.1: Frensing Model Parameter Values

Parameter	Value	Description
k_1	2.12×10^{-9} mL/virion/h	viral infection rate constant
k_2	7.13×10^{-3} 1/h	infected cell death rate constant
k_3	168 virion/cell/h	virus production rate constant
k_4	0.035 1/h	viral degradation rate constant
k_{33}	168 virion/cell/h	DIP production rate constant
μ	0.027 1/h	cell growth rate
D	0.0396 1/h	reactor dilution rate
f	10^{-3}	fraction of infected cells producing DIPs
T_{in}	3×10^6 cells/mL	feed cell concentration

$$\frac{dV_s}{dt} = k_3 I_s - \left(k_1 \left(T + I_d + I_s + I_c\right) + D + k_4\right) V_s, \tag{1.5}$$

and

$$\frac{dV_d}{dt} = k_{33} I_c + f k_3 I_s - \left(k_1 \left(T + I_d + I_s + I_c\right) + D + k_4\right) V_d, \tag{1.6}$$

which describe the time evolution of six species within a single continuous stirred tank reactor (CSTR) [13]. The species consist of target cells denoted as T, standard virus particles (STVs) denoted by V_{s}, defective interfering particles (DIPs) denoted by V_{d}, and three infected cellular species denoted by I. The subscripts d, s, and c for the infected cell species refer to DIP-, STV- and co-infected, respectively. The remaining parameters are defined in Table 1.1.

This model was used as the basis for much of my thesis work contained herein. Written in the form of species balances as above, it is easy to see there are six states within the model including four cellular species and two viral. Gaining a deeper understanding of how these states interact, as well as how they are connected through the remaining parameters in the model, was of the utmost importance for my work.

1.4 Outline of Thesis Document

The primary goal of my thesis work was to build a better understanding of certain cell-virus infectivity systems that are already being applied in industry. Specifically, the cell-virus systems most relevant to my work are those that exhibit oscillatory behavior due to the Von

Magnus Effect. In Chapter 1, I present the main background and motivation as a necessary basis to understanding the work herein. Viral vaccines have been an integral part of our world since their inception decades ago. Yet even today we struggle to develop these life-changing medicines to combat certain diseases. While the methods most commonly employed today allow the manufacturing of these viral vaccines, it is becoming ever-clearer that egg-based viral replication or other batch mode processes have vital drawbacks that must be addressed. Finally, Chapter 1 examines the influenza A infectivity model that forms the basis for much of my work and discusses its relevance and the modifications I made to the original model from Frensing [13].

Chapter 2 delves into a more detailed look at the oscillatory nature of the model. The approach here was to generate a methodology to reduce or eliminate oscillatory behavior through the application of first priniciples. Of course, with a basic understanding of the biomanufacturing industry, it is clear that large changes in existing processes can be difficult to adopt. Thus, Chapter 2 begins with an open loop analysis of the Frensing model. This analysis examines each variable within the model and, through systematically modifying one variable at a time, provides a more concrete idea of how we can simply change parameter values to reduce oscillations. While this is simple, it is not always effective at completely smoothing the relevant states. The chapter continues with the construction of a p-only controller that can successfully eliminate oscillations over time. Finally, a third approach is offered by using residence time distributions to demonstrate that by adding more tanks in series to a bio-process, we can buffer the viral and cellular states and stabilize them by the exit of the final reactor in the series.

In Chapter 3, I present a novel bioreactor for the manufacturing of viral vaccines. This new reactor is based on hollow fiber bioreactors, with some key modifications. By passing the cell and virus slurry through the lumenal space of the reactor, we can confine the infectivity of the system and better control the rate at which this occurs. Media passed in parallel through the extracapillary space provides oxygen and nutrients, via diffusion across the membrane, for the cells' survival. Using this reactor setup, I was able to demonstrate successfully that there is no oscillatory behavior in this system. Over the run time, the states are not monotonic, and thus there is room for optimization of reactor parameters including reactor

length, diameter, and feed flow rates. This chapter analyzes the reactor using infectivity kinetics from the Frensing model, but is constructed in such a way that other cell-virus systems could be substituted with few modifications.

As cell populations age, they often exhibit changes on a physical or physiological level that can affect their productivity, particularly when considering cell populations used for drug production. With this in mind, I wanted to apply population balance models (PBMs) to track the various age groups of cells within the population. Chapters 4 and 5 lay the groundwork for this application of PBMs by analyzing a numerical solution method that contains no discretization error. These chapters are written pedagogically, and they take the reader through the application of my approach beginning with the simplest cell population balance equation and progressing to the general case. More specifically, Chapter 4 details the numerical method and shows the relevant examples, and Chapter 5 uses the method of characteristics to develop analytical solutions that support the proofs from Chapter 4.

Chapter 2

Stabilization of Oscillatory Behavior in Continuous Stirred Tank Reactors for Viral Propagation

To gain insight into the oscillatory nature of certain cell-virus infectivity systems, I began with the Frensing model in its original form. The goal at this point was simply to reproduce what Frensing had done, and then use the design paramters already contained within the model to perform an open-loop analysis. The results of the open-loop analysis provided key relationships within the model, which translate directly to physical situations that arise within the bioreactor as infection is occuring. From here, I turned to control theory to construct a simple feedback controller, choosing manipulated and control variables with my understanding gained in the open loop analysis. Feedback control allows companies to apply new technology to their already existing processes, so as to reduce up front capital costs in moving toward stabilization. The alternative to feedback control is utilizing residence time distributions of the process. By adding more CSTRs in series, we can effectively manipulate the residence time distribution of the species we care about, and thus stabilize it over the course of the entire process.

2.1 Open Loop Analysis of Infectivity System

Frensing et al. were able to show that their model, when run with the parameter values shown in Table 1, resulted in all six states exhibiting stable oscillations over time, which they attributed to the accumulation of defective interfering particles within the system [13]. As the Frensing et al. model is the most relevant to my work, I chose it as the base on which much of my work was built. Of course, this model was constructed specifically for Influenza A infection using a certain avian cell line. However, a long-term goal of my work is to build a "plug and play" model that would allow users to select a cell and virus type and simply update the kinetic values as needed. It is important to first understand how the system behaves at different values of relevant parameters. The model itself contains nine parameters, of which seven are rate constants, cell growth rate and fraction of cells producing defective virus particles. These seven parameters are directly related to the cell type and virus chosen for the system, and are thus assumed to be fixed once both a virus and cell type are chosen. Note, however, that the values for these parameters are likely to change with the cell/virus combination chosen.

The remaining parameters in the model are the concentration of cells in the feed stream, T_{in}, and the dilution rate, D, which is equivalent to the ratio of flow rate, F, divided by reactor volume, V. In essence, this leaves three tunable parameters. Knowing this, these three parameters were individually varied in an attempt to gauge how the system's states respond to each, and, perhaps more importantly, to determine, in a more quantitative manner, how the productivity of the system varies with each. As productivity can be measured in a number of ways, the metric chosen here, for the sake of consistency, was the cumulative number of standard virus particles harvested from the reactor over time.

2.1.1 Productivity Versus Inlet Target Cell Concentration

The concentration of target cells in the feed stream was the first parameter analyzed. The parameter space was gridded using logarithmic spacing between 10^4 and 10^7 cells/mL. The resulting concentration plots for the cellular states are shown in Figure 2-1, while plots of the viral states and the productivity are shown in Figure 2-2.

18

Figure 2-1: Concentration plots of cellular species at various reactor volumes with fixed flow rate of 19.8 mL/h demonstrate that increasing feed concentration causes oscillatory behavior to worsen.

One trend immediately evident in Figure 2-1 is that the number of target cells in the system, T, generally increases as the concentration of these cells in the feed increases. While this trend is expected given that cells are entering the system at a higher rate, it is not as obvious that increasing the concentration of target cells in the feed should increase the oscillations of all of the other states. This is likely due to the fact that increasing the feed concentration promotes an immediate increase in the accumulation of target cells within the CSTR. This, in turn, increases the production rate of STVs and the STV-infected cell species - a fraction of which create DIPs according to degradation of the viral genome over time, or rounds of infection, described by the von Magnus effect. Finally, increases in these species promote increases in the production rate of the DIP- and co-infected species, both of which consume target cells via infection reactions. Thus, it makes sense that an increase in the rate of addition of target cells would result in a sharp increase in all states followed by a

19
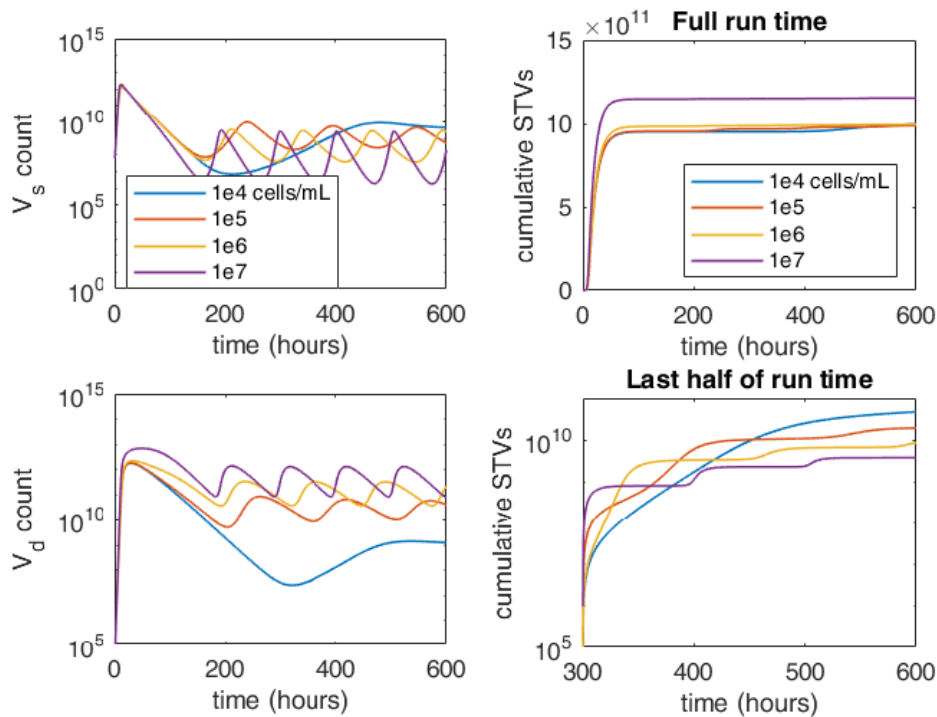
Figure 2-2: Concentration plots of viral states at various values of target cell concentration in the feed stream further demonstrate that increasing feed concentration causes larger oscillations. Productivity, measured in terms of cumulative number of standard virus particles produced over time, decreases as a result.

sharp decline in all states, thereby causing the larger oscillations exhibited by the system at higher feed concentrations. Of course, the opposite is then also true in that these oscillations should be tempered at lower target cell feed rates.

2.1.2   Productivity versus V

Next, the effect of the volume of the infection reactor was analyzed. Plots of cellular and viral state concentrations and productivity are shown in Figure 2-3 and Figure 2-4. It should be noted that the initial conditions for these simulations were set to constant concentration rather than constant mass. Thus, as reactor volume was increased, so too was the amount of target cells and STVs present initially.

Here again, it is immediately evident that increasing the reactor volume increases the oscillations of all states within the reactor. This is easily explained by the fact that increasing
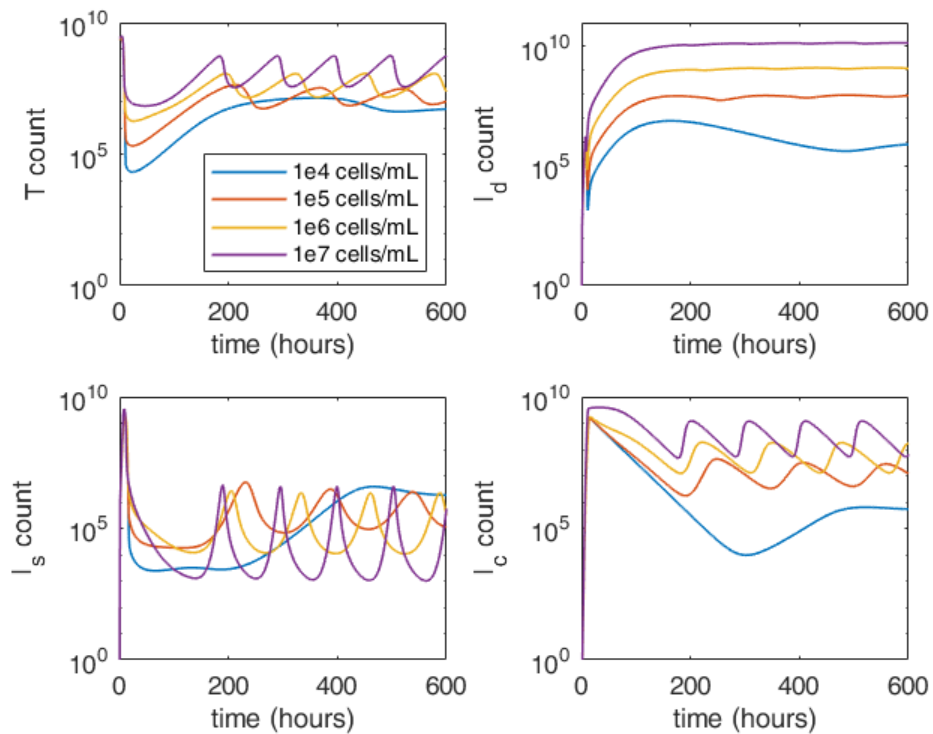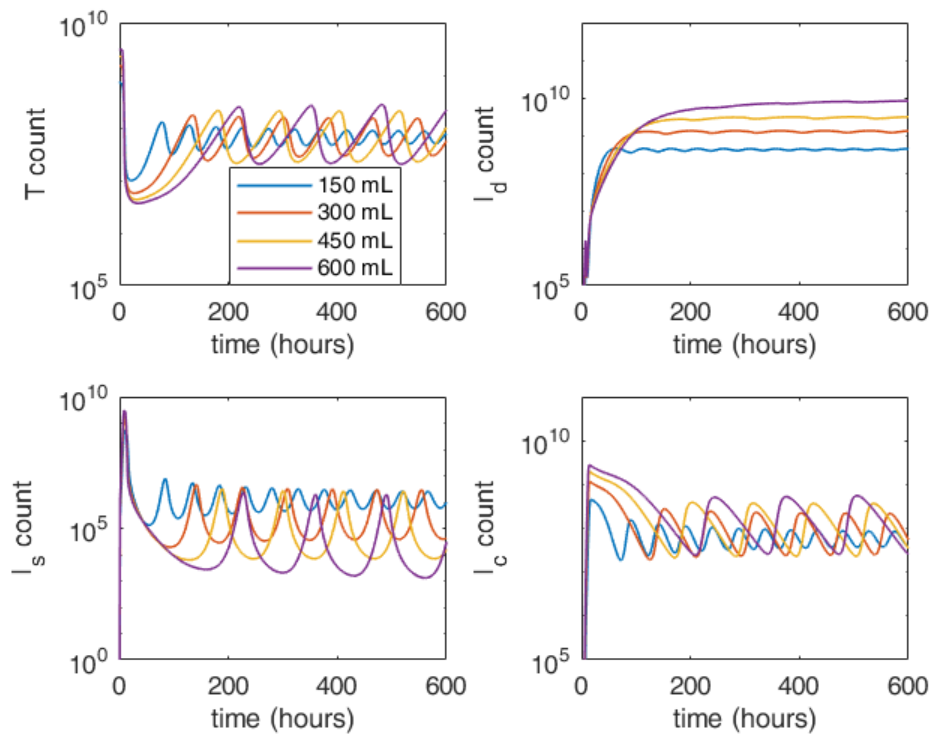
Figure 2-3: Concentration plots of cellular species at various reactor volumes with fixed flow rate of 19.8 mL/h demonstrate that increasing volume causes larger oscillations

the reactor volume at a fixed flow rate increases the residence time of the system. Thus, target cells remain in the system for a longer period of time, giving them a greater chance to become infected by STVs. Furthermore, the now greater number of STVs and STV-infected cells have a larger chance to produce DIPs and DIP-infected cells. Similar to the previous section, the increased amount of each species causes a greater rate of degradation as well as a greater rate of exodus from the reactor. From this analysis it is clear that increasing the volume of the reactor should cause greater oscillations in the species. On the other hand, decreasing reactor volume at a fixed flow rate has the opposite effect.

Despite the larger fluctuations in all species, Figure 6 shows that increasing the reactor volume increases the cumulative number of standard virus particles produced over the reactor run time. This may be due, at least in part, to the use of constant concentration initial conditions across trials. As reactor volume increases from 150 mL to 600 mL, the number of standard virus particles initially present in the reactor is increased by a factor of 4. It

is not surprising then that the final number of standard virus particles in the 600 mL trial is 2-3 times greater than that in the 150 mL trial. Interestingly, when considering only the last 10 days of a 20 day run, the trend in cumulative STVs produced is reversed. In fact, the number of STVs produced in the final 10 days for a reactor volume of 150 mL is nearly 10^{11}, while that for the 600 mL trial is 1.5 orders of magnitude lower. This result suggests that, when performing longer runs in a single CSTR system, it is beneficial to utilize a lower working volume after the first 5-10 days. As this may not be physically realizable, a similar effect could be obtained by manipulating the flow rate of the reactor such that the dilution rate increases at later times.

2.1.3   Productivity versus F

The last parameter to be explored was the reactor flow rate, F. The flow rate was varied from 25 to 100 mL/h in a reactor of constant volume at 500 mL. Results of these trials are shown in Figure 2-5 and Figure 2-6.

As expected based on the relationship between reactor flow rate, volume and dilution rate, the trend exhibited in Figure 2-5 shows that as flow rate is increased at a fixed reactor volume, the oscillations of all states diminish over time. This stabilization of species occurs more quickly at larger flow rates, which also tends to result in larger numbers of target, STV-infected, and co-infected cells. Similarly, the average number of STVs in the system also increases with flow rate, while the number of DIPs decreases, if only slightly. Much of these trends can be explained with an analysis similar to that in the previous section. Flow rate is proportional to dilution rate, which is inversely proportional to reactor residence time. This suggests that as flow rate increases (and residence time decreases), there is a lower chance overall that DIPs will be produced from standard virus particles. This is also in accordance with the von Magnus effect in that with a lower residence time, fewer infection cycles will occur leading to a smaller fraction of STVs that produce DIPs.

In this part of the analysis, the highest flow rate tested was 100 mL/h in a reactor with a 500 mL volume. This is equivalent to a dilution rate of 0.2/h, which is relatively large for any real system. However, because of the noticeably increasing trend in cumulative STVs produced with increasing flow rates at both early and late times of the run, larger values of

flow rate (and thus dilution rate) were tested (Figure 2-7 and Figure **??**).

Here, flow rates of 250-520 ml/h were examined in the same 500 mL reactor. Of course, without some mechanism for recycling media, these flow rates would likely result in exorbitantly large operational costs. However, assuming that media recycle is possible, it is apparent that further increases in reactor flow rate lead to greater amounts of standard virus particles within the reactor, and therefore greater numbers of cumulative STVs produced, at least up to a point. As flow rate is increased toward the point at which dilution rate approaches $1\ h^{-1}$, the cumulative number of STVs produced over time begins to drop. At flow rates resulting in dilution rates greater than $1\ h^{-1}$, productivity decreases sharply, indicating that the residence time of the system has become lower than the time it takes target cells to become infected by STVs. Realistically, moving the reactor contents through the system at these speeds may be harmful to the cells and/or virus particles in terms of the shear stresses they would encounter, but this is a limitation of the current model.
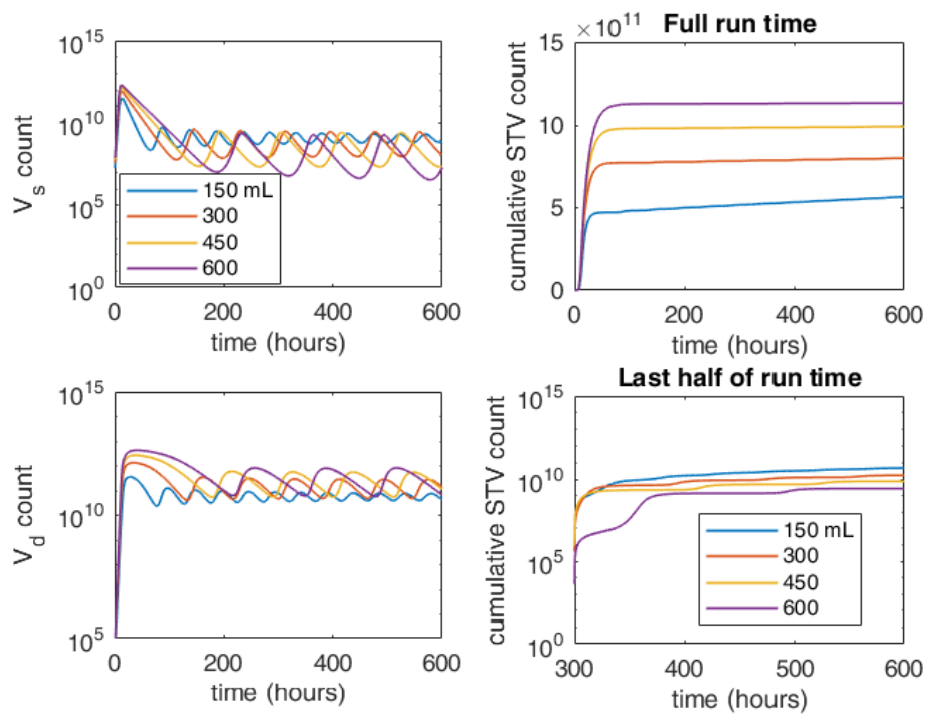
Figure 2-4: Concentration plots of viral states at various reactor volumes with fixed flow rate of 19.8 mL/h. Oscillations increase with increased reactor volume because of increased residence time.
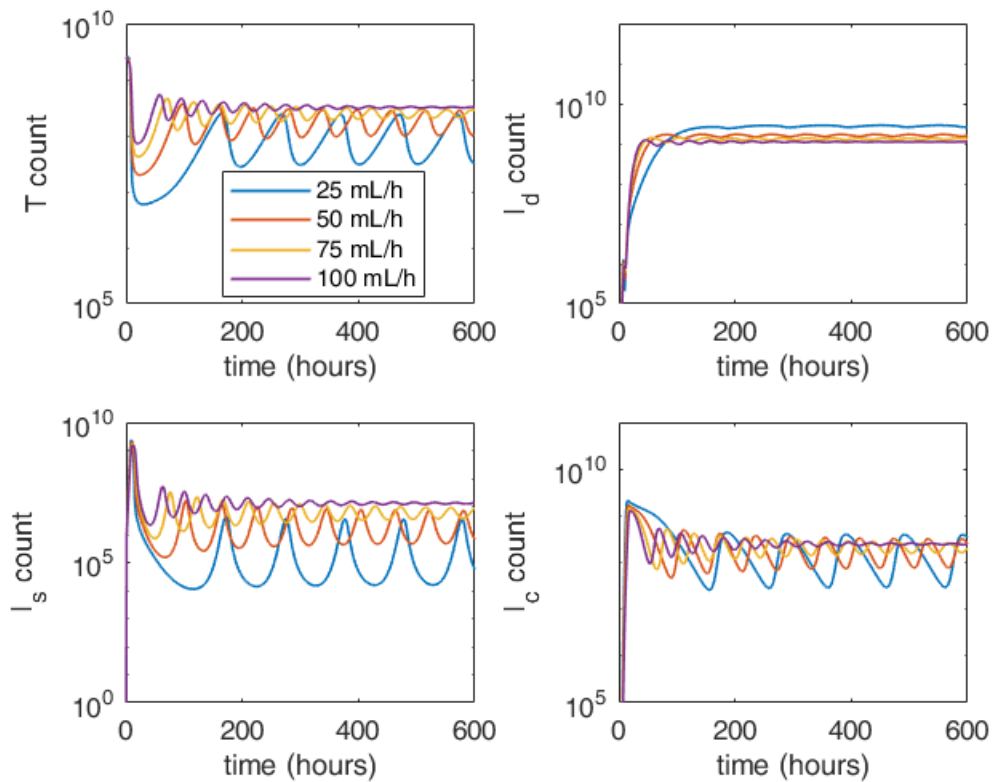
Figure 2-5: Concentration plots of cellular species at various flow rates at constant reactor volume of 500 mL. Decreases in residence time reduces the amplitude of oscillations because of reduced contact time between cells and virus.
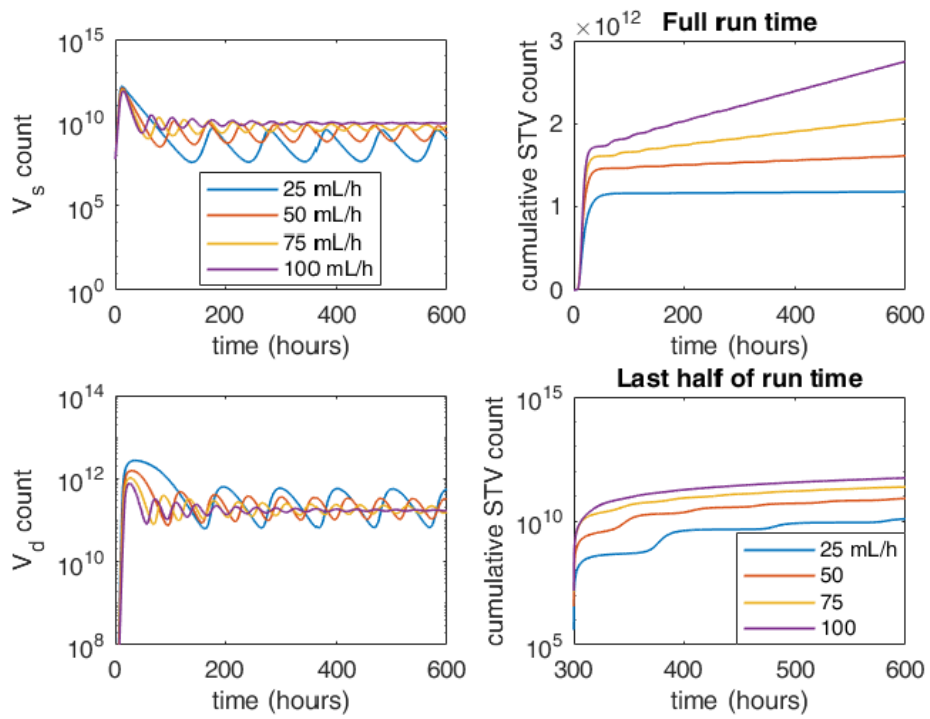
Figure 2-6: Reducing residence time on these scales causes reduced oscillations in the viral states and increased productivity
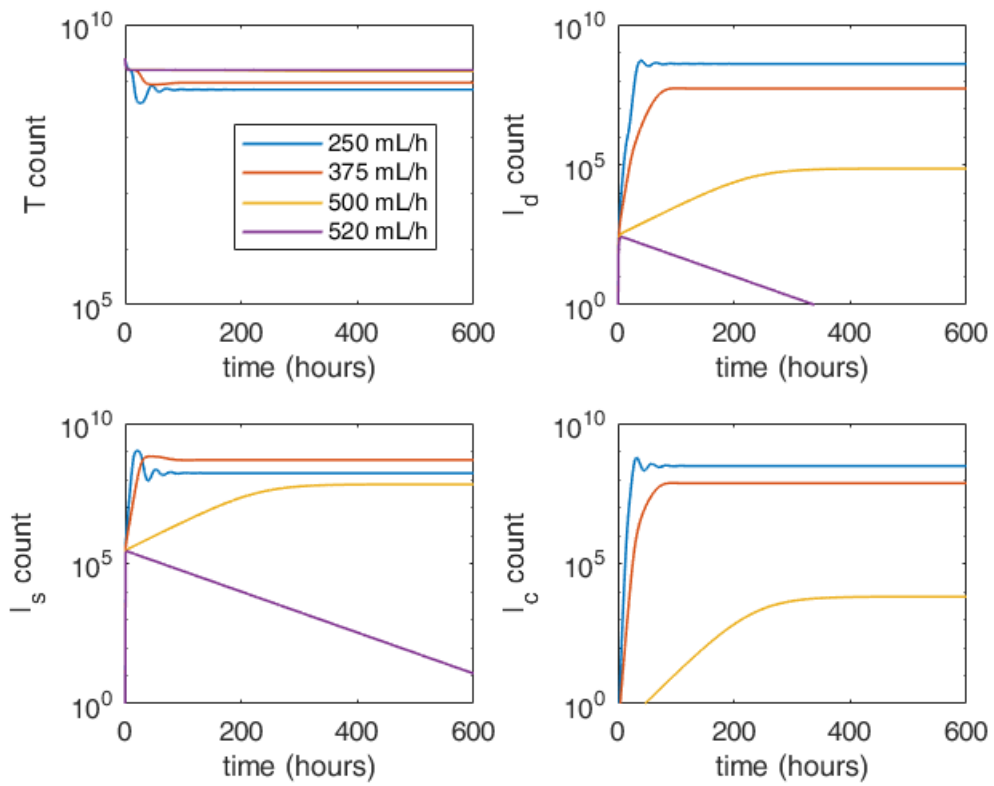
Figure 2-7: Using high dilution rates leads to reduced oscillations in cellular states. However, shear stress may limit maximum allowable flow rates.
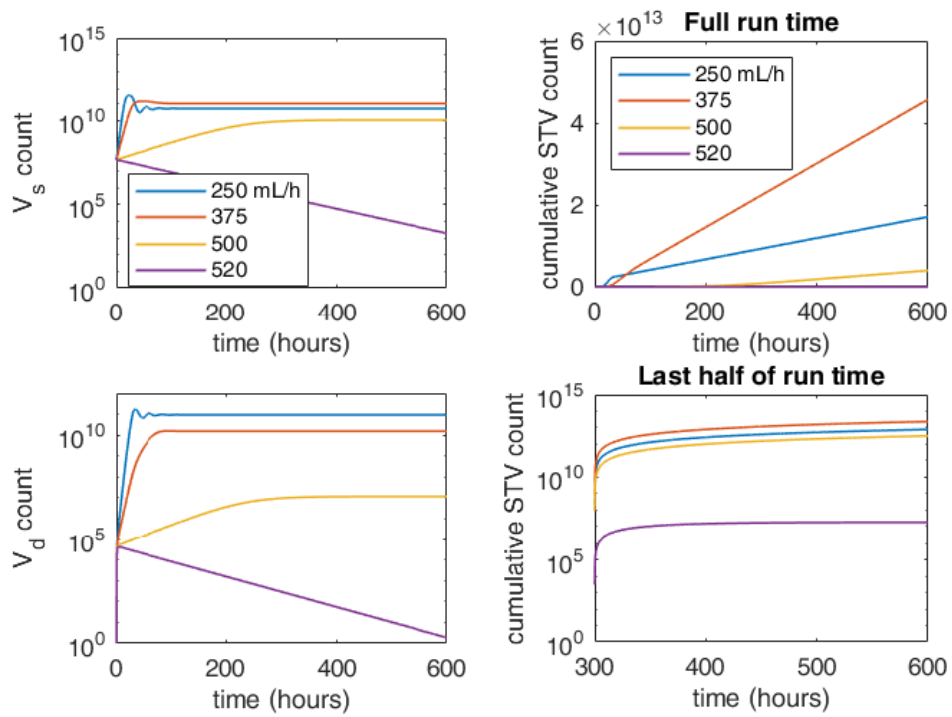
Figure 2-8: Up to a certain point, high diluation rates can increase productivity.

2.2 Feedback Control

Although a measure of productivity versus system parameters is important, designing a system to operate robustly and stably is perhaps more industrially relevant. To this end, simple feedback controllers were designed using the parameters analyzed previously as manipulated variables in order to control a subset of the system states and stabilize them around their steady state values. As a proof of concept, proportional-only controllers (P controllers) were designed first. It was assumed that all relevant states could be measured directly, there are no disturbances affecting the system, and there is no uncertainty in the parameters. The controller equation then becomes

$$\hat{u} = k\hat{x}, \tag{2.1}$$

where u represents the manipulated variables T_{in}, V and F, k is the proportional gain, x represents the corresponding state, and the carrots above u and x denote that these are deviation variables. The deviation variables are determined by subtracting the steady state value from the state in question or by subtracting the value of the manipulated variable at that steady state. For this analysis, x includes the target cells, STVs and DIPs.

First, T_{in} was used to control all three states individually. For each case, the system was run for 600 hours with the parameter values used by Frensing et al. (Table 1.1). Then, providing the system was at steady state, the steady state value was determined by using the peak to peak average value, and the new value of the manipulated variable for that case was determined using the controller equation. This value was updated every two hours to approximate continuous control action, and the system was run for another 1200 hours. The concentration and T_{in} plots resulting from the most effective gain values tested are shown in Figures 2-9 through 2-12.

As is evident from the concentration plots, the oscillations in the system can be largely, if not entirely, reduced using simple P-only controllers. In some cases, particularly when using T_{in} to control the viral states, some offset can be observed. This suggests that adding integral action to the controllers may be beneficial. However, there are many instances in which adding integral action to unstable systems drives the system to further instabilities. It should be noted that a large variety of gain values were tested for each combination of

29
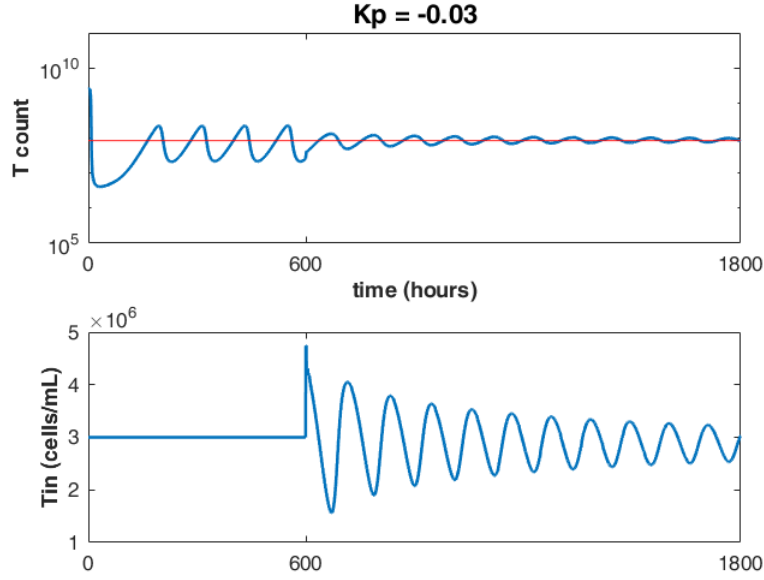
Figure 2-9: Controlling the concentration of target cells using concentration of target cells in the feed stream

state and manipulated variable. However, beyond those shown here, none of the designed controllers were able to effectively stabilize the relevant states.

It is interesting to note that utilizing proportional-only controllers allows the stabilization of T, V_s, and V_d around their steady states. This suggests that it may be possible to force the system to operate at other steady states by manipulating parameters in the right combinations. If this is true, it is likely that the system's productivity can be increased, simply by adding feedback control. At this point, only one manipulated variable has been varied at a time, but adding multiple, interacting control loops is clearly the next step in such an analysis. Furthermore, more robust controllers can be designed by linearizing the bioreactor model around the desired state using a Taylor series expansion. Such a model takes the form

$$f(x, u) \approx f(x, u)|_{x_{ss}, u_{ss}} + \left.\frac{\partial f(x, u)}{\partial x}\right|_{x_{ss}, u_{ss}} (x - x_{ss}) + \left.\frac{\partial f(x, u)}{\partial u}\right|_{x_{ss}, u_{ss}} (u - u_{ss}) + h.o.t. \quad (2.2)$$

where $h.o.t.$ represent second and higher ordered derivatives (assumed to be negligible), and

Figure 2-10: Controlling the concentration of standard virus particles using concentration of target cells in the feed stream

the subscript ss represents the steady state value. The function $f(x, u)$ represents the model ODE equations presented previously, and when these are evaluated at their steady states, they are equal to 0. Thus, the first term on the right-hand side disappears, and we can represent the system as

$$\frac{d}{dt}x = A(x - x_{ss}) + B(u - u_{ss}). \tag{2.3}$$

In this way, the system is linearized around a steady state. Furthermore, A is a matrix that represents the jacobian of the model equations evaluated at the steady state, and B represents the analogous matrix of derivatives with respect to parameters evaluated at steady state. The individual values of A and B provide estimates of the process and controller gain values.

2.3 Steady State Analysis

When designing the feedback controllers tested with the model analyzed here, the steady state values obtained after running the model for 600 hours at a constant parameter set were
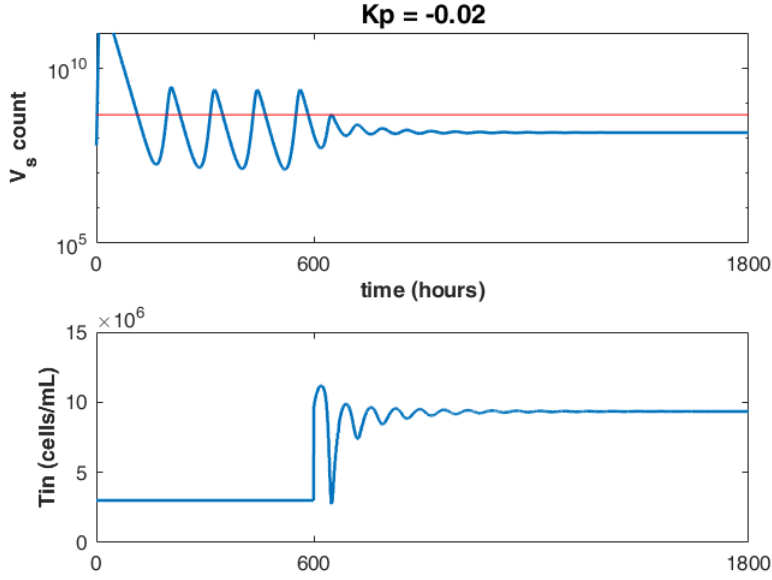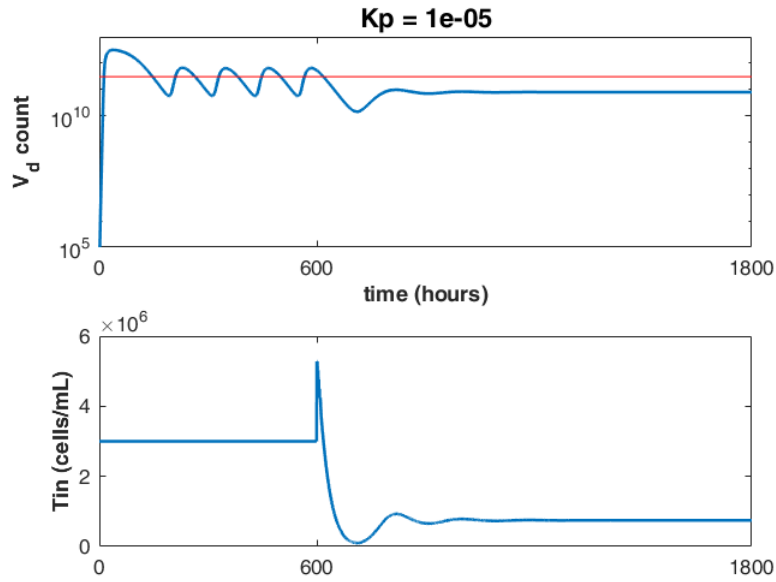
Figure 2-11: Controlling the concentration of defective virus particles using concentration of target cells in the feed stream
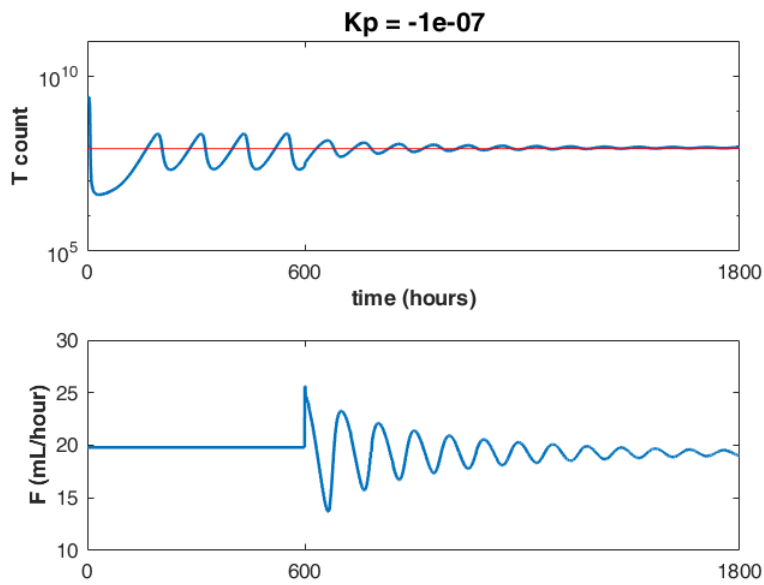
Figure 2-12: Controlling the concentration of target cells using flow rate

used to calculate the necessary deviation variables. However, for the sake of completeness, a full steady state analysis is necessary to ensure that all possible steady states are accounted

for.

To analyze the steady states of the system in more detail, the lefthand sides of the model equations were set to 0, and the equations were subsequently solved for the steady state value of their respective states. The steady state model is given by

$$\bar{T} = \frac{DT_{\text{in}}}{k_1\left(\bar{V}_{\text{s}} + \bar{V}_{\text{d}}\right) + D - \mu},$$
(2.4)

$$\bar{I}_{\text{d}} = \frac{k_1\bar{V}_{\text{d}}\bar{T}}{k_1\bar{V}_{\text{s}} + D - \mu},$$
(2.5)

$$\bar{I}_{\text{s}} = \frac{k_1\bar{V}_{\text{s}}\bar{T}}{k_1\bar{V}_{\text{d}} + k_2 + D},$$
(2.6)

$$\bar{I}_{\text{c}} = \frac{k_1\left(\bar{V}_{\text{s}}\bar{I}_{\text{d}} + \bar{V}_{\text{d}}\bar{I}_{\text{s}}\right)}{k_2 + D},$$
(2.7)

$$\bar{V}_{\text{s}} = \frac{k_3\bar{I}_{\text{s}}}{k_1\left(\bar{T} + \bar{I}_{\text{d}} + \bar{I}_{\text{s}} + \bar{I}_{\text{c}}\right) + D + k_4},$$
(2.8)

and

$$\bar{V}_{\text{d}} = \frac{k_{33}\bar{I}_{\text{c}} + fk_3\bar{I}_{\text{s}}}{k_1\left(\bar{T} + \bar{I}_{\text{d}} + \bar{I}_{\text{s}} + \bar{I}_{\text{c}}\right) + D + k_4},$$
(2.9)

where states with overbars represent the steady state value.

Because of the coupled nature of the system, an analytical solution for individual steady state values cannot be obtained. Thus, Matlab's fsolve function was utilized to obtain these values numerically. Approximately 15000 combinations of initial conditions were tested, with each state being allowed to take on an initial value of 0, 10^3, 10^5, 10^7 or 10^9 cells (or virions) per mL. The converged solutions were able to be divided into four groups, indicating four different steady states. Two of these resulted in the concentrations of some species taking on negative values, which means they are infeasible. Another steady state occurs when all species concentration except the target cells are reduced to zero. This is the trivial steady state which simply balances cell growth and influx with reactor dilution rate, and it can only be reached if no viruses originate in the system. The fourth steady state is non-trivial and feasible, and it is that which is seen when running the system with the initial conditions specified by Frensing et al.

Knowing that there is one nontrivial, feasible steady state, it is interesting to determine if that steady state can be optimized to result in a greater number of STVs. This can be done by performing a full optimization allowing the parameters T_{in}, V, and F to be varied over physical values so as to maximize the number of STVs produced over time. A first step toward this end is gridding the parameter space and testing various combinations within that space.

2.4   CSTRs in Series

Although applying a closed loop, feedback controller was effective at dampening the oscillatory nature of the cell-virus system, it may not always be possible to design such a control system. In these cases, another option is to manipulate the residence time distribution of the virus particles. Specifically, by having the infection aspect of the vaccine production platform contained within a series of CSTRs, it is possible to dampen any oscillations by the exit of the final reactor in series. It is well known within chemical engineering that connecting an infinite number of CSTRs in series constructs a system that acts like a plug flow reactor, or PFR, which does not allow the accumulation of particles like in a CSTR. Of course, it is unrealistic to supply an infinite number of CSTRs, and instead we would like to know how many CSTRs are needed to sufficiently dampen oscillatory behavior in a given system. The Frensing system was used as a basis to study this question as well, and it was determined that with this system, approximately 5 reactors are needed in series, as seen in Figure 2-13. This approximation can be refined by applying an optimization algorithm around the Frensing system, incrementally increasing the number of reactors in the series, and analyzing the 2-norm (or other function indicative of a system's stability) of the relevant states.

2.5   Future Work

An analysis of initial conditions used in the system must be performed including the difference in effect of using constant mass versus constant concentration conditions. It is expected
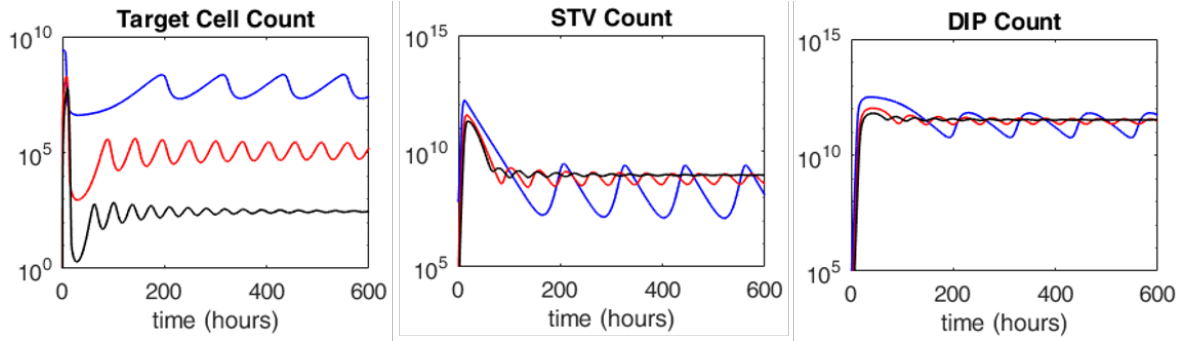
Figure 2-13: Smoothing of final concentrations occurs through the addition of multiple reactors in series. For this system, approximately 5 reactors are needed.

that there will be little difference, but the information may be useful nonetheless. This is especially true when considering that allotments of the seed virus may be in short supply, and using constant concentration when scaling up reactor sizes would require more material. Secondly, now that the single CSTR system is well-understood, new reactor configurations must be explored. It is expected that a series of CSTRs can be utilized to reduce the system's oscillatory behavior, particularly when more robust controllers are added. Next, if very high dilution rates are of interest, estimates of the effect of these high throughputs on the cells and virus particles, in terms of shear and other stresses, must be undertaken to make the model more complete.

Chapter 3

In silico Analysis of an Alternative Hollow Fiber Bioreactor Configuration for Vaccine Production in Suspension Cell Cultures

For years, animal cell lines have been studied as sources of biopharmaceuticals such as vaccines and antibodies [12, 44]. Many studies have focused on the selection of suitable bioreactors within which the animal cell culture is grown and used for production. Well-stirred bioreactors, which are easy to implement in the laboratory, are scalable, and have been widely employed at production scale, have been the standard choice in the bioprocessing industry for many years. Viral products, such as vaccines, produced on animal-cell substrates will benefit from the development of new cell lines amenable to suspension culture [25,36,37]. Suspension culture expands the development space by enabling the separation of cell population growth and viral propagation, allowing the application of separate process control strategies to each stage [13]. The well-stirred bioreactor system for influenza production as described in Frensing et al. is limited for continuous propagation because the wide residence time distribution allows significant formation of late-forming, undesirable byproducts called defective interfering particles (DIPs) which lead to undesirable oscillations in cell and

virus concentrations that span orders of magnitude [13]. Several alternatives to stirred-tank bioreactors have been described in literature, with the goal of addressing the accumulation of undesirable byproducts and resulting oscillatory behavior. One such configuration is the hollow fiber bioreactor (HFBR), which consists of a bundle of thin hollow-fiber tubes in parallel within a cartridge [35, 47, 48, 58]. An immobilized animal cell culture occupies the extra-capillary space (ECS) within the cartridge, which surrounds the fibers. Culture medium containing oxygen, glucose, amino-acids, etc. flows through the fiber lumen and enables the delivery of nutrients via diffusion through the porous wall to the cells, while waste products such as lactic acid, ammonia, and carbon dioxide are returned to the flowing media for disposal. This material exchange is accomplished by transport in the radial direction consisting primarily of molecular diffusion and a small amount of convective transport through the fiber wall pores and extracellular matrix in the extra-capillary space. Nurturing of the cell culture is accomplished by introducing, at a high rate, nutrient-rich medium into the lumen of the hollow fibers. A fraction of these nutrients are transported by diffusion through the hollow fiber membrane into the ECS, and the remainder is recycled. This bioreactor configuration is problematic in a number of ways, including that harvesting of viruses must be done from the ECS outlet and that it is difficult to monitor and control the health of the culture during all phases of the reaction. Furthermore, if cells, rather than antibodies or viruses, are the intended product, harvesting from the ECS can lead to cell damage. We propose the alternative HFBR configuration in Figure 3-1, in which a cell-medium slurry enters the front of the HFBR and flows through the fiber lumen, which we designate as the fiber-lumen stream (FLS). The slurry is created immediately before the bioreactor entrance by injecting a stream containing viral particles into the stream containing cells, which ensures a constant inlet concentration. Another stream of medium, called the perfusion fluid, enters the extra-capillary space and flows parallel to the hollow-fiber tubes. The inner portion of the fiber membrane is permeable to the nutrient and waste molecules, and is impermeable to cells and virus reactants and products, which remain in the lumen stream. This inner portion of the membrane is called the ultrafiltration skin. Nutrients depleted by cell growth and viral infection in the lumen stream are resupplied by membrane transport from the extra-capillary stream. Waste products are transported from the lumen stream through the membrane into
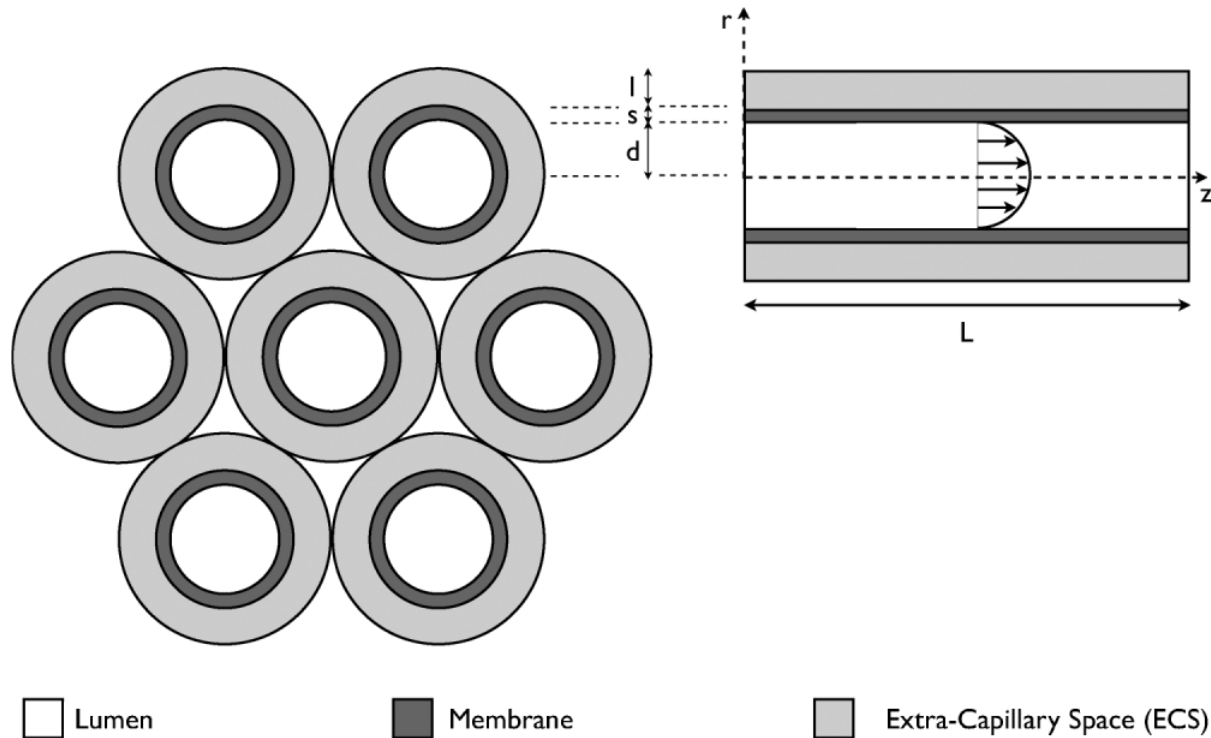
Figure 3-1: Structure within a hollow fiber bioreactor cartridge. In this model, cells and viruses are suspended in slurry flowing through the lumen. Additional media flows through the ECS as perfusion fluid to provide nutrients.

the ECS, alleviating their effect on cell vitality, and cells and viruses are easily harvested by sending the outflow from the FLS to a storage vessel.

3.1 Hollow Fiber Bioreactor Model

The model used to examine the alternative HFBR is based on the Krogh Cylinder models (KCM) of earlier investigators, as shown in Figure 3-1 [48]. Computationally, this model offers the convenience of radial symmetry, which promotes ease of extension to an entire HFBR cartridge by simulating a single fiber. There are three zones in the radial domain: the lumen of the hollow fiber, the membrane of the hollow fiber, and the extra-capillary region. In the KCM, we assume that the extra-capillary space is annular, with an imaginary wall for the outer boundary. All three zones are occupied by the smaller species, but the cells and viruses only inhabit the hollow fiber lumen. The curved triangular zones in the ECS defined by coincident edges of three imaginary outer boundaries are excluded in the

39

analysis, but perfusion fluid flows through them as well. As metabolites in these areas can still be transported to the Krogh cylinder zone by diffusion, the actual delivery of nutrients by perfusion flow is underestimated in this model. Thus, the performance of the alternative HFBR will be better than that predicted by the Krogh cylinder model, and this analysis actually predicts a lower bound of performance in terms of nutrient delivery from the ECS. Within the alternate HFBR model, a number of variables impact design considerations including the flow rates of the lumen and perfusion streams, the radius of the fiber lumen, the length of the bioreactor system, and the cell growth and viral infection rates. A subset of these, specifically the cell growth and viral infection rates, are determined once a specific cell line and virus type have been chosen for the system. This work primarily focuses on delineating trends in productivity in terms of viral production and target cell consumption with bioreactor dimensions (lumen radius and system length) and flow rates through the lumen and ECS. Several cell growth rates were tested, however, to demonstrate how this parameter affects productivity as well as to show that the alternate HFBR is somewhat robust to the choice of the cell line. Timescales on the order of hours are required for cellular production of influenza viruses, so the velocities in the lumen are purposefully limited to low values (i.e., on the order of a few centimeters per hour) to maintain high enough residence times) [13]. The correspondingly low Reynolds numbers necessitate the use of parabolic velocity profiles, creating a wider residence time distribution for slowly diffusing entities such as cells. This problem is somewhat alleviated by shear-induced migration of particles [9]. The rate constants used in our simulations of cell and virus dynamics are those for avian cell line AGE1.CR.pIX, which is used to generate influenza virus [36, 37]. Cell-virus kinetics are obtained from Frensing et al., and cell-specific uptake coefficients of nutrients and production coefficients for waste species are taken from Lohr et al [13, 36]. In the following equations, the independent variables are the radial (r) and axial (z) positions in the bioreactor. The hollow fiber membrane keeps cells and viruses inside the lumen, but allows for transport of smaller species like glucose, amino acids, oxygen, ammonium, and lactate. Furthermore, axial diffusion and radial convection are ignored in this analysis. First, we present the governing continuity equations for the hollow fiber lumen, which contains nutrient and waste species as well as cells and viruses. Those equations are followed by the models for the porous fiber

membrane and the extra-capillary space, which are occupied only by nutrient and waste species. At steady state, the system is described by a set of algebraic and parabolic, second-order partial differential equations, solvable by various numerical techniques. For this work, the model equations are solved by the method-of-lines in which the finite difference method is applied to the radial derivatives to produce a system of ordinary differential equations in terms of the axial coordinate, which are solved using MATLAB's ODE15s function.

3.1.1   Lumen of the Hollow Fiber

For cells and virus that are confined to the hollow fiber lumen, the governing equations and inlet conditions are

$$v_z(r)\frac{\partial T(z,r)}{\partial z} = D_T\left(\frac{\partial^2 T(z,r)}{\partial r^2} + \frac{1}{r}\frac{\partial T(z,r)}{\partial r}\right) + \mu T(z,r)$$
$$- k_1\left(V_s(z,r) + V_d(z,r)\right)T(z,r), \quad T(0,r) = T_0, \quad (3.1)$$

$$v_z(r)\frac{\partial I_s(z,r)}{\partial z} = D_{I_s}\left(\frac{\partial^2 I_s(z,r)}{\partial r^2} + \frac{1}{r}\frac{\partial I_s(z,r)}{\partial r}\right)$$
$$+ k_1 V_s(z,r)T(z,r) - \left(k_2 + k_1 V_s(z,r)\right)I_s(z,r), \quad I_s(0,r) = I_{s0}, \quad (3.2)$$

$$v_z(r)\frac{\partial I_d(z,r)}{\partial z} = D_{I_d}\left(\frac{\partial^2 I_d(z,r)}{\partial r^2} + \frac{1}{r}\frac{\partial I_d(z,r)}{\partial r}\right)$$
$$+ k_1 V_d(z,r)T(z,r) + \mu I_d(z,r) - k_1 V_s(z,r)I_d(z,r), \quad I_d(0,r) = I_{d0}, \quad (3.3)$$

$$v_z(r)\frac{\partial I_c(z,r)}{\partial z} = D_{I_c}\left(\frac{\partial^2 I_c(z,r)}{\partial r^2} + \frac{1}{r}\frac{\partial I_c(z,r)}{\partial r}\right)$$
$$+ k_1\left(V_s(z,r)I_d(z,r) + V_d(z,r)I_s(z,r)\right) - k_d I_c(z,r), \quad I_c(0,r) = I_{c0}, \quad (3.4)$$

41

$$v_{\mathrm{z}}(r)\frac{\partial V_{\mathrm{s}}(z,r)}{\partial z} = D_{V_{\mathrm{s}}}\left(\frac{\partial^2 V_{\mathrm{s}}(z,r)}{\partial r^2} + \frac{1}{r}\frac{\partial V_{\mathrm{s}}(z,r)}{\partial r}\right)$$

$$+ k_3 I_{\mathrm{s}}(z,r) - \left(k_1\psi\left(T(z,r) + I_{\mathrm{s}}(z,r) + I_{\mathrm{d}}(z,r) + I_{\mathrm{c}}(z,r)\right) + k_4\right)V_{\mathrm{s}}(z,r), \quad V_{\mathrm{s}}(0,r) = V_{\mathrm{s}0},$$

$$(3.5)$$

and

$$v_{\mathrm{z}}(r)\frac{\partial V_{\mathrm{d}}(z,r)}{\partial z} = D_{V_{\mathrm{d}}}\left(\frac{\partial^2 V_{\mathrm{d}}(z,r)}{\partial r^2} + \frac{1}{r}\frac{\partial V_{\mathrm{d}}(z,r)}{\partial r}\right) + k_3 3 I_{\mathrm{c}}(z,r) + f k_3 I_{\mathrm{s}}(z,r)$$

$$- \left(k_1\psi\left(T(z,r) + I_{\mathrm{s}}(z,r) + I_{\mathrm{d}}(z,r) + I_{\mathrm{c}}(z,r)\right) + k_4\right)V_{\mathrm{d}}(z,r), \quad V_{\mathrm{d}}(0,r) = V_{\mathrm{d}0}. \quad (3.6)$$

This model was derived based on the kinetic scheme for the interaction among cells and viruses used by Frensing et al., which discusses influenza virus production from the avian cell line AGE1.CR6, where T, I_{s}, I_{d}, and I_{c} are concentrations of uninfected target cells, cells infected by standard virus, cells infected by defective interfering particles (DIPs), and cells infected both by standard and defective viruses, respectively [13]; V_{s} and V_{d} are the concentrations of standard virus and DIPs, respectively; and the lumen velocity (v_z) has a parabolic profile given by

$$v_z(r) = 2v_{z,0}\left(1 - \frac{r^2}{R_{\mathrm{lum}}^2}\right), \tag{3.7}$$

where $R_{textrmlum}$ is the lumen radius and is the average flow velocity in the lumen.

The kinetic parameters in 3.1 to 3.6 are the growth rate of the target cell population μ (1/h), the target cell concentration in the feed T_0 (cells/mL), the viral infection rate k_1 (mL/virion-h), the apoptosis rate of infected cells k_2 (1/h), the standard virus production rate k_3 (virions/cell-h), the DIPs production rate, k_{33} (virions/cell-h), the virus degradation rate k_4 (1/h), the fraction f of DIPs produced relative to standard viruses in the standard virus infected cell species, and a factor ψ for unit conversion which is equal to one when Vs and Vd are quantified in units of virions/cell. Values for the other parameters are given in Table 3.1. Viral production within the system is driven in part by the kinetics of the infection process. Target cells are fed to the system and produced through mitosis. The target cells are converted to infected states through infection either with standard virus or with defective-interfering particles. Both I_{s} and I_{d} are converted to co-infected cells through

cross infection by the other virus particle. Standard- and co-infected cells are the primary source of standard virus particles and DIPs, respectively. The model is structured such that viruses are produced by the appropriately infected cells only while they are alive, and considers cell death via apoptosis for these species using first-order kinetics. Although nearly all virus particles produced by the STV-infected cells are the standard type, a small fraction (1/1000) are DIPs instead, as a result of genetic degradation. All particles produced from co-infected cells, on the other hand, are the defective variant [13].

Within the lumen, the conservation equation for the smaller molecules that can pass through the hollow-fiber membrane is

$$v_z(r)\frac{\partial c_i(z,r)}{\partial z} = D_i \left(\frac{\partial^2 c_i(z,r)}{\partial r^2} + \frac{1}{r}\frac{\partial c_i(z,r)}{\partial r} \right) + Q_i(z,r), \quad c_i(0,r) = c_0, \qquad (3.8)$$

where z is the axial position, r is the radial position, c_i is the concentration of species i $\in$ G, Gl, O2, NH4+, L, G denotes glucose, Gl denotes the amino acid glutamine, O2 is dissolved oxygen, NH4+ is ammonium ion representing nitrogenous waste, and L is lactate, a byproduct of glucose metabolism. The diffusivity of species i is denoted by D_i, and Q_i is nutrient consumption rate (or waste production rate, where appropriate) for species i.

The consumption and production rates of smaller species are proportional to cell concentration and are given by

$$Q_G = -q_G(T + I_\text{s} + I_\text{d} + I_\text{c}), \qquad (3.9)$$

$$Q_{Gl} = -q_{Gl}(T + I_\text{s} + I_\text{d} + I_\text{c}), \qquad (3.10)$$

$$Q_{O_2} = -q_{O_2}(T + I_\text{s} + I_\text{d} + I_\text{c}), \qquad (3.11)$$

$$Q_L = -q_L(T + I_\text{s} + I_\text{d} + I_\text{c}), \qquad (3.12)$$

and

$$Q_{NH4+} = -q_{NH4+}(T + I_\text{s} + I_\text{d} + I_\text{c}), \qquad (3.13)$$

where the q_i and p_i are the cell-specific consumption and production coefficients, respectively, for species i. These rates are assumed to be the same across all cell states in the model. Although the consumption or production rates may change when a cell becomes in-

43

fected, such variations are not well characterized in the literature, and would not change the main conclusions of this study. The diffusivities for viruses are obtained by Stokes-Einstein equation,

$$D = \frac{k_B T}{6\pi R_v \mu_{\mathrm{visc}}}, \tag{3.14}$$

and for cells are given by Higgins, et al.,

$$D = C\dot{\gamma}_h R_{\mathrm{cell}}^2, \tag{3.15}$$

where R_v is the virus radius, and γ_h is the hydrodynamic shear rate [10, 40].

Cell-specific coefficients for consumption and production appear in Table 3.2 and are inferred from Lohr et al. and Petiot et al., except for that of oxygen, which was suggested as a typical value by Piret and Cooney [36, 46, 48]. Values for diffusivities as well as other parameters appearing in the model are also listed in Table 3.2, and Table 3.3 contains solution parameters and ranges of certain parameters tested in the model.

3.1.2 Membrane of the Hollow Fiber

There are two components of the membrane of the hollow fiber: the very thin ultrafiltration skin, which is at the interface of the lumen, and a thicker spongy material, which encompasses the outer portion of the membrane and interface with the extra-capillary space. The ultrafiltration skin prevents viruses and cells from entering the sponge, and has an approximate thickness of $\Delta R_u = 0.5$ microns and a fractional porosity ϵ_u of about 0.03 . The spongy portion of the membrane is about 75 microns in thickness, and only nutrient and waste molecules are capable of entering the spongy portion through the ultrafiltration skin. Convection terms in the membrane are assumed negligible due to the low axial flow, that is, the hydraulic pressures between the lumen and extra-capillary space are the same. Furthermore, no nutrient consumption or waste production occurs in the membrane due to the exclusion of cells and virus. The governing equations for the concentrations of the permeable

species in the spongy region are

$$D_{m,i}\frac{1}{r}\frac{\partial}{\partial r}\left(r\frac{\partial c_{m,i}}{\partial r}\right) = 0. \tag{3.16}$$

3.1.3   Extra-capillary Space

Only the smaller molecules are present in the extra-capillary space. The continuity equations in this region are

$$u_z(r)\frac{\partial c_i(z,r)}{\partial z} = D_i\left(\frac{\partial^2 c_i(z,r)}{\partial r^2} + \frac{1}{r}\frac{\partial c_i(z,r)}{\partial r}\right), \quad c_i(0,r) = c_{i,\text{ext}}(z) \tag{3.17}$$

where $u_z(r)$ is the flow velocity in the ECS. The flow is laminar and velocity profile is parabolic and described by

$$u_z(r) = 2u_{z,0}\left(1 - \frac{\left(r - left(\frac{1}{2}(R_\text{ext} - R_\text{m}) + R_\text{m}\right)^2}{\left(\frac{1}{2}(R_\text{ext} - R_\text{m})\right)^2}\right) \tag{3.18}$$

where R_m is the radius at the intersection of the membrane and extra capillary space, R_{ext} is the external radius of the system which occurs at the outer edge of the ECS and u_{z0} represents the average flow velocity in the ECS.

3.1.4   Radial Boundary Conditions

The cells and viruses occupy only the lumen of the hollow fiber. For $X(z,r)$ representing the concentration of a cell or virus, its boundary conditions are

$$\frac{\partial X(z,r)}{\partial r} = 0 \, at \, r = 0 \tag{3.19}$$

and

$$\frac{\partial X(z,r)}{\partial r} = 0 \, at \, r = R_\text{lum}. \tag{3.20}$$

The first equation is a symmetry condition, while the latter enforces that neither cells nor virus particles can diffuse through the membrane.

For the smaller species, which occupy the lumen, membrane, and extra-capillary domains, six radial boundary conditions are required. For the lumen region, the symmetry condition at the lumen center is

$$\frac{\partial c_i}{\partial r} = 0 \; at \; r = 0, \tag{3.21}$$

and the flux continuity conditions at the intersection of the lumen and inner surface of the ultrafiltration skin are

$$D_i \left. \frac{\partial c_i}{\partial r} \right|_{r=R_{\mathrm{lum}}^-} = \epsilon_u D_i \left. \frac{\partial c_i}{\partial r} \right|_{r=R_{\mathrm{lum}}^+}, \tag{3.22}$$

where ϵ_u is the porosity of the ultrafiltration skin.

For the spongy region of the membrane, the flux continuity condition at the intersection of the outer surface of ultrafiltration skin and the inner surface of the spongy region of the membrane is

$$\epsilon_u D_i \left. \frac{\partial c_i}{\partial r} \right|_{r=R_{\mathrm{lum}}^-} = \epsilon_m D_i \left. \frac{\partial c_i}{\partial r} \right|_{r=R_{\mathrm{lum}}^+}, \tag{3.23}$$

where ϵ_m is the porosity of the membrane sponge.

The intersection of the sponge and the extra-capillary space must satisfy the flux continuity condition

$$-\epsilon_m D_i \left. \frac{\partial c_i}{\partial r} \right|_{r=R_{\mathrm{lum}}+\Delta R_{\mathrm{u}}+\Delta R_{\mathrm{m}}} = -D_i \left. \frac{\partial c_i}{\partial r} \right|_{r=R_{\mathrm{lum}}+\Delta R_{\mathrm{u}}+\Delta R_{\mathrm{m}}}, \tag{3.24}$$

where there will be a discontinuity in $\frac{\partial c}{\partial r}$, since ϵ_m is less than 1. Also imposed at this interface is the continuity condition

$$c_i(z, R_{\mathrm{lum}} + \Delta R_{\mathrm{u}} + \Delta R_{\mathrm{m}-}) = c_i(z, R_{\mathrm{lum}} + \Delta R_{\mathrm{u}} + \Delta R_{\mathrm{m}+}), \tag{3.25}$$

where ΔR_{m+} and ΔR_{m-} denote positions just inside and outside, respectively, the spongy and extra-capillary space interface.

Finally, a no-flux condition is specified at the outer boundary of the extra-capillary space:

$$-D_i \left. \frac{\partial c_i}{\partial r} \right|_{r=R_{\text{ext}}} = 0. \tag{3.26}$$

This condition indicates an impermeable boundary for our imaginary outer wall surrounding the extra-capillary space. Here, the assumption is that the concentrations of nutrients and waste species reach a maximum and minimum, respectively, at the interface with the extra-capillary space surrounding adjacent hollow fibers.

3.2   Hollow Fiber Bioreactor Design Considerations

The novelty of the alternate hollow fiber bioreactor presented here promotes using a design-based approach to acquire trends between system parameters and bioreactor productivity. Rather than using a single metric for productivity, we considered the resultant consumption of target cells (process feedstock), production of standard virus particles (desired product), and production of defective interfering particles which are an undesired byproduct. Bioreactor length and radius, FLS and ECS flow rates, cell doubling times, and small-molecule consumption and production rates are parameters which were varied between bioreactor setups using various cell substrates and viral species. Once a cell line and virus are chosen, however, only bioreactor sizing parameters can be modified. Thus, we explored the effects of bioreactor length and fiber radius (200 to 500 microns) on the production of standard virus particles. Multiple cell doubling times (24, 30, and 36 hours) were explored as well in order to show that the alternate HFBR is a valid consideration for a variety of cell types. It is common with bioprocesses involving animal cell substrates to use a residence time on the order of 20 hours [56, 59]. Simulation results quickly demonstrated, however, that standard virus production for that residence time reaches a peak well before the end of the bioreactor for a variety of combinations of bioreactor length and flow rate (Figure 3-2). Any production after this point consists primarily of defective interfering particles, which indicates that a 20-hour residence time is too long for this system. We reduced the residence time to a final value of 12 hours, to ensure near-maximal production of standard virus without diluting this
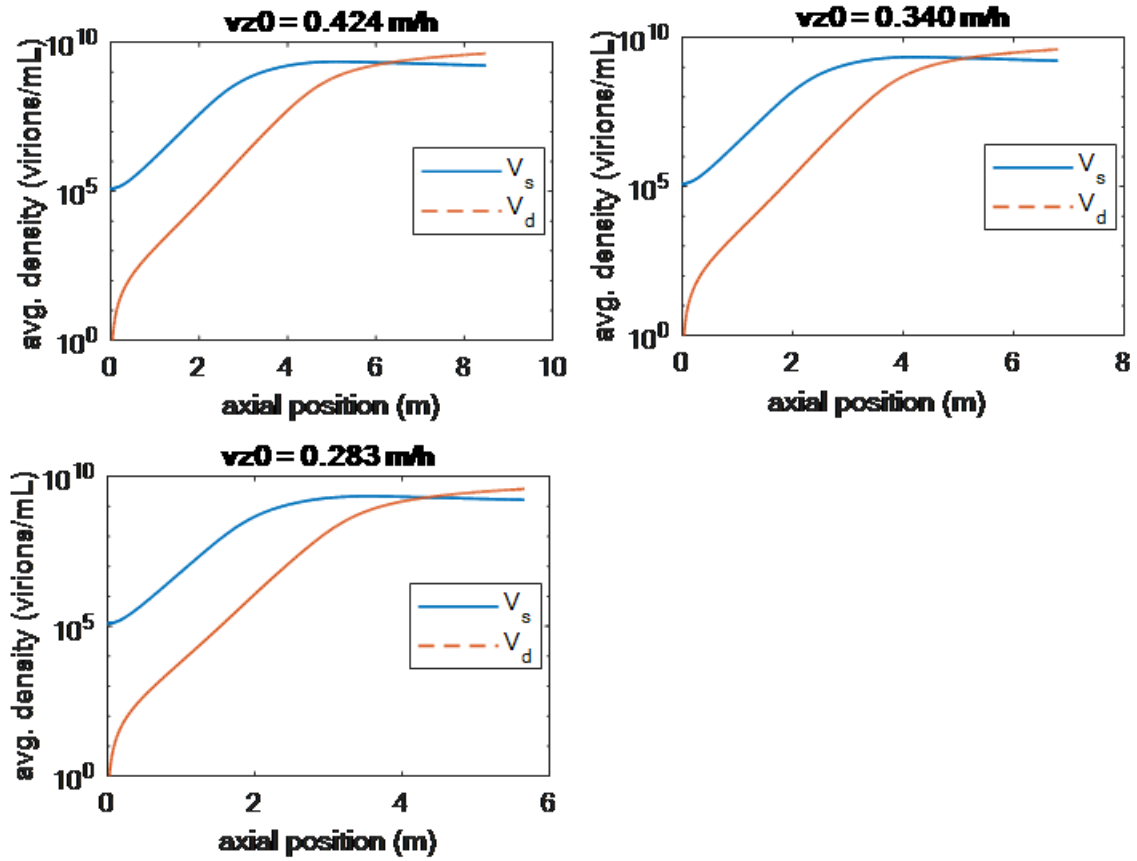
Figure 3-2: Using a 20 hour residence time results in a decline in standard virus production before the exit of the reactor, even at a variety of combinations of flow rate and reactor length. Furthermore, defective interfering particle production, which occurs more rapidly, causes the concentration of the defective species to overtake that of the standard particle. Reducing the residence time to 12 hours allows the capture of standard virus concentration peak without diluting it unnecessarily with DIPs.

species with excess DIPs which would be produced at longer times. Bioreactors modeled in this study were designed by first choosing linear flow rates based on desired production rates and typical feed flow rates, and then determining the bioreactor length to maintain a residence time of 12 hours. As oxygen is oftentimes the growth rate-limiting species, a suitable velocity for the perfusion flow through the ECS is determined by requiring the oxygen depletion per pass to be no more than half of the original value [48]. This moderate depletion is similar to that obtained by Piret and Cooney for a traditional HFBR [47]. Using this metric, the perfusion fluid flow rate is set to twice that of the lumen stream, giving the ECS a residence time of 6 hours.

3.3   Results and Discussion

Simulations of the model equations presented in this chapter indicate that lumen radius has the largest effect on the key species concentrations throughout the bioreactor. Bioreactor radii less than 250 μm were necessary to ensure adequate cell densities over the entire cross-section. For example, when , the radial profiles of the target and STV-infected cells at downstream axial locations indicates serious depletion of these cells near the lumen wall (Figure 3-3). The low value of the cell diffusivity was insufficient for radial diffusion to compensate for the slow residence time in the outer lumen. This point is further illustrated by the mixed-cup averages of the cells and viruses in Figure 3-4, when $R_{lum} = 500\mu$ m. The severe decline in standard virus precursor cell concentrations T and I_s upstream of the outlet of the bioreactor causes STV production to halt and the concentration of this species to be overtaken by that of its defective counterpart. On the other hand, radial profiles for indicate an adequate distribution of cells over most of the cross-section (Figure 3-5). The radial profiles of the virions show less spatial variation due to their higher diffusivities (Figure 3-6). The target cell doubling time had a low impact on species concentrations throughout the bioreactor when compared to the effects of modifying bioreactor dimensions. Increasing cell doubling time from 24 to 30 to 36 hours caused target cell and STV concentrations to decrease by 1–2% down the length of the bioreactor (Figures 3-7 and 3-8), and similar small effects on the other variables. The target cell concentration drops sharply by in the first half of the bioreactor (Figure 3-7), in which the cells have only been in the hollow fibers for 6 hours. As such, the target cells spend insufficient time in the bioreactor to have significant proliferation for any value of their doubling times. In other words, the growth kinetics of the target cells are much slower than the viral infection kinetics, so the resulting dynamics have a weak dependency on variation in the cell growth kinetics. Because it is clear that the alternative HFBR system is more effective at smaller lumen radii, and to make these results industrially applicable, the remainder of the results are posed as a case study using a bioreactor with a lumen radius of 250 microns, which matches commercially available hollow fibers. Based on the above modeling results, the residence time is kept at 12 hours, and the target cells are chosen to have a 24-hour doubling time. Figure 3-9

shows the axial profiles of the mixed-cup average of the concentrations of cells and virions, respectively. Target cells are almost depleted at the outlet of the bioreactor, while standard virus-infected cells – which are the only cells that can produce standard viruses – are more plentiful but declining. The DIP-infected cell concentration remains low throughout the bioreactor. Only the concentration of co-infected cells – which can produce only defective virions – is increasing at the outlet. These results imploy that the effluent cells should not be recycled, and that the only material leaving the bioreactor that could be potentially recycled (modulo any regulatory considerations) would be standard virus particles. The maximum concentration of standard virus particles for the 250-micron lumen is 44% higher than for the 500-micron lumen (compare Figures 3-5 and 3-9), which provides additional support for the lowering of the hollow fiber radius. Figure 3-10 displays the radial profiles of the nutrient concentrations at the axial locations z = 0 , 0.10, 0.20, 0.30 and 0.38 m, respectively. The flat profiles at z = 0 reflect the inlet conditions. At z = 0.10 m, the glucose, amino acid, and oxygen concentrations are nearly flat, due to high diffusivities and small radial dimensions, with a slight decline from the outer edge of the ECS to the lumen center at , as expected. Replenishment of glucose and amino acids from the highly perfused extra-capillary space is sufficient to maintain exit levels above 90% of the entrance concentrations. The discontinuity in radial gradients at the membrane reflects the use of the overall membrane resistance. Oxygen is more depleted near the outlet of the bioreactor, but its concentration is still more than half of the inlet concentration, which is in line with results for traditional HFBRs. For overall reduction of the consumption of consumables, the outlet perfusion fluid could be boosted with more glucose and amino acids, re-oxygenated, and recycled to the medium reservoir . The radial profiles for ammonium ion and lactate concentrations are relatively flat (Figure 3-11), as for the nutrient profiles. The exit levels of ammonium are lower than for mammalian cells, as avian cells consume far less glutamine [17]. Thus avian cells offer a benefit as high levels of ammonium are toxic to some mammalian cells. Lactate levels are similar as in mammalian cells, but lactate toxicity does not appear to be a problem, given the success of Frensing's experiments [13, 17]. A higher perfusion rate through the ECS would lead to even lower consumption of nutrients and buildup of waste, making the exit ECS fluid a better candidate for recycling. With recycling, the perfusion rate would need to

Table 3.1: Cell and Virus Kinetic Parameter Values

Parameter	Value
$D_{\text{cell}}(m/s^2)$	2.08×10^{-13}
$D_{\text{virus}}(m/s^2)$	5.0×10^{-12}
$I_{\text{d,0}}(cells/m^3)$	0
$I_{\text{s,0}}(cells/m^3)$	0
$I_{\text{c,0}}(cells/m^3)$	0
$k_1(mL/virion/h)$	2.12×10^{-9}
$k_2(1/h)$	7.13×10^{-3}
$k_3(virion/cell/h)$	168
$k_4(1/h)$	0.035
$k_{33}(virion/cell/h)$	168
$K_{\text{m,Gl}}(mmol/m^3)$	0.5×10^6
μ (1/h)	0.027
f	10^{-3}
$R_{\text{cell}}(m)$	7.5×10^{-6}
$R_{\text{virus}}(m)$	50×10^{-9}
$T_0(cells/m^3)$	3×10^{12}
$V_{\text{d,0}}(virions/m^3)$	0
$V_{\text{s,0}}(virions/m^3)$	1.25×10^{11}

be optimized to trade off cell health and costs.

3.4 Conclusions

Hollow fiber bioreactors provide a narrow residence time distribution for cell-virus cultures, thus curtailing the creation of late-forming defective viruses in the case of the AGE1.CR.pIX/influenza virus system. Because DIPs cannot accumulate periodically in an alternative HFBR, the oscillatory behavior that occurs in certain cell/virus systems is eliminated. To obtain a sufficient output of standard virus that is not diluted with DIPs, the alternative HFBR model using model parameters fit to data by Frensing et al.6 indicates that the average residence time of cells should set to about 12 hours. This value can likely be optimized to further improve STV to DIP collection ratio, or similar productivity metrics. The results presented here indicate an upper limit of 250 microns on the radius of the hollow fiber lumen is necessary to ensure adequate cell densities throughout the bioreactor to maintain a high

Table 3.2: Nutrient and Waste Kinetic Parameter Values

Parameter	Value
$c_{\mathrm{G},0}(mmol/m^3)$	20×10^3
$c_{\mathrm{Gl},0}(mmol/m^3)$	3.6×10^3
$c_{\mathrm{O2},0}(mmol/m^3)$	0.2×10^3
$c_{\mathrm{NH4},0}^{+}(mmol/m^3)$	0
$c_{\mathrm{L},0}(mmol/m^3)$	0
$D_{\mathrm{G}}(m^2/s)$	6.7×10^{-10}
$D_{\mathrm{Gl}}(m^2/s)$	7.6×10^{-10}
$D_{\mathrm{O2}}(m^2/s)$	2.0×10^{-9}
$D_{\mathrm{NH4}}^{+}(m^2/s)$	1.97×10^{-9}
$D_{\mathrm{L}}(m^2/s)$	4.9×10^{-10}
$q_{\mathrm{G}}(mmol/s/cell)$	3.737×10^{-13}
$q_{\mathrm{Gl}}(mmol/s/cell)$	7.958×10^{-14}
$q_{\mathrm{O2}}(mmol/s/cell)$	4.290×10^{-15}
$p_{\mathrm{NH4}}^{+}(mmol/s/cell)$	5.363×10^{-14}
$p_{\mathrm{L}}(mmol/s/cell)$	6.557×10^{-13}
ϵ_{m}	0.86
ϵ_{u}	0.03

Table 3.3: Other Parameter Values

Parameter	Value
$R_{\mathrm{ext}}(m)$	475×10^{-6}
$R_{\mathrm{lum}}(m)$: (tested)	200×10^{-6} to 500×10^{-6}
$R_{\mathrm{lum}}(m)$: (final value)	250×10^{-6}
$u_z(m/h)$	0.024
$v_{z,0}(m/h)$	0.03
$z_L(m)$: (tested)	0.2 to 0.5
$z_L(m)$: (final value)	0.38
$\Delta R_m(m)$	75×10^{-6}
$\Delta R_u(m)$	0.5×10^{-6}

volumetric production of standard virus. This maximum radius is primarily set by the low diffusivities of cells. For larger lumen radii, the target and standard-virus-infected cells are depleted in the outer regions of the lumen, which leads to lower production of standard virus per unit volume of hollow fiber. Using hollow fibers with smaller radii might improve performance, but potential plugging is a concern, depending on choice of cell line and typical cell diameters. The diffusivities of the metabolites are sufficiently high to keep their radial profiles relatively uniform in the alternative HFBR. By using high perfusion rates of medium through the ECS, sufficient nutrients can be supplied, and the effluent nutrient stream can be recycled. Recycling of cells after a single pass through the hollow fiber is not advisable as 80% are incapable of producing standard virus; i.e., they are DIP- and co-infected cells. This depletion of useful cells is due to the cell-virus kinetics revealed by Frensing's experiments. The alternative HFBR enables the disposal of the spent cells, as does a harvested well-stirred bioreactor. A conventional HFBR, with cells anchored in the extra-capillary space, would eventually suffer the same problem, so the spent cells would have to be removed and the ECS re-cultured.

Figure 3-3: 500-micron reactor, 24 hour target cell doubling time. Radial profiles of target and STV-infected cells (precursors to standard virus particles) show severe depletion, particularly at the lumen wall, before the exit of the reactor. This is caused by the low diffusivity of these species.
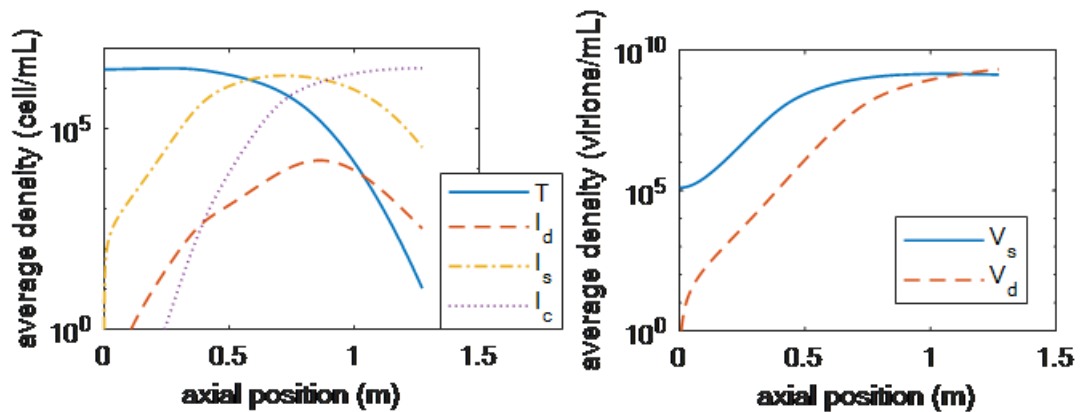
Figure 3-4: 500-micron reactor, 24 hour target cell doubling time. Concentration of target and STV-infected cells decline rapidly before the end of the reactor, while the co-infected species concentration remains high. This causes STV production to end prior to the reactor outlet, while DIP production is maintained by the large co-infected population.
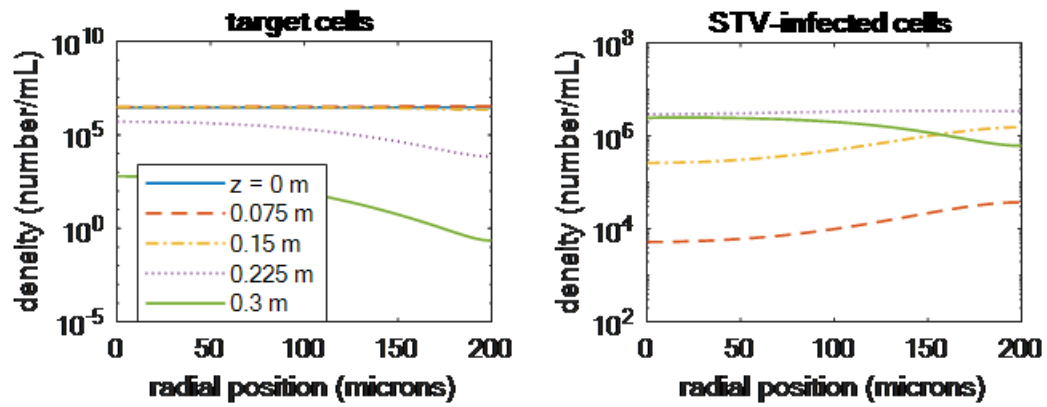
Figure 3-5: 200-micron reactor, 24 hour target cell doubling time. Both STV-precursor species are adequately distributed across the radius of the reactor which promotes viral production throughout the entire reactor volume.
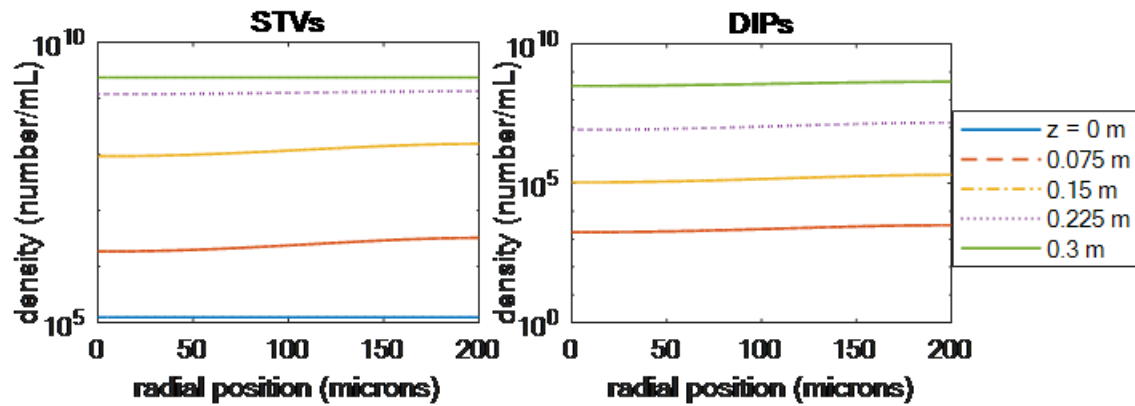
Figure 3-6: 200-micron reactor, 24 hour target cell doubling time.
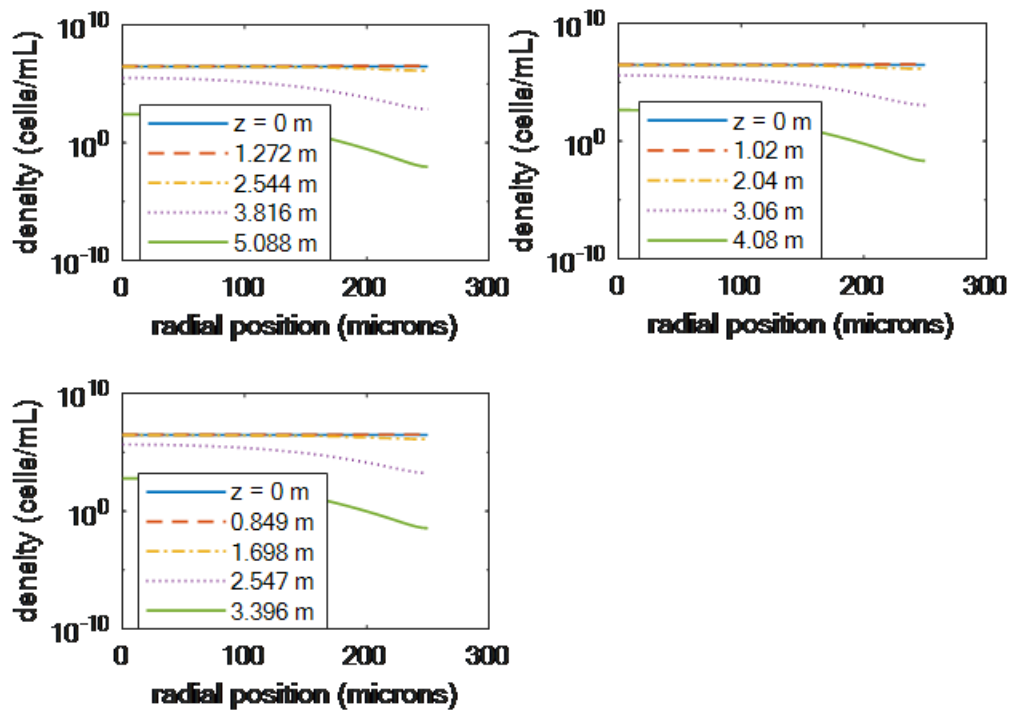
Figure 3-7: 250 micron reactor. Increasing target cell doubling time from 24 to 30 to 36 hours results in lower concentrations of this species throughout the reactor. However, the decrease is only 1-2% of the concentration entering the reactor.
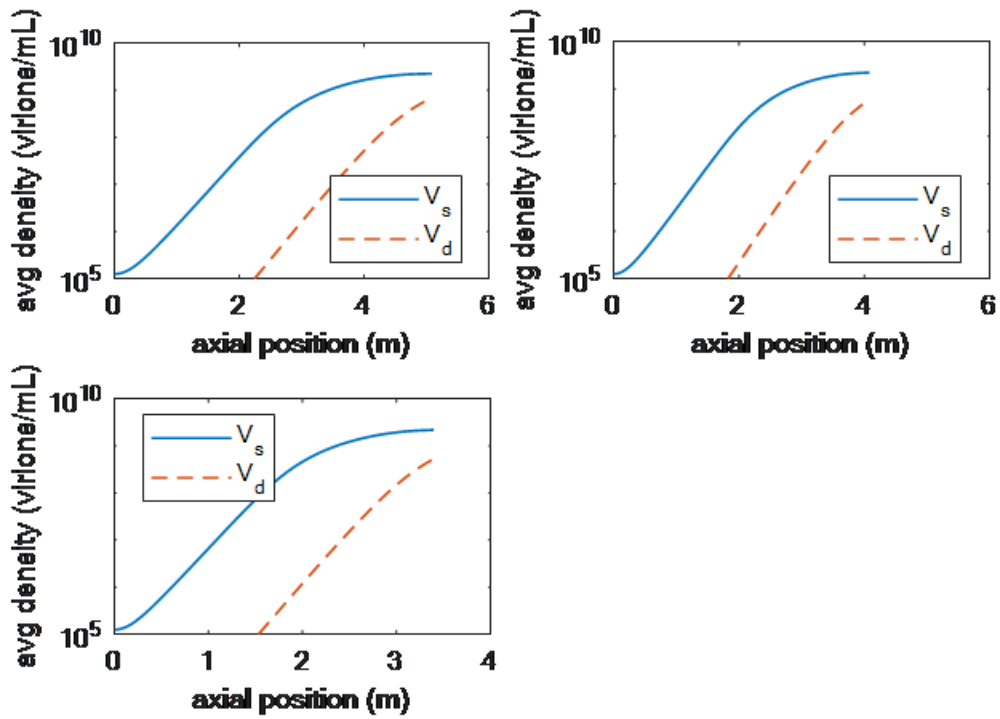
Figure 3-8: 250 micron reactor. Increasing target cell doubling times increases STV production by 1-2%.
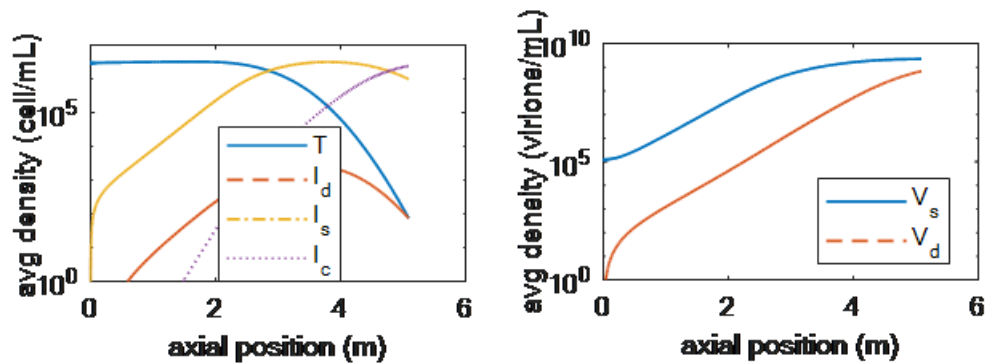
Figure 3-9: 250-micron reactor, 24 hour target cell doubling time. Results for the case study reactor show adequate cell densities throughout the reactor, as well as production of STVs that exceeds that of the defective variant.
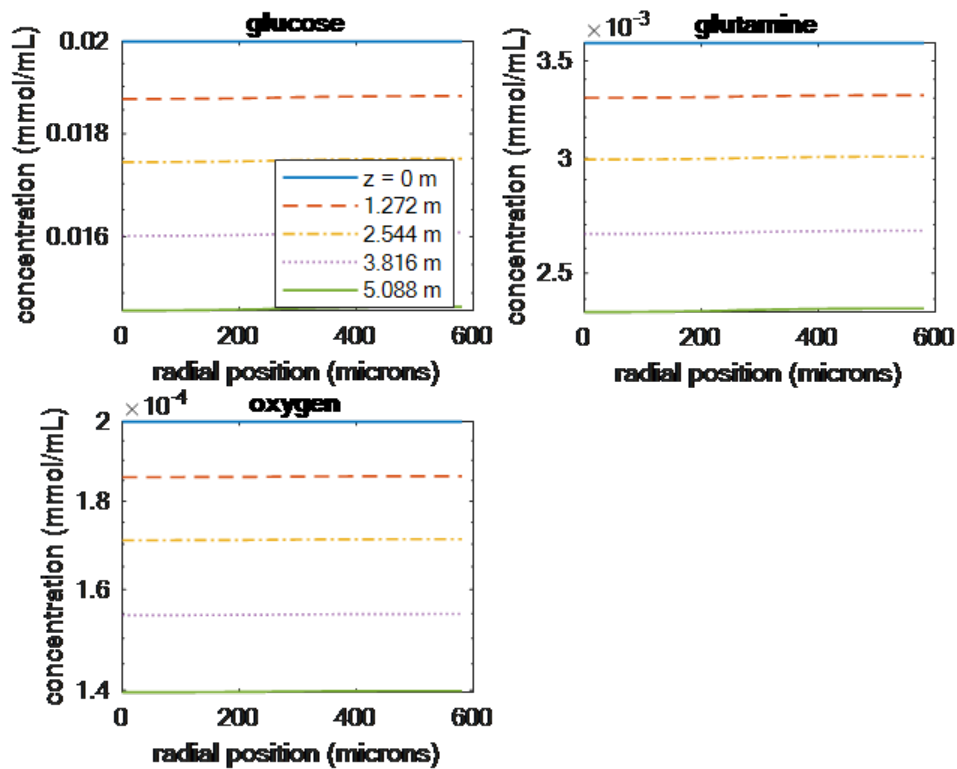
Figure 3-10: 250-micron reactor, 24 hour target cell doubling time. Nutrient profiles remain relatively flat, indicating ease of diffusion relative to cell and virus species. The discontinuity that occurs at the membrane (at a radial position of 250 microns) is expected from analysis of the equations. Note that oxygen depletion is only 30% here, which indicates that the perfusion flow rate can potentially be reduced.
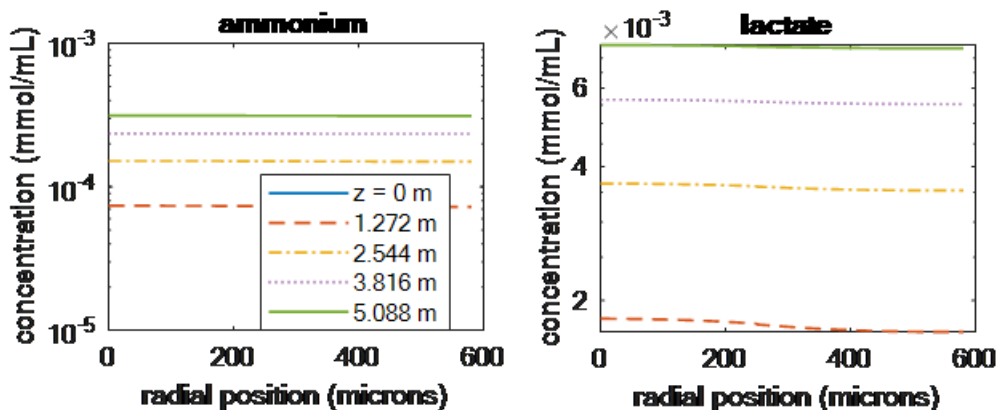
Figure 3-11: 250-micron reactor, 24 hour target cell doubling time. Radial profiles of waste species demonstrate that neither accumulate to toxic levels within the reactor.

Chapter 4

Finite Difference Simulation of Population Balance Models with No Discretization Error

Population balance models are used to describe an exceptionally wide array of chemical and biological processes which have a distribution over some intrinsic property as their main state. Because of the ubiquitous nature of these problems, it is important to have a generalizable approach for the solution of population balance equations. The finite difference and finite volume methods typically utilized to solve these equations rely on increasingly higher ordered approximations, which can be computationally expensive. This chapter proposes a simple finite difference scheme that results in no numerical discretization error for certain classes of population balances. The proposed finite difference method results in zero error for constant growth rate, and nonzero error expressions are derived for more complicated systems including time or age-dependent growth and non-homogeneous problems. These error expressions confirm the zero error in the simpler cases. Further, they demonstrate that it is appropriate to apply the finite difference methods to more complicated classes of problems, with the expectation that the error will transition from first-order error to zero error as the growth rate and/or nonhomogeneous terms become smoother functions of time or the intrinsic variable.

The spatiotemporal dynamics of populations are described by population balance models.

These models are applicable to a wide variety of biological processes for populations that include cells, viruses, aggregates, bubbles, droplets, crystals, or precipitates. A large literature derives finite difference and finite volume methods for the numerical simulation of population balance models, as well as for more general partial differential equations, with the focus being to minimize discretization errors (e.g., see [20], [50], [68], [38], [39], [70] and citations therein). Especially important for this class of hyperbolic partial differential equations is the need to reduce numerical diffusion (i.e., smearing of the numerical solution compared to the true solution) and numerical dispersion (i.e., aphysical oscillations in the numerical solution that do not arise in the true solution). This chapter describes a finite difference method with *no discretization error* for the simulation of classes of population balance models that arise in many applications.

This chapter summarizes the population balance model and describes the finite difference method with associated analysis for a series of successively more complicated population balance models. The intent is for this chapter to be pedagogical. That is, the chapter shows the main idea of the finite difference method first for a relatively simple case, and then shows how to generalize the approach. The chapter also derives error expressions that quantify the error for more general population balance models, which show that the finite difference method behaves benignly, and is also suitable for application to those systems.

4.1   Population Balance Models

Species balances for spatially well-mixed systems can be written as ordinary differential equations (ODEs),

$$\frac{df(t)}{dt} = h(t, f), \tag{4.1}$$

where f is the species density (e.g., concentration), t is time, and h is a forcing function that can be a function of f and t. Both f and h can be vectors in general, with each element corresponding to each species in the system. For the derivation and analysis of finite difference methods, f and h can be treated as scalars without loss of generality, as the extension to the vector case is trivial.

When a species has an additional intrinsic variable, such as size or age, the partial

differential equation (PDE) corresponding to the ODE model is

$$\frac{\partial f(t,a)}{\partial t} + \frac{\partial (Gf(t,a))}{\partial a} = h(t,a,f) \tag{4.2}$$

where a is the additional intrinsic variable and $G = da/dt$ is the rate of change of the intrinsic variable with respect to time. The term G is referred to as "growth rate" in the population balance literature. While this is an accurate term for most populations, it is somewhat of a misnomer in that da/dt is not associated with a rate of growth for some applications, e.g., when a is the age of a cell and G represents the aging of a cell rather than its growth. To be consistent with the literature, this chapter also refers to G as the growth rate.

This equation describes the time evolution of the distribution of f with respect to a. For example, in cell population balance models which define the variable a as the age of a cell, $G = 1$ [60]. When the intrinsic variable a is the size or mass of the cell, or the number or concentration of organelles within a cell, then G is rarely equal to one but may be describable by a constant or a function of a and/or t. The forcing function h can also be a function of the intrinsic variable a. When the growth rate is not a function of a, then G can be factored of the second term,

$$\frac{\partial f(t,a)}{\partial t} + G\frac{\partial f(t,a)}{\partial a} = h(t,a,f) \tag{4.3}$$

The above population balance models, as well as the results of this chapter, can also be generalized to the case with multiple intrinsic variables, e.g.,

$$\frac{\partial f(t,a_1,\ldots,a_m)}{\partial t} + \sum_{i=1}^{m} G_i \frac{\partial f(t,a_i)}{\partial a_i} = h(t,a_1,\ldots,a_m,f) \tag{4.4}$$

in a straightforward manner, where m is the number of intrinsic variables. Also, the same population balance model and results can be extended to populations in a steady-state slug or plug flow through a tube by replacing the time t with the residence time τ, or to the dynamic slug or plug flow through a tube by including both derivatives with respect to time and residence time, e.g.,

$$\frac{\partial f(t,a_1,\ldots,a_m)}{\partial t} + \frac{\partial f(t,a_1,\ldots,a_m)}{\partial \tau} + \sum_{i=1}^{m} G_i \frac{\partial f(t,a_i)}{\partial a_i} = h(t,a_1,\ldots,a_m,f) \tag{4.5}$$

where $\tau = z/u$ where z is the axial position down the tube and u is the flow velocity.

4.2 Numerical Method and Associated Error Analysis

Finite difference methods are used to approximate partial differentials, e.g., on the left-hand side of (5.6). To reduce the numerical error, that is, the difference between the numerical approximation described by the discretized equation and the true solution described by the PDE, the well established strategy is to use increasingly complicated and higher order accurate finite difference expansions. While this approach reduces the number of discretization points needed to achieve a specified level of numerical accuracy, the computational cost per discretization point increases.

This chapter describes a different approach, which is to select a special choice of first-order finite difference expressions so that the discretization error is **zero**. This approach both results in the lowest cost per discretization point and allows the user to select the number of discretization points based on the level of detail desired in the solution rather than achieving a desired numerical error. Specifically, this approach employs a first-order forward difference for the time derivative and a first-order backward difference for the derivative with respect to the intrinsic variable.

As is standard in the numerical analysis literature (e.g., [49]), the finite difference method is first applied to homogeneous population balance models, both to simplify the algebra and because the presence of a nonhomogeneous term does not affect whether the finite difference method gives zero discretization error in the sum of the partial derivatives. The first set of results also show that the finite difference method, when transformations are included, results in zero error for large mesh sizes for homogeneous population balance models.

The numerical analysis in this chapter starts by studying the homogeneous form of the partial differential equations, as that simplifes the analysis and is by far the most common practice in the engineering and science literature [29, 49]. Then the chapter analyzes the overall error between the numerical solution and the exact solution for the nonhomogeneous partial differential equation, which is the type of analysis employed by mathematicians who specialize in numerical methods for PDEs (e.g., [11, 31]). This latter analysis quantifies the

effects of mesh sizes on the overall error for nonhomogeneous population balance models, and shows how the overall error converges to zero as the time or size dependency weakens in the nonhomogeneous term.

4.2.1 Case 1: Cell Population Balance Models

First let's illustrate the approach by considering the homogeneous population balance model in which the growth rate G is equal to 1,

$$\frac{\partial f(t,a)}{\partial t} + \frac{\partial f(t,a)}{\partial a} = 0, \quad f(0,a) = f_0(a), \tag{4.6}$$

over the real domains $a \geq 0$ and $t \geq 0$. The value of $G = da/dt = 1$ applies to cell populations in which a is the age and is defined to have the same unit as the time t [28].

Applying the aforementioned finite difference scheme yields

$$\frac{f_{i+1}^j - f_i^j}{\Delta t} + \frac{f_i^j - f_i^{j-1}}{\Delta a} = 0 \tag{4.7}$$

where i is the time index and j is the index for the intrinsic variable. The Taylor series expansions for f in terms of t and a, respectively, are

$$f(t+\Delta t, a) = f(t,a) + \Delta t \frac{\partial f}{\partial t}\Big|_{t,a} + \frac{(\Delta t)^2}{2!}\frac{\partial^2 f}{\partial t^2}\Big|_{t,a} + \frac{(\Delta t)^3}{3!}\frac{\partial^3 f}{\partial t^3}\Big|_{t,a} + \cdots + \frac{(\Delta t)^n}{n!}\frac{\partial^n f}{\partial t}\Big|_{t,a} + \cdots \tag{4.8}$$

$$f(t, a-\Delta a) = f(t,a) - \Delta a \frac{\partial f}{\partial a}\Big|_{t,a} + \frac{(\Delta a)^2}{2!}\frac{\partial^2 f}{\partial a^2}\Big|_{t,a} - \frac{(\Delta a)^3}{3!}\frac{\partial^3 f}{\partial a^3}\Big|_{t,a} + \cdots + (-1)^n\frac{\partial^n f}{\partial a^n}\Big|_{t,a} + \cdots \tag{4.9}$$

These expressions can be rearranged into the form

$$\frac{f_{i+1}^j - f_i^j}{\Delta t} = \frac{\partial f}{\partial t}\Big|_{t,a} + \frac{\Delta t}{2!}\frac{\partial^2 f}{\partial t^2}\Big|_{t,a} + \frac{(\Delta t)^2}{3!}\frac{\partial^3 f}{\partial t^3}\Big|_{t,a} + \cdots + \frac{(\Delta t)^{n-1}}{n!}\frac{\partial^n f}{\partial t^n}\Big|_{t,a} + \cdots \tag{4.10}$$

$$\frac{f_i^j - f_i^{j-1}}{\Delta a} = \frac{\partial f}{\partial a}\Big|_{t,a} - \frac{\Delta a}{2!}\frac{\partial^2 f}{\partial a^2}\Big|_{t,a} + \frac{(\Delta a)^2}{3!}\frac{\partial^3 f}{\partial a^3}\Big|_{t,a} + \cdots + (-1)^{n-1}\frac{(\Delta a)^{n-1}}{n!}\frac{\partial^n f}{\partial a^n}\Big|_{t,a} + \cdots \tag{4.11}$$

and inserted into the left-hand side of (4.7) to give an expression for the discretization error

63

of

$$\text{error} = \frac{f_{i+1}^j - f_i^j}{\Delta t} + \frac{f_i^j - f_i^{j-1}}{\Delta a}$$

$$= \frac{\partial f}{\partial t}\bigg|_{t,a} + \frac{\partial f}{\partial a}\bigg|_{t,a} + \frac{\Delta t}{2!}\frac{\partial^2 f}{\partial t^2}\bigg|_{t,a} - \frac{\Delta a}{2!}\frac{\partial^2 f}{\partial a^2}\bigg|_{t,a} + \frac{(\Delta t)^2}{3!}\frac{\partial^3 f}{\partial t^3}\bigg|_{t,a} + \frac{(\Delta a)^2}{3!}\frac{\partial^3 f}{\partial a^3}\bigg|_{t,a}$$
$$+ \cdots + \frac{(\Delta t_i)^{n-1}}{n!}\frac{\partial^n f}{\partial t^n}\bigg|_{t_i,a_j} + (-1)^{n-1}\frac{(\Delta a_j)^{n-1}}{n!}\frac{\partial^n f}{\partial a^n}\bigg|_{t_i,a_j} + \cdots \quad (4.12)$$

From (4.6), the first two terms on the right-hand side sum to 0. Taking successive derivatives of (4.6) with respect to t and a and rearranging gives the equalities:

$$\frac{\partial^2 f}{\partial t^2} = \frac{\partial^2 f}{\partial a^2} \quad (4.13)$$

$$\frac{\partial^3 f}{\partial t^3} = -\frac{\partial^3 f}{\partial a^3} \quad (4.14)$$

such that the remaining terms in (4.12) (if the fourth and sixth terms are re-written) are

$$\text{error} = \frac{\Delta t - \Delta a}{2!}\frac{\partial^2 f}{\partial t^2}\bigg|_{t,a} + \frac{(\Delta t)^2 - (\Delta a)^2}{3!}\frac{\partial^3 f}{\partial t^3}\bigg|_{t,a} + \cdots + \frac{(\Delta t)^{n-1} - (\Delta a)^{n-1}}{n!}\frac{\partial^n f}{\partial t^n}\bigg|_{t,a} + \cdots$$
$$(4.15)$$

where induction is used to derive the nth-order term. By choosing $\Delta t = \Delta a$, all terms on the right-hand side of (4.12) cancel, proving that this finite difference scheme has no discretization error.

For $\Delta t = \Delta a$, the finite difference expression (4.7) simplifies to

$$f_{i+1}^j = f_i^{j-1}. \quad (4.16)$$

This difference equation is an analytical solution to the population balance model (4.6). Writing in terms of the original variables, this expression is

$$f(t_i + \Delta t, a) = f(t_i, a - \Delta t). \quad (4.17)$$

64

Applying this equation for $t_0 = 0$ and $i = 1$ gives

$$f(t_1, a) = f(t_0, a - t_1) = f_0(a - t_1), \tag{4.18}$$

which is

$$f(t, a) = f_0(a - t) \tag{4.19}$$

for $t = t_1$ – the exact analytical solution to (4.6). This expression is exact for any value of Δt. Writing the equation for $i = 2$ gives

$$f(t_2, a) = f(t_1, a - (t_2 - t_1)) = f(t_0, a - (t_2 - t_1) - t_1) = f_0(a - t_2), \tag{4.20}$$

which is the exact analytical expression (4.30) for $t = t_2$. Although the above numerical analysis treated all of the Δt to be equal, to simplify the analysis, we see that the numerical method gives the exact analytical solutions for nonuniform Δt, as long as Δa_i is set equal to Δt_i.

The above finite difference expression is very cheap, as it does not actually involve any floating point operations, e.g., plus, minus, multiplication, or division. Instead, the algorithm just shifts the elements in the vector whose elements are f_i^j by one position.

4.2.2   Case 2: Population Balance Models with Constant Growth Rate

Next let's analyze the homogeneous population balance model in which $G = g$ constant,

$$\frac{\partial f(t, a)}{\partial t} + g \frac{\partial f(t, a)}{\partial a} = 0, \quad f(0, a) = f_0(a), \tag{4.21}$$

over the real domains $t \geq 0$ and $a \geq 0$. This population balance model arises when the driving force for growth is constant. A common example is in crystallization where a is the crystal size and the supersaturation that appears in the growth rate is held constant by a feedback control system to provide high molecular purity while suppressing nucleation (e.g., see [3, 6, 19, 41, 54, 65–67] and citations therein).

The population balance model (4.21) can be transformed to be the same as the cell population balance model (4.6) by redefining the time coordinate as $\tilde{t} = gt$, in which case the same finite difference method results in zero discretization error. The below analysis avoids that transformation, so as to clearly show how the growth rate enters into the exact cancellation of discretization error and the numerical stability condition.

Applying the finite difference scheme yields

$$\frac{f_{i+1}^j - f_i^j}{\Delta t} + g\frac{f_i^j - f_i^{j-1}}{\Delta a} = 0. \tag{4.22}$$

Inserting the Taylor series for f in (4.10) and (4.11) into this equation gives the discretization error of

$$\text{error} = \frac{f_{i+1}^j - f_i^j}{\Delta t} + g\frac{f_i^j - f_i^{j-1}}{\Delta a}$$

$$= \left.\frac{\partial f}{\partial t}\right|_{t,a} + g\left.\frac{\partial f}{\partial a}\right|_{t,a} + \frac{\Delta t}{2}\left.\frac{\partial^2 f}{\partial t^2}\right|_{t,a} - \frac{g\Delta a}{2}\left.\frac{\partial^2 f}{\partial a^2}\right|_{t,a} + \frac{(\Delta t)^2}{3!}\left.\frac{\partial^3 f}{\partial t^3}\right|_{t,a} + \frac{g(\Delta a)^2}{3!}\left.\frac{\partial^3 f}{\partial a^3}\right|_{t,a}$$
$$+ \cdots + \frac{(\Delta t)^{n-1}}{n!}\left.\frac{\partial^n f}{\partial t^n}\right|_{t,a} + (-1)^{n-1}\frac{g(\Delta a)^{n-1}}{n!}\left.\frac{\partial^n f}{\partial a^n}\right|_{t,a} + \cdots \tag{4.23}$$

As before, the first two terms on the right-hand side sum to 0 according to (4.21). Furthermore, successive derivatives of (4.21) can be taken and rearranged to yield

$$g\frac{\partial^2 f}{\partial a^2} = \frac{1}{g}\frac{\partial^2 f}{\partial t^2} \tag{4.24}$$

$$g\frac{\partial^3 f}{\partial a^3} = -\frac{1}{g^2}\frac{\partial^3 f}{\partial t^3} \tag{4.25}$$

such that the remaining terms in (4.23) (if the fourth and sixth terms are rewritten) are

$$\text{error} = \frac{1}{2}\left(\Delta t - \frac{\Delta a}{g}\right)\left.\frac{\partial^2 f}{\partial t^2}\right|_{t,a} + \frac{1}{3!}\left((\Delta t)^2 - \frac{(\Delta a)^2}{g^2}\right)\left.\frac{\partial^3 f}{\partial t^3}\right|_{t,a} + \cdots + \frac{1}{n!}\left((\Delta t)^{n-1} - \frac{(\Delta a)^{n-1}}{g^{n-1}}\right)\left.\frac{\partial^n f}{\partial t^n}\right|_{t,a} + \cdots \tag{4.26}$$

where induction is used to derive the nth-order derivative. Choosing $\Delta a = g\Delta t$ results in the cancellation of the remaining terms on the right-hand side of (4.23), showing that the finite difference approximation results in no numerical discretization error.

The choice of $\Delta a = g\Delta t$ is exactly the Courant–Friedrichs–Lewy (CFL) necessary condition [5] for numerical stability of a finite difference method for the population balance model (4.21). The above analysis shows that the CFL condition not only provides numerical stability but also results in zero discretization error.

The above and subsequent analyses apply independent of the boundary conditions and so hold for any physically meaningful boundary conditions, e.g., for the birth of cells at $a = 0$.

For $\Delta a = g\Delta t$, the finite difference expression (4.22) simplifies to

$$f_{i+1}^{j} = f_i^{j-1} \tag{4.27}$$

This difference equation is an analytical solution to the population balance model (4.21). Writing in terms of the original variables, this expression is

$$f(t_i + \Delta t, a) = f(t_i, a - g\Delta t). \tag{4.28}$$

Applying this equation for $t_0 = 0$ and $i = 1$ gives

$$f(t_1, a) = f(t_0, a - gt_1) = f_0(a - gt_1), \tag{4.29}$$

which is

$$f(t, a) = f_0(a - gt) \tag{4.30}$$

for $t = t_1$ – the exact analytical solution to (4.6). This expression is exact for any value of Δt. Writing the equation for $i = 2$ gives

$$f(t_2, a) = f(t_1, a - g(t_2 - t_1)) = f(t_0, a - g(t_2 - t_1) - gt_1) = f_0(a - gt_2), \tag{4.31}$$

which is the exact analytical expression (4.30) for $t = t_2$. Although the above numerical analysis treated all of the Δt to be equal, to simplify the analysis, we see that the numerical method gives the exact analytical solutions for nonuniform Δt, as long as Δa_i is set equal to $g\Delta t_i$.

As above, the finite difference expression only requires a memory reallocation.

4.2.3 Case 3: Population Balance Models with Growth Rate $G(a)$

Next, let's analyze the homogeneous population balance in which $G = G(a)$ such that

$$\frac{\partial \hat{f}(t,a)}{\partial t} + \frac{\partial(G(a)\hat{f}(t,a))}{\partial a} = 0, \quad \hat{f}(0,a) = \hat{f}_0(a), \tag{4.32}$$

with $G(a)$ continuous in a and $G(a) > 0, \forall a$ (similar results can be derived for the case where $G(a) < 0, \forall a$ by a small change in the discretization scheme). The expression $G(a)$ models size-dependent growth, which has been heavily studied in the literature on precipitation and crystallization, e.g., see $[1, 2, 4, 22, 23]$ and citations therein. When a is the age of a growing cell, then $G(a) \neq 0$ models age-dependent growth.

The first step in the zero-error finite difference method for solving (4.32) is to multiply the population balance model (4.32) by $G(a)$ and define a new variable $f = G(a)\hat{f}(t,a)$, to give

$$\frac{\partial f(t,a)}{\partial t} + G(a)\frac{\partial f(t,a)}{\partial a} = 0, \quad f(0,a) = f_0(a). \tag{4.33}$$

The second step is to define a change in variables of

$$\tilde{a} = \int_0^a G(\hat{a})d\hat{a} \tag{4.34}$$

and

$$\tilde{f}(t,\tilde{a}) = f(t,a), \tag{4.35}$$

which results in the transformed population balance model

$$\frac{\partial \tilde{f}(t,\tilde{a})}{\partial t} + \frac{\partial \tilde{f}(t,\tilde{a})}{\partial \tilde{a}} = 0, \quad \tilde{f}(0,\tilde{a}) = \tilde{f}_0(\tilde{a}). \tag{4.36}$$

The PDE is just the cell population balance model, to which the numerical discretization can be applied to produce zero discretization error. For a growth rate that is always positive or always negative, (4.34) can be solved off-line and used afterwards to map the $\tilde{f}(t,\tilde{a})$ values, to calculate the values $f(t,a)$ with zero error. This method can also be applied to growth rates that can have any value, including zero, by (1) splitting the simulation into segments in which the value of $G(a)$ is positive, negative, or zero in each segment, (2) applying the finite

difference method to each segment, and (3) subsequently summing the resulting solutions.

The below analysis directly applies the finite difference discretization to (4.33), which shows that the method has a graceful increase in numerical error when applied without first applying the suggested change of variables.

Applying the aforementioned finite difference scheme results in

$$\frac{f_{i+1}^j - f_i^j}{\Delta t_i} + G(a_j)\frac{f_i^j - f_i^{j-1}}{\Delta a_j} = 0. \tag{4.37}$$

The Taylor series expansions for f in terms of t and a, respectively, are

$$f(t_i+\Delta t_i, a_j) = f(t_i, a_j)+\Delta t_i \left.\frac{\partial f}{\partial t}\right|_{t_i,a_j} +\frac{(\Delta t_i)^2}{2!}\left.\frac{\partial^2 f}{\partial t^2}\right|_{t_i,a_j} +\frac{(\Delta t_i)^3}{3!}\left.\frac{\partial^3 f}{\partial t^3}\right|_{t_i,a_j} +\cdots+\frac{(\Delta t_i)^n}{n!}\left.\frac{\partial^n f}{\partial t^n}\right|_{t_i,a_j} +\cdots \tag{4.38}$$

$$f(t_i, a_j-\Delta a_j) = f(t_i, a_j)-\Delta a_j \left.\frac{\partial f}{\partial a}\right|_{t_i,a_j} +\frac{(\Delta a_j)^2}{2!}\left.\frac{\partial^2 f}{\partial a^2}\right|_{t_i,a_j} -\frac{(\Delta a_j)^3}{3!}\left.\frac{\partial^3 f}{\partial a^3}\right|_{t_i,a_j} +\cdots+(-1)^n\frac{(\Delta a_j)^n}{n!}\left.\frac{\partial^n f}{\partial a^n}\right|_{t_i,a_j} +\cdots \tag{4.39}$$

Insertion of these expansions into (4.37) results in a discretization error of

$$\text{error} = \frac{f_{i+1}^j - f_i^j}{\Delta t_i} + G(a_j)\frac{f_i^j - f_i^{j-1}}{\Delta a_j}$$

$$= \left.\frac{\partial f}{\partial t}\right|_{t_i,a_j} + G(a_j)\left.\frac{\partial f}{\partial a}\right|_{t_i,a_j} + \frac{\Delta t_i}{2!}\left.\frac{\partial^2 f}{\partial t^2}\right|_{t_i,a_j} - G(a_j)\frac{\Delta a_j}{2!}\left.\frac{\partial^2 f}{\partial a^2}\right|_{t_i,a_j} + \frac{(\Delta t_i)^2}{3!}\left.\frac{\partial^3 f}{\partial t^3}\right|_{t_i,a_j}$$

$$+ G(a_j)\frac{(\Delta a_j)^2}{3!}\left.\frac{\partial^3 f}{\partial a^3}\right|_{t_i,a_j} + \cdots + \frac{(\Delta t_i)^{n-1}}{n!}\left.\frac{\partial^n f}{\partial t^n}\right|_{t_i,a_j} + (-1)^{n-1}\frac{(\Delta a_j)^{n-1}}{n!}\left.\frac{\partial^n f}{\partial a^n}\right|_{t_i,a_j} + \cdots \tag{4.40}$$

The sum of the first two terms on the right-hand side is zero due to (4.33). Taking successive derivatives of (4.33) gives

$$\frac{\partial^2 f}{\partial t^2} = -G(a)\frac{\partial^2 f}{\partial t \partial a}, \tag{4.41}$$

$$G(a)\frac{\partial^2 f}{\partial a^2} = -\frac{\partial^2 f}{\partial t \partial a} - \frac{dG}{da}\frac{\partial f}{\partial a}, \tag{4.42}$$

$$\frac{\partial^3 f}{\partial t^3} = -G(a)\frac{\partial^3 f}{\partial t^2 \partial a}, \tag{4.43}$$

69

and

$$G(a)\frac{\partial^3 f}{\partial a^3} = -\frac{\partial^3 f}{\partial t \partial a^2} - \frac{d^2 G}{da^2}\frac{\partial f}{\partial a} - 2\frac{dG}{da}\frac{\partial^2 f}{\partial a^2}. \qquad (4.44)$$

Insertion of these expressions into (4.40), and applying induction for the nth-order derivatives gives

$$
\begin{aligned}
\text{error} = &-G(a_j)\frac{\Delta t_i}{2!}\frac{\partial^2 f}{\partial t \partial a}\bigg|_{t_i,a_j} + \frac{\Delta a_j}{2!}\left[\frac{\partial^2 f}{\partial t \partial a} + \frac{dG}{da}\frac{\partial f}{\partial a}\right]_{t_i,a_j} \\
&-G(a_j)\frac{(\Delta t_i)^2}{3!}\frac{\partial^3 f}{\partial t^2 \partial a}\bigg|_{t_i,a_j} - \frac{(\Delta a_j)^2}{3!}\left[\frac{\partial^3 f}{\partial t \partial a^2} + \frac{d^2 G}{da^2}\frac{\partial f}{\partial a} + 2\frac{dG}{da}\frac{\partial^2 f}{\partial a^2}\right]_{t_i,a_j} + \cdots \\
&-G(a_j)\frac{(\Delta t_i)^{n-1}}{n!}\frac{\partial^n f}{\partial t^{n-1} \partial a}\bigg|_{t_i,a_j} + (-1)^n\frac{(\Delta a_j)^{n-1}}{n!}\left[\frac{\partial^n f}{\partial t \partial a^{n-1}} + \sum_{k=1}^{n-1}c_k^n\frac{d^k G}{da^k}\frac{\partial^{n-k} f}{\partial a^{n-k}}\right]_{t_i,a_j} + \cdots
\end{aligned}
$$
$$(4.45)$$

where the binomial coefficient c_k^n is given by

$$c_k^n = \frac{(n-1)!}{(n-k-1)!k!}, \quad \forall k = 1, 2, \ldots, n-1. \qquad (4.46)$$

Choosing $\Delta a_j = G(a_j)\Delta t_i$ results in the expression

$$
\begin{aligned}
\text{error} = &\, G(a_j)\frac{\Delta t_i}{2!}\left[\frac{dG}{da}\frac{\partial f}{\partial a}\right]_{t_i,a_j} - G^2(a_j)\frac{(\Delta t_i)^2}{3!}\left[\frac{1}{G(a_j)}\frac{\partial^3 f}{\partial t^2 \partial a} + \frac{\partial^3 f}{\partial t \partial a^2} + \frac{d^2 G}{da^2}\frac{\partial f}{\partial a} + 2\frac{dG}{da}\frac{\partial^2 f}{\partial a^2}\right]_{t_i,a_j} + \cdots \\
&- G^{n-1}(a_j)\frac{(\Delta t_i)^{n-1}}{n!}\left[\frac{1}{G^{n-2}(a_j)}\frac{\partial^n f}{\partial t^{n-1} \partial a} + (-1)^{n-1}\left(\frac{\partial^n f}{\partial t \partial a^{n-1}} + \sum_{k=1}^{n-1}c_k^n\frac{d^k G}{da^k}\frac{\partial^{n-k} f}{da^{n-k}}\right)\right]_{t_i,a_j} + \cdots
\end{aligned}
$$
$$(4.47)$$

Taking the partial derivative of (4.42) with respect to t gives

$$G(a)\frac{\partial^3 f}{\partial t \partial a^2} = -\frac{\partial^3 f}{\partial t^2 \partial a} - \frac{dG}{da}\frac{\partial^2 f}{\partial t \partial a}, \qquad (4.48)$$

which can be rearranged to

$$\frac{1}{G(a)}\frac{\partial^3 f}{\partial t^2 \partial a} + \frac{\partial^3 f}{\partial t \partial a^2} = -\frac{1}{G(a)}\frac{dG}{da}\frac{\partial^2 f}{\partial t \partial a}. \qquad (4.49)$$

Insertion of this expression into the error (4.47) results in

$$
\text{error} = G(a_j) \frac{\Delta t_i}{2!} \left[\frac{dG}{da} \frac{\partial f}{\partial a} \right]_{t_i, a_j} - G^2(a_j) \frac{(\Delta t_i)^2}{3!} \left[-\frac{1}{G} \frac{dG}{da} \frac{\partial^2 f}{\partial t \partial a} + \frac{d^2 G}{da^2} \frac{\partial f}{\partial a} + 2 \frac{dG}{da} \frac{\partial^2 f}{\partial a^2} \right]_{t_i, a_j} + \cdots
$$

$$
- G^{n-1}(a_j) \frac{(\Delta t_i)^{n-1}}{n!} \left[\frac{1}{G^{n-2}(a_j)} \frac{\partial^n f}{\partial t^{n-1} \partial a} + (-1)^{n-1} \left(\frac{\partial^n f}{\partial t \partial a^{n-1}} + \sum_{k=1}^{n-1} c_k^n \frac{d^k G}{da^k} \frac{\partial^{n-k} f}{da^{n-k}} \right) \right]_{t_i, a_j} + \cdots
$$

$$
\tag{4.50}
$$

The overall discretization error is first order when the growth rate varies with a, with the first-order term being proportional to dG/da. Consistent with the zero error observed for constant G in Case 2, the second-order term is equal to zero for $d^n G/da^n = 0$. We know from the error analysis for Case 2 that all of the higher order terms are also equal to zero for $d^n G/da^n = 0$.

The above error expression shows that the discretization error continuously transitions from first-order accurate to zero error as $d^n G/da^n$ decreases. As the change in growth rate with respect to a approaches zero, the discretization error approaches zero, which motivates the use of the aforementioned finite difference approach for the population balance model (4.33) for Case 3 as long as the growth rate has a weak dependancy on a.

The choice of $\Delta a_j = G(a_j) \Delta t_i$ is exactly the Courant–Friedrichs–Lewy (CFL) necessary condition [5] for numerical stability of a finite difference method for the population balance model (4.33) evaluated for the current value of $a = a_j$ whenever the discretization formula (4.37) is applied. This above analysis shows that the CFL condition not only provides numerical stability but also, when applied in the right way, discretization error that approaches zero as $d^n G/da^n$ approaches zero.

The above and subsequent analyses apply independent of the boundary conditions and so hold for any physically meaningful boundary conditions, e.g., for the nucleation of crystals at some small size.

For the choice $\Delta a_j = G(a_j) \Delta t_i$, the finite difference expression (4.37) simplifies to

$$
f_{i+1}^j = f_i^{j-1}. \tag{4.51}
$$

As above, the finite difference expression only requires a memory reallocation.

4.2.4 Case 4: Population Balance Models with Time-Varying Growth Rate $G(t)$

Next, let's analyze the homogeneous population balance model with time-varying growth rate,

$$\frac{\partial f(t,a)}{\partial t} + \frac{\partial (G(t)f(t,a))}{\partial a} = 0, \quad f(0,a) = f_0(a). \tag{4.52}$$

The growth rate can be pulled outside of the partial derivative with respect to a, to give

$$\frac{\partial f(t,a)}{\partial t} + G(t)\frac{\partial f(t,a)}{\partial a} = 0, \quad f(0,a) = f_0(a) \tag{4.53}$$

over the real domains $t \geq 0$ and $a \geq 0$ with $G(t)$ continuous in t and $G(t) > 0, \forall t$. This population balance model is applicable to populations of varying driving force, e.g., growing crystals or precipitants under conditions of varying supersaturation [52], or growing cells in bioreactors with varying nutrients or substrate concentrations [51, 70].

The first step of the finite difference method is to define

$$\tilde{t} = \int_0^t G(\hat{t})d\hat{t} \tag{4.54}$$

and

$$\tilde{f}(\tilde{t},a) = f(t,a) \tag{4.55}$$

and use a change in variables to derive the transformed population balance model

$$\frac{\partial \tilde{f}(\tilde{t},a)}{\partial \tilde{t}} + \frac{\partial \tilde{f}(\tilde{t},a)}{\partial a} = 0, \quad \tilde{f}(0,a) = \tilde{f}_0(a), \tag{4.56}$$

which is just the cell population balance model to which the numerical discretization can be applied to produce zero discretization error. For a growth rate that is always positive or always negative, (4.54) can be solved off-line and used afterwards to map the $\tilde{f}(\tilde{t},a)$ values, to the calculate the values $f(t,a)$ with zero error. This method can also be applied to growth

rates that can have any value, including zero, by (1) splitting the simulation into segments in which the value of $G(t)$ is positive, negative, or zero in each segment, (2) applying the finite difference method to each segment, and (3) subsequently summing the resulting solutions.

The below analysis directly applies the finite difference discretization to (4.53) to show that numerical error behaves benignly when the growth rate is time varying.

Applying the finite difference scheme yields

$$\frac{f_{i+1}^j - f_i^j}{\Delta t_i} + G(t_i)\frac{f_i^j - f_i^{j-1}}{\Delta a_j} = 0. \tag{4.57}$$

The function f can be expanded with Taylor series in t and a to give

$$f(t_i+\Delta t_i, a_j) = f(t_i, a_j)+\Delta t_i\left.\frac{\partial f}{\partial t}\right|_{t_i,a_j}+\frac{(\Delta t_i)^2}{2!}\left.\frac{\partial^2 f}{\partial t^2}\right|_{t_i,a_j}+\frac{(\Delta t_i)^3}{3!}\left.\frac{\partial^3 f}{\partial t^3}\right|_{t_i,a_j}+\cdots+\frac{(\Delta t_i)^n}{n!}\left.\frac{\partial^n f}{\partial t^n}\right|_{t_i,a_j}+\cdots \tag{4.58}$$

$$f(t_i, a_j-\Delta a_j) = f(t_i, a_j)-\Delta a_j\left.\frac{\partial f}{\partial a}\right|_{t_i,a_j}+\frac{(\Delta a_j)^2}{2!}\left.\frac{\partial^2 f}{\partial a^2}\right|_{t_i,a_j}-\frac{(\Delta a_j)^3}{3!}\left.\frac{\partial^3 f}{\partial a^3}\right|_{t_i,a_j}+\cdots+(-1)^{n-1}\frac{(\Delta a_j)^n}{n!}\left.\frac{\partial^n f}{\partial a^n}\right|_{t_i,a_j}+\cdots \tag{4.59}$$

Insertion of these expansions into (4.57) yields

$$\text{error} = \frac{f_{i+1}^j - f_i^j}{\Delta t_i} + G(t_i)\frac{f_i^j - f_i^{j-1}}{\Delta a_j}$$

$$= \left.\frac{\partial f}{\partial t}\right|_{t_i,a_j} + G(t_i)\left.\frac{\partial f}{\partial a}\right|_{t_i,a_j} + \frac{\Delta t_i}{2!}\left.\frac{\partial^2 f}{\partial t^2}\right|_{t_i,a_j} - G(t_i)\frac{\Delta a_j}{2!}\left.\frac{\partial^2 f}{\partial a^2}\right|_{t_i,a_j} + \frac{(\Delta t_i)^2}{3!}\left.\frac{\partial^3 f}{\partial t^3}\right|_{t_i,a_j}$$

$$+ G(t_i)\frac{(\Delta a_j)^2}{3!}\left.\frac{\partial^3 f}{\partial a^3}\right|_{t_i,a_j} + \cdots + \frac{(\Delta t_i)^{n-1}}{n!}\left.\frac{\partial^n f}{\partial t^n}\right|_{t_i,a_j} + (-1)^{n-1}G(t_i)\frac{(\Delta a_j)^{n-1}}{n!}\left.\frac{\partial^n f}{\partial a^n}\right|_{t_i,a_j} + \cdots \tag{4.60}$$

The first two terms on the right-hand side sum to zero according to (4.53), and taking successive derivatives of (4.53) and rearranging results in the expressions,

$$\frac{\partial^2 f}{\partial t^2} = -\frac{dG}{dt}\frac{\partial f}{\partial a} - G(t)\frac{\partial^2 f}{\partial t\partial a}, \tag{4.61}$$

$$G(t)\frac{\partial^2 f}{\partial a^2} = -\frac{\partial^2 f}{\partial t \partial a}, \tag{4.62}$$

$$\frac{\partial^3 f}{\partial t^3} = -\frac{d^2 G}{dt^2}\frac{\partial f}{\partial a} - 2\frac{dG}{dt}\frac{\partial^2 f}{\partial t \partial a} - G(t)\frac{\partial^3 f}{\partial t^2 \partial a}, \tag{4.63}$$

and

$$G(t)\frac{\partial^3 f}{\partial a^3} = -\frac{\partial^3 f}{\partial t \partial a^2}. \tag{4.64}$$

Substituting these expressions into (4.60) results in

$$
\begin{aligned}
\text{error} = &-\frac{\Delta t_i}{2!}\left[\frac{dG}{dt}\frac{\partial f}{\partial a} + G(t)\frac{\partial^2 f}{\partial t \partial a}\right]_{t_i,a_j} + \frac{\Delta a_j}{2!}\frac{\partial^2 f}{\partial t \partial a}\bigg|_{t_i,a_j} \\
&-\frac{(\Delta t_j)^2}{3!}\left[\frac{d^2 G}{dt^2}\frac{\partial f}{\partial a} + 2\frac{dG}{dt}\frac{\partial^2 f}{\partial t \partial a} + G(t)\frac{\partial^3 f}{\partial t^2 \partial a}\right]_{t_i,a_j} - \frac{(\Delta a_j)^2}{3!}\frac{\partial^3 f}{\partial t \partial a^2}\bigg|_{t_i,a_j} + \cdots \\
&-\frac{(\Delta t_i)^{n-1}}{n!}\left[\sum_{k=0}^{n-1} c_k^n \frac{d^k G(t)}{dt^k}\frac{\partial^{n-k} f}{\partial t^{n-1-k}\partial a}\right]_{t_i,a_j} + (-1)^{n-1}\frac{(\Delta a_j)^{n-1}}{n!}\frac{\partial^n f}{\partial t \partial a^{n-1}}\bigg|_{t_i,a_j} + \cdots \quad (4.65)
\end{aligned}
$$

where c_k^n is the binomial coefficient

$$c_k^n = \frac{(n-1)!}{(n-k-1)!k!}, \quad \forall k = 0,1,2,\ldots,n-1. \tag{4.66}$$

Choosing $\Delta a_j = G(t_i)\Delta t_i$ and some rearrangement results in

$$
\begin{aligned}
\text{error} = &-\frac{\Delta t_i}{2!}\left[\frac{dG}{dt}\frac{\partial f}{\partial a}\right]_{t_i,a_j} - \frac{(\Delta t_i)^2}{3!}\left[\frac{d^2 G}{dt^2}\frac{\partial f}{\partial a} + 2\frac{dG}{dt}\frac{\partial^2 f}{\partial t \partial a} + G(t)\frac{\partial^3 f}{\partial t^2 \partial a} + G^2(t)\frac{\partial^3 f}{\partial t \partial a^2}\right]_{t_i,a_j} \\
&+\cdots - \frac{(\Delta t_i)^{n-1}}{n!}\left[\left(\sum_{k=0}^{n-1} c_k^n \frac{d^k G}{dt^k}\frac{\partial^{n-k} f}{\partial t^{n-1-k}\partial a}\right) + (-1)^{n-1}G^{n-1}(t)\frac{\partial^n f}{\partial t \partial a^{n-1}}\right]_{t_i,a_j} + \cdots \quad (4.67)
\end{aligned}
$$

which shows that the numerical discretization error is first order in Δt_i and approaches zero error as $G(t)$ approaches a constant value.

Taking the partial derivative of (4.61) with respect to a gives

$$\frac{\partial^3 f}{\partial t^2 \partial a} = -\frac{dG}{dt}\frac{\partial f}{\partial a^2} - G(t)\frac{\partial^2 f}{\partial t \partial a^2}. \tag{4.68}$$

Multiplying by $G(t)$ gives

$$G(t)\frac{\partial^3 f}{\partial t^2 \partial a} = -G(t)\frac{dG}{dt}\frac{\partial f}{\partial a^2} - G^2(t)\frac{\partial^2 f}{\partial t \partial a^2}, \tag{4.69}$$

which can be inserted into the error (4.67) to give

$$\text{error} = -\frac{\Delta t_i}{2!}\left[\frac{dG}{dt}\frac{\partial f}{\partial a}\right]_{t_i,a_j} - \frac{(\Delta t_i)^2}{3!}\left[\frac{d^2G}{dt^2}\frac{\partial f}{\partial a} + 2\frac{dG}{dt}\frac{\partial^2 f}{\partial t \partial a} - G(t)\frac{dG}{dt}\frac{\partial f}{\partial a^2}\right]_{t_i,a_j} + \cdots$$
$$- \frac{(\Delta t_i)^{n-1}}{n!}\left[\left(\sum_{k=0}^{n-1} c_k^n \frac{d^k G}{dt^k}\frac{\partial^{n-k} f}{\partial t^{n-1-k}\partial a}\right) + (-1)^{n-1}G^{n-1}(t)\frac{\partial^n f}{\partial t \partial a^{n-1}}\right]_{t_i,a_j} + \cdots \tag{4.70}$$

The overall discretization error is first order when the growth rate varies with t, with the first-order term being proportional to dG/dt. Consistent with the zero error observed for constant G in Case 2, the second-order term is equal to zero for $d^n G/dt^n = 0$. We know from the error analysis for Case 2 that all of the higher order terms are also equal to zero for $d^n G/dt^n = 0$.

The above error expression shows that the discretization error continuously transitions from first-order accurate to zero error as $d^n G/dt^n$ decreases. As the growth rate with respect to a approaches zero, the discretization error approaches zero, which motivates the use of the aforementioned finite difference approach for the population balance model (4.53) for Case 4 as long as the growth rate has a weak dependency on t.

The choice of $\Delta a_j = G(t_i)\Delta t_i$ is exactly the CFL necessary condition [5] for numerical stability of a finite difference method for the population balance model (4.53) evaluated for the current value of $t = t_i$ whenever the discretization formula (4.57) is applied. This above analysis shows that the CFL condition not only provides numerical stability but also, when applied in the right way, discretization error that approaches zero as $d^n G/dt^n$ approaches zero.

The finite difference expression is the same as in Cases 1 to 3.

4.2.5 Case 5: Population Balance Models with Separable Time- and Size-dependent Growth Rate

This section shows how zero discretization error is achieved for the population balance model

$$\frac{\partial f(t,a)}{\partial t} + \frac{\partial (G_t(t)G_a(a)f(t,a))}{\partial a} = 0, \quad f(0,a) = f_0(a). \tag{4.71}$$

in which the growth rate is separable. Nearly all growth rates reported in the literature have this form, in which the growth rates $G(t,a)$ can be written as the product of time- and size-dependent algebraic functions [20].

The first step in the finite difference method is pull the $G_t(t)$ outside of the partial derivative with respect to a, define

$$\tilde{t} = \int_0^t G_t(\hat{t})d\hat{t} \tag{4.72}$$

and

$$\tilde{f}(\tilde{t}, a) = f(t,a), \tag{4.73}$$

and use a change in variables to derive the transformed population balance model

$$\frac{\partial \tilde{f}(\tilde{t},a)}{\partial \tilde{t}} + \frac{\partial (G_a(a)\tilde{f}(\tilde{t},a))}{\partial a} = 0, \quad \tilde{f}(0,a) = \tilde{f}_0(a). \tag{4.74}$$

The next step is to multiply the equations by $G_a(a)$ to give

$$G_a(a)\frac{\partial \tilde{f}(\tilde{t},a)}{\partial \tilde{t}} + G_a(a)\frac{\partial (G_a(a)\tilde{f}(\tilde{t},a))}{\partial a} = 0, \quad G_a(a)\tilde{f}(0,a) = G_a(a)\tilde{f}_0(a). \tag{4.75}$$

Define a new variable

$$\hat{f}(\tilde{t}, a) = G_a(a)\tilde{f}(\tilde{t}, a)) \tag{4.76}$$

and pull the $G_a(a)$ into the partial with respect to $\tilde{t}$ in the first term of the PDE to give

$$\frac{\partial \hat{f}(\tilde{t},a)}{\partial \tilde{t}} + G_a(a)\frac{\partial (\hat{f}(\tilde{t},a))}{\partial a} = 0, \quad \hat{f}(0,a) = \hat{f}_0(a). \tag{4.77}$$

The next step is to define the change in variables

$$\tilde{a} = \int_0^a G_a(\hat{a})d\hat{a} \tag{4.78}$$

and

$$\bar{f}(\tilde{t}, \tilde{a}) = \hat{f}(\tilde{t}, a), \tag{4.79}$$

which results in the transformed population balance model

$$\frac{\partial \bar{f}(\tilde{t}, \tilde{a})}{\partial t} + \frac{\partial \bar{f}(\tilde{t}, \tilde{a})}{\partial \tilde{a}} = 0, \quad \bar{f}(0, \tilde{a}) = \bar{f}_0(\tilde{a}). \tag{4.80}$$

The PDE is just the cell population balance model, to which the numerical discretization method can be applied to produce zero discretization error. For a growth rate that is always positive or always negative, (4.34) can be solved off-line and used afterwards to map the $\tilde{f}(t, \tilde{a})$ values, to calculate the values $f(t, a)$ with zero error. This method can also be applied to growth rates that can have any value, including zero, by (1) splitting the simulation into segments in which the value of $G_a(a)$ and $G_t(a)$ are positive, negative, or zero in each segment, (2) applying the finite difference method to each segment, and (3) subsequently summing the resulting solutions.

The numerical analysis for the situation in which the numerical discretization is directly applied intermediate transformed population balance models is not derived here, as the results would look like the concatenation of the results of the previous two sections.

The finite difference expression is the same as in Cases 1 to 4.

4.2.6 Case 6: Nonhomogeneous Population Balance Models with Constant Growth

This section considers the effect of including nonhomogeneous terms within the population balance model. To simplify the analysis while still being able to make all of the main points, consider the case of constant growth,

$$\frac{\partial f(t, a)}{\partial t} + g\frac{\partial f(t, a)}{\partial a} = h(t, a), \quad f(0, a) = f_0(a). \tag{4.81}$$

Let's first analyze the case in which h is a constant,

$$\frac{\partial f}{\partial t} + g\frac{\partial f}{\partial a} = h. \tag{4.82}$$

Applying the numerical discretization yields

$$\frac{f_{i+1}^j - f_i^j}{\Delta t_i} + g\frac{f_i^j - f_i^{j-1}}{\Delta a_j} = h. \tag{4.83}$$

Substituting the Taylor series expansions of f,

$$f(t_i+\Delta t_i, a_j) = f(t_i, a_j)+\Delta t_i \left.\frac{\partial f}{\partial t}\right|_{t_i,a_j} + \frac{(\Delta t_i)^2}{2!}\left.\frac{\partial^2 f}{\partial t^2}\right|_{t_i,a_j} + \frac{(\Delta t_i)^3}{3!}\left.\frac{\partial^3 f}{\partial t^3}\right|_{t_i,a_j} + \cdots + \frac{(\Delta t_i)^n}{n!}\left.\frac{\partial^n f}{\partial t^n}\right|_{t_i,a_j} + \cdots \tag{4.84}$$

and

$$f(t_i, a_j-\Delta a_j) = f(t_i, a_j)-\Delta a_j \left.\frac{\partial f}{\partial a}\right|_{t_i,a_j} + \frac{(\Delta a_j)^2}{2!}\left.\frac{\partial^2 f}{\partial a^2}\right|_{t_i,a_j} - \frac{(\Delta a_j)^3}{3!}\left.\frac{\partial^3 f}{\partial a^3}\right|_{t_i,a_j} + \cdots + (-1)^n\frac{(\Delta a_j)^n}{n!}\left.\frac{\partial^n f}{\partial a^n}\right|_{t_i,a_j} + \cdots \tag{4.85}$$

into (4.83) gives

$$\text{error} = -h + \frac{f_{i+1}^j - f_i^j}{\Delta t_i} + g\frac{f_i^j - f_i^{j-1}}{\Delta a_j}$$

$$= -h + \left.\frac{\partial f}{\partial t}\right|_{t_i,a_j} + g\left.\frac{\partial f}{\partial a}\right|_{t_i,a_j} + \frac{\Delta t_i}{2!}\left.\frac{\partial^2 f}{\partial t^2}\right|_{t_i,a_j} - g\frac{\Delta a_j}{2!}\left.\frac{\partial^2 f}{\partial a^2}\right|_{t_i,a_j} + \frac{(\Delta t_i)^2}{3!}\left.\frac{\partial^3 f}{\partial t^3}\right|_{t_i,a_j}$$

$$+ g\frac{(\Delta a_j)^2}{3!}\left.\frac{\partial^3 f}{\partial a^3}\right|_{t_i,a_j} + \cdots + \frac{(\Delta t_i)^{n-1}}{n!}\left.\frac{\partial^n f}{\partial t^n}\right|_{t_i,a_j} + (-1)^{n-1}g\frac{(\Delta a_j)^{n-1}}{n!}\left.\frac{\partial^n f}{\partial a^n}\right|_{t_i,a_j}. \tag{4.86}$$

Equation (4.82) implies that the sum of the first three terms on the right-hand side is zero, and taking successive derivatives of (4.82) yields

$$\frac{\partial^2 f}{\partial t^2} + g\frac{\partial^2 f}{\partial a\partial t} = 0 \text{ and } \frac{\partial^2 f}{\partial t\partial a} + g\frac{\partial^2 f}{\partial a^2} = 0 \longrightarrow \frac{\partial^2 f}{\partial t^2} - g^2\frac{\partial^2 f}{\partial a^2} = 0 \longrightarrow \boxed{g\frac{\partial^2 f}{\partial a^2} = \frac{1}{g}\frac{\partial^2 f}{\partial t^2}}$$

$$\longrightarrow g\frac{\partial^3 f}{\partial a^3} = \frac{1}{g}\frac{\partial^3 f}{\partial a\partial t^2} \tag{4.87}$$

$$\frac{\partial^2 f}{\partial t^2} + g\frac{\partial^2 f}{\partial a \partial t} = 0 \quad \longrightarrow \quad \frac{\partial^3 f}{\partial t^3} + g\frac{\partial^3 f}{\partial a \partial t^2} = 0 \quad \longrightarrow \quad \frac{\partial^3 f}{\partial a \partial t^2} = -\frac{1}{g}\frac{\partial^3 f}{\partial t^3} \tag{4.88}$$

Insertion of the rightmost equation in (4.88) into (4.87) gives

$$\boxed{g\frac{\partial^3 f}{\partial a^3} = -\frac{1}{g^2}\frac{\partial^3 f}{\partial t^3}}. \tag{4.89}$$

Substituting the boxed equations and their generalization derived by induction into (4.86) gives

$$\text{error} = \frac{1}{2!}\left(\Delta t_i - \frac{\Delta a_j}{g}\right)\frac{\partial^2 f}{\partial t^2}\bigg|_{t_i,a_j} + \frac{1}{3!}\left((\Delta t_i)^2 - \left(\frac{\Delta a_j}{g}\right)^2\right)\frac{\partial^3 f}{\partial t^3}\bigg|_{t_i,a_j}$$
$$+ \cdots + \frac{1}{n!}\left((\Delta t_i)^{n-1} - \left(\frac{\Delta a_j}{g}\right)^{n-1}\right)\frac{\partial^n f}{\partial t^n}\bigg|_{t_i,a_j} + \cdots \tag{4.90}$$

Choosing $\Delta a_j = g\Delta t_i$ allows the cancellation of the remaining terms on the right-hand side, showing that the finite difference method results in no numerical discretization error.

Now let's consider the case where $h = h(a)$ such that the population balance model (4.81) can be written as

$$\frac{\partial f}{\partial t} + g\frac{\partial f}{\partial a} = h(a). \tag{4.91}$$

Applying the numerical discretization scheme results in

$$\frac{f_{i+1}^j - f_i^j}{\Delta t_i} + g\frac{f_i^j - f_i^{j-1}}{\Delta a_j} = h(a_j) \tag{4.92}$$

Substituting the Taylor expansions for f in (4.84) and (4.85) into the finite difference approximation yields

$$\text{error} = -h(a_j) + \frac{f_{i+1}^j - f_i^j}{\Delta t_i} + g\frac{f_i^j - f_i^{j-1}}{\Delta a_j}$$

$$= -h(a_j) + \frac{\partial f}{\partial t}\bigg|_{t_i,a_j} + g\frac{\partial f}{\partial a}\bigg|_{t_i,a_j} + \frac{\Delta t_i}{2!}\frac{\partial^2 f}{\partial t^2}\bigg|_{t_i,a_j} - g\frac{\Delta a_j}{2!}\frac{\partial^2 f}{\partial a^2}\bigg|_{t_i,a_j} + \frac{(\Delta t_i)^2}{3!}\frac{\partial^3 f}{\partial t^3}\bigg|_{t_i,a_j}$$
$$+ g\frac{(\Delta a_j)^2}{3!}\frac{\partial^3 f}{\partial a^3}\bigg|_{t_i,a_j} + \cdots + \frac{(\Delta t_i)^{n-1}}{n!}\frac{\partial^n f}{\partial t^n}\bigg|_{t_i,a_j} + (-1)^{n-1}g\frac{(\Delta a_j)^{n-1}}{n!}\frac{\partial^n f}{\partial a^n}\bigg|_{t_i,a_j} + \cdots \tag{4.93}$$

Equation (4.91) implies that the first three terms sum to zero, and taking successive derivatives of (4.91) yields

$$\frac{\partial^2 f}{\partial t^2} + g\frac{\partial^2 f}{\partial a \partial t} = 0 \text{ and } \frac{\partial^2 f}{\partial t \partial a} + g\frac{\partial^2 f}{\partial a^2} = \frac{dh}{da} \longrightarrow \frac{\partial^2 f}{\partial t^2} - g^2\frac{\partial^2 f}{\partial a^2} + g\frac{dh}{da} = 0 \longrightarrow \boxed{g\frac{\partial^2 f}{\partial a^2} = \frac{1}{g}\frac{\partial^2 f}{\partial t^2} + \frac{dh}{da}}$$

$$\longrightarrow \quad g\frac{\partial^3 f}{\partial a^3} = \frac{1}{g}\frac{\partial^3 f}{\partial a \partial t^2} + \frac{d^2 h}{da^2} \tag{4.94}$$

$$\frac{\partial^2 f}{\partial t^2} + g\frac{\partial^2 f}{\partial a \partial t} = 0 \longrightarrow \frac{\partial^3 f}{\partial t^3} + g\frac{\partial^3 f}{\partial a \partial t^2} = 0 \longrightarrow \frac{\partial^3 f}{\partial a \partial t^2} = -\frac{1}{g}\frac{\partial^3 f}{\partial t^3} \tag{4.95}$$

Insertion of the rightmost equation in (4.95) into (4.94) gives

$$\boxed{g\frac{\partial^3 f}{\partial a^3} = -\frac{1}{g^2}\frac{\partial^3 f}{\partial t^3} + \frac{d^2 h}{da^2}}. \tag{4.96}$$

The expression for the error (4.93) can be simplified by using the boxed equations to give

$$\text{error} = \frac{1}{2!}\left(\Delta t_i - \frac{\Delta a_j}{g}\right)\frac{\partial^2 f}{\partial t^2}\bigg|_{t_i,a_j} - \frac{\Delta a_j}{2!}\frac{dh}{da}\bigg|_{a_j} + \frac{1}{3!}\left((\Delta t_i)^2 - \left(\frac{\Delta a_j}{g}\right)^2\right)\frac{\partial^3 f}{\partial t^3}\bigg|_{t_i,a_j}$$
$$+ \frac{(\Delta a_j)^2}{3!}\frac{d^2 h}{da^2}\bigg|_{a_j} + \cdots + \frac{1}{n!}\left((\Delta t_i)^{n-1} - \left(\frac{\Delta a_j}{g}\right)^{n-1}\right)\frac{\partial^n f}{\partial t^n}\bigg|_{t_i,a_j} + (-1)^n\frac{(\Delta a_j)^{n-1}}{n!}\frac{d^{n-1} h}{da^{n-1}}\bigg|_{a_j} + \cdots$$
$$\tag{4.97}$$

Choosing $\Delta a_j = g\Delta t_i$ cancels of all of the terms on the right-hand side that involve derivatives of f, to give

$$\text{error} = -\frac{\Delta a_j}{2!}\frac{dh}{da}\bigg|_{a_j} + \frac{(\Delta a_j)^2}{3!}\frac{d^2 h}{da^2}\bigg|_{a_j} + \cdots + (-1)^n\frac{(\Delta a_j)^{n-1}}{n!}\frac{d^{n-1} h}{da^{n-1}}\bigg|_{a_j} + \cdots \tag{4.98}$$

The remaining terms depend on successively higher order derivatives of $h(a)$. While the error is strictly first-order accurate in Δa_j, the error approaches zero as the dependancy of the nonhomogeneous term h on age becomes weaker. The coefficients converge to zero faster at higher orders as the nonhomogeneous term becomes smoother. In applications, the nonhomogeneous term is typically a smooth function of a, and the higher order terms would become zero. For example, consider the case in which $h(a)$ has a mild quadratic curvature,

e.g., $h(a) = 1 + 0.1a + 0.01a^2$. Then $[dh/dt|_{a_j} = 0.1 + 0.02a_j$, $d^2h/dt^2 = 0.01$, and $d^n h/dt^n = 0$ for all $n > 2$. The coefficient in the first-order term is small, the coefficient in the second order term is smaller, and the coefficients of the higher order terms are exactly equal to zero.

For completeness, the finite difference scheme (4.92) for $\Delta a_j = g\Delta t_i$ simplifies to

$$f_{i+1}^j = f_i^{j-1} + h(a_j)\Delta t_i. \tag{4.99}$$

In contrast to Cases 1 to 4, this finite difference expression require one summation, one multiplication, and one function evaluation – in addition to the memory reallocation. The computational cost remains very low compared to numerical algorithms reported in the literature for simulating population balance models.

Next, let's analyze the case in which the nonhomogeneous term in the population balance model (4.81) is time varying,

$$\frac{\partial f}{\partial t} + g\frac{\partial f}{\partial a} = h(t). \tag{4.100}$$

The finite difference approximation is

$$\frac{f_{i+1}^j - f_i^j}{\Delta t_i} + g\frac{f_i^j - f_i^{j-1}}{\Delta a_j} = h(t_i). \tag{4.101}$$

Substituting the Taylor expansions for f in (4.84) and (4.85) into the finite difference expression yields

$$\text{error} = \frac{f_{i+1}^j - f_i^j}{\Delta t_i} + g\frac{f_i^j - f_i^{j-1}}{\Delta a_j} - h(t_i)$$

$$= -h(t_i) + \frac{\partial f}{\partial t}\bigg|_{t_i,a_j} + g\frac{\partial f}{\partial a}\bigg|_{t_i,a_j} + \frac{\Delta t_i}{2!}\frac{\partial^2 f}{\partial t^2}\bigg|_{t_i,a_j} - g\frac{\Delta a_j}{2!}\frac{\partial^2 f}{\partial a^2}\bigg|_{t_i,a_j} + \frac{(\Delta t_i)^2}{3!}\frac{\partial^3 f}{\partial t^3}\bigg|_{t_i,a_j} + g\frac{(\Delta a_j)^2}{3!}\frac{\partial^3 f}{\partial a^3}\bigg|_{t_i,a_j}$$

$$+ \cdots + \frac{(\Delta t_i)^{n-1}}{n!}\frac{\partial^n f}{\partial t^n}\bigg|_{t_i,a_j} + (-1)^{n-1}g\frac{(\Delta a_j)^{n-1}}{n!}\frac{\partial^n f}{\partial a^n}\bigg|_{t_i,a_j} + \cdots \tag{4.102}$$

The first three terms on the right-hand side sum to zero according to (4.100). Taking

successive derivatives of the PDE (4.100) gives

$$\frac{\partial^2 f}{\partial a \partial t} + g \frac{\partial^2 f}{\partial a^2} = 0 \text{ and } \frac{\partial^2 f}{\partial t^2} + g \frac{\partial^2 f}{\partial t \partial a} = \frac{dh}{dt} \longrightarrow \boxed{g \frac{\partial^2 f}{\partial a^2} = \frac{1}{g} \frac{\partial^2 f}{\partial t^2} - \frac{1}{g} \frac{dh}{dt}} \longrightarrow g \frac{\partial^3 f}{\partial a^3} = \frac{1}{g} \frac{\partial^3 f}{\partial a \partial t^2}$$
(4.103)

$$\frac{\partial^2 f}{\partial t^2} + g \frac{\partial^2 f}{\partial t \partial a} = \frac{dh}{dt} \longrightarrow \frac{\partial^3 f}{\partial t^3} + g \frac{\partial^3 f}{\partial^2 t \partial a} = \frac{d^2 h}{dt^2} \longrightarrow \frac{1}{g} \frac{\partial^3 f}{\partial^2 t \partial a} = \frac{1}{g^2} \frac{d^2 h}{dt^2} - \frac{1}{g^2} \frac{\partial^3 f}{\partial t^3}$$
(4.104)

$$\longrightarrow \boxed{g \frac{\partial^3 f}{\partial a^3} = \frac{1}{g^2} \frac{d^2 h}{dt^2} - \frac{1}{g^2} \frac{\partial^3 f}{\partial t^3}},$$
(4.105)

which can be used to simplify the error expression to

$$\text{error} = \frac{1}{2!} \left(\Delta t_i - \frac{\Delta a_j}{g} \right) \frac{\partial^2 f}{\partial t^2} \bigg|_{t_i, a_j} + \frac{1}{2!} \frac{\Delta a_j}{g} \frac{dh}{dt} \bigg|_{t_i} + \frac{1}{3!} \left((\Delta t_i)^2 - \left(\frac{\Delta a_j}{g} \right)^2 \right) \frac{\partial^3 f}{\partial t^3} \bigg|_{t_i, a_j} + \frac{1}{3!} \left(\frac{\Delta a_j}{g} \right)^2 \frac{d^2 h}{dt^2} \bigg|_{t_i}$$

$$+ \cdots + \frac{1}{n!} \left((\Delta t_i)^{n-1} - \left(\frac{\Delta a_j}{g} \right)^{n-1} \right) \frac{\partial^n f}{\partial t^n} \bigg|_{t_i, a_j} + \frac{1}{n!} \left(\frac{\Delta a_j}{g} \right)^{n-1} \frac{d^{n-1} h}{dt^{n-1}} \bigg|_{t_i} + \cdots \quad (4.106)$$

Choosing $\Delta a_j = g \Delta t_i$ cancels all of the terms involving derivatives of f, to give

$$\text{error} = \frac{1}{2!} \frac{\Delta a_j}{g} \frac{dh}{dt} \bigg|_{t_i} + \frac{1}{3!} \left(\frac{\Delta a_j}{g} \right)^2 \frac{d^2 h}{dt^2} \bigg|_{t_i} + \cdots + \frac{1}{n!} \left(\frac{\Delta a_j}{g} \right)^{n-1} \frac{d^{n-1} h}{dt^{n-1}} \bigg|_{t_i} + \cdots \quad (4.107)$$

which can alternatively be written as

$$\text{error} = \frac{\Delta t_i}{2!} \frac{dh}{dt} \bigg|_{t_i} + \frac{\Delta t_i^2}{3!} \frac{d^2 h}{dt^2} \bigg|_{t_i} + \cdots + \frac{\Delta t_i^{n-1}}{n!} \frac{d^{n-1} h}{dt^{n-1}} \bigg|_{t_i} + \cdots \quad (4.108)$$

The error is first order in Δa_j with the coefficients on higher order terms becoming smaller as $h(t)$ becomes smoother.

For $\Delta a_j = g \Delta t_i$, the finite difference expression (4.101) simplifies to

$$f_{i+1}^j = f_i^{j-1} + h(t_i) \Delta t_i, \quad (4.109)$$

which has the same low computational cost as for an age-dependent forcing function.

Finally, consider the case in which $h = h(t, a)$ where the PDE (4.81) and the discretized

population balance model, respectively, are

$$\frac{\partial f}{\partial t} + g\frac{\partial f}{\partial a} = h(t, a) \tag{4.110}$$

and

$$\frac{f_{i+1}^j - f_i^j}{\Delta t_i} + g\frac{f_i^j - f_i^{j-1}}{\Delta a_j} = h(t_i, a_j). \tag{4.111}$$

Substituting the Taylor expansions for f in (4.84) and (4.85) also into the finite difference expression yields

$$\text{error} = \frac{f_{i+1}^j - f_i^j}{\Delta t_i} + g\frac{f_i^j - f_i^{j-1}}{\Delta a_j} - h(t_i, a_j)$$

$$= -h(t_i, a_j) + \frac{\partial f}{\partial t}\bigg|_{t_i,a_j} + g\frac{\partial f}{\partial a}\bigg|_{t_i,a_j} + \frac{\Delta t_i}{2!}\frac{\partial^2 f}{\partial t^2}\bigg|_{t_i,a_j} - g\frac{\Delta a_j}{2!}\frac{\partial^2 f}{\partial a^2}\bigg|_{t_i,a_j} + \frac{(\Delta t_i)^2}{3!}\frac{\partial^3 f}{\partial t^3}\bigg|_{t_i,a_j}$$

$$+ g\frac{(\Delta a_j)^2}{3!}\frac{\partial^3 f}{\partial a^3}\bigg|_{t_i,a_j} + \cdots + \frac{(\Delta t_i)^{n-1}}{n!}\frac{\partial^n f}{\partial t^n}\bigg|_{t_i,a_j} + g(-1)^{n-1}\frac{(\Delta a_j)^{n-1}}{n!}\frac{\partial^n f}{\partial a^n}\bigg|_{t_i,a_j} + \cdots \tag{4.112}$$

Equation (4.110) implies that the first three terms on the right-hand side sum to zero. Taking successive derivatives of (4.110) yields

$$\frac{\partial^2 f}{\partial t^2} + g\frac{\partial^2 f}{\partial t\partial a} = \frac{\partial h}{\partial t} \text{ and } \frac{\partial^2 f}{\partial a\partial t} + g\frac{\partial^2 f}{\partial a^2} = \frac{\partial h}{\partial a} \longrightarrow \boxed{g\frac{\partial^2 f}{\partial a^2} = \frac{\partial h}{\partial a} - \frac{1}{g}\frac{\partial h}{\partial t} + \frac{1}{g}\frac{\partial^2 f}{\partial t^2}}$$

$$\longrightarrow g\frac{\partial^3 f}{\partial a^3} = \frac{\partial^2 h}{\partial a^2} - \frac{1}{g}\frac{\partial^2 h}{\partial a\partial t} + \frac{1}{g}\frac{\partial^3 f}{\partial a\partial t^2} \tag{4.113}$$

and

$$\frac{\partial^2 f}{\partial t^2} + g\frac{\partial^2 f}{\partial t\partial a} = \frac{\partial h}{\partial t} \longrightarrow \frac{\partial^3 f}{\partial t^3} + g\frac{\partial^3 f}{\partial t^2\partial a} = \frac{\partial^2 h}{\partial t^2} \longrightarrow \frac{1}{g}\frac{\partial^3 f}{\partial a\partial t^2} = \frac{1}{g^2}\frac{\partial^2 h}{\partial t^2} - \frac{1}{g^2}\frac{\partial^3 f}{\partial t^3}. \tag{4.114}$$

Combining and rearranging the latter two PDEs gives

$$\boxed{g\frac{\partial^3 f}{\partial a^3} = \frac{\partial^2 h}{\partial a^2} - \frac{1}{g}\frac{\partial^2 h}{\partial t\partial a} + \frac{1}{g^2}\frac{\partial^2 h}{\partial t^2} - \frac{1}{g^2}\frac{\partial^3 f}{\partial t^3}} \tag{4.115}$$

Substituting the boxed equations into (4.112) and rearranging gives

$$
\begin{aligned}
\text{error} =\ & \frac{1}{2!}\left(\Delta t_i - \frac{\Delta a_j}{g}\right)\frac{\partial^2 f}{\partial t^2}\bigg|_{t_i,a_j} - \frac{\Delta a_j}{2!}\left[\frac{\partial h}{\partial a} - \frac{1}{g}\frac{\partial h}{\partial t}\right]\bigg|_{t_i,a_j} \\
& + \frac{1}{3!}\left((\Delta t_i)^2 - \left(\frac{\Delta a_j}{g}\right)^2\right)\frac{\partial^3 f}{\partial t^3}\bigg|_{t_i,a_j} + \frac{(\Delta a_j)^2}{3!}\left[\frac{\partial^2 h}{\partial a^2} - \frac{1}{g}\frac{\partial^2 h}{\partial t\partial a} + \frac{1}{g^2}\frac{\partial^2 h}{\partial t^2}\right]\bigg|_{t_i,a_j} + \cdots \\
& + \frac{1}{n!}\left((\Delta t_i)^{n-1} - \left(\frac{\Delta a_j}{g}\right)^{n-1}\right)\frac{\partial^n f}{\partial t^n}\bigg|_{t_i,a_j} + \frac{(\Delta a_j)^{n-1}}{n!}\left[\sum_{k=0}^{n-1}\frac{(-1)^k}{g^k}\frac{\partial^{n-1}h}{\partial t^k\partial a^{n-k-1}}\right]\bigg|_{t_i,a_j} + \cdots \quad (4.116)
\end{aligned}
$$

Choosing $\Delta a_j = g\Delta t_i$ cancels all the terms involving derivatives of f,

$$
\begin{aligned}
\text{error} =\ & \frac{\Delta a_j}{2!}\left[-\frac{\partial h}{\partial a} + \frac{1}{g}\frac{\partial h}{\partial t}\right]\bigg|_{t_i,a_j} + \frac{(\Delta a_j)^2}{3!}\left[\frac{\partial^2 h}{\partial a^2} - \frac{1}{g}\frac{\partial^2 h}{\partial t\partial a} + \frac{1}{g^2}\frac{\partial^2 h}{\partial t^2}\right]\bigg|_{t_i,a_j} \\
& + \frac{(\Delta a_j)^{n-1}}{n!}\left[\sum_{k=0}^{n-1}\frac{(-1)^k}{g^k}\frac{\partial^{n-1}h}{\partial t^k\partial a^{n-k-1}}\right]\bigg|_{t_i,a_j} + \cdots \quad (4.117)
\end{aligned}
$$

The error is technically first order in Δa_j, with the coefficients being sums of successively higher order derivatives of the nonhomogeneous term h with respect to t and a. The discretization error approaches higher order accuracy as the nonhomgeneous term varies more slowly with respect with t and a.

The choice $\Delta a_j = g\Delta t_i$ simplifies the finite difference expression (4.111) to

$$
f_{i+1}^j = f_i^{j-1} + h(t_i, a_j)\Delta t_i, \quad (4.118)
$$

which has the same low computational cost as when the forcing function is an explicit function of only age or time.

4.2.7 Case 7: Population Balance Models with Linear Nonhomogeneous Term

A large proportion of population balance models have a linear nonhomogenous term, e.g., Von Foerster's equation [60],

$$\frac{\partial f(t,a)}{\partial t} + \frac{\partial f(t,a)}{\partial a} = -\lambda(t,a)f(t,a), \quad f(0,a) = f_0(a). \tag{4.119}$$

Let's first illustrate the finite difference method for the case in which λ is a constant. The first step is to multiply the population balance model by $e^{\lambda t}$,

$$e^{\lambda t}\frac{\partial f(t,a)}{\partial t} + e^{\lambda t}\frac{\partial f(t,a)}{\partial a} = -\lambda e^{\lambda t}f(t,a), \quad f(0,a) = f_0(a), \tag{4.120}$$

and do the replacement

$$\frac{\partial}{\partial t}(e^{\lambda t}f(t,a)) = \lambda e^{\lambda t}f(t,a) + e^{\lambda t}\frac{\partial f(t,a)}{\partial t} \tag{4.121}$$

to derive

$$\frac{\partial}{\partial t}(e^{\lambda t}f(t,a)) + \frac{\partial}{\partial a}(e^{\lambda t}f(t,a)) = 0, \quad f(0,a) = f_0(a). \tag{4.122}$$

Defining

$$\tilde{f}(t,a) = e^{\lambda t}f(t,a) \tag{4.123}$$

results in the homogeneous cell population balance model

$$\frac{\partial \tilde{f}(t,a)}{\partial t} + \frac{\partial \tilde{f}(t,a)}{\partial a} = 0, \quad \tilde{f}(0,a) = f_0(a), \tag{4.124}$$

which was solved as Case 1. This approach is basically the same as the integrating factor employed in the analytical solution of first-order ordinary differential equations. This method applies to λ being a function of a or t, with a slight tweak to the definitions.

For example, consider

$$\frac{\partial f(t,a)}{\partial t} + \frac{\partial f(t,a)}{\partial a} = -\lambda(t)f(t,a), \quad f(0,a) = f_0(a). \tag{4.125}$$

Multiply the population balance model by $\exp\left(\int_0^t \lambda(\tilde{t})d\tilde{t}\right)$ to give

$$\exp\left(\int_0^t \lambda(\tilde{t})d\tilde{t}\right)\frac{\partial f(t,a)}{\partial t}+\exp\left(\int_0^t \lambda(\tilde{t})d\tilde{t}\right)\frac{\partial f(t,a)}{\partial a} = -\lambda(t)\exp\left(\int_0^t \lambda(\tilde{t})d\tilde{t}\right)f(t,a), \quad f(0,a)=f_0,$$
(4.126)

and do the replacement

$$\frac{\partial}{\partial t}\left(\exp\left(\int_0^t \lambda(\tilde{t})d\tilde{t}\right)f(t,a)\right)=\lambda(t)\exp\left(\int_0^t \lambda(\tilde{t})d\tilde{t}\right)f(t,a)+\exp\left(\int_0^t \lambda(\tilde{t})d\tilde{t}\right)\frac{\partial f(t,a)}{\partial t} \quad (4.127)$$

to derive

$$\frac{\partial}{\partial t}\left(\exp\left(\int_0^t \lambda(\tilde{t})d\tilde{t}\right)f(t,a)\right)+\frac{\partial}{\partial a}\left(\exp\left(\int_0^t \lambda(\tilde{t})d\tilde{t}\right)f(t,a)\right)=0, \quad f(0,a)=f_0(a). \quad (4.128)$$

Defining

$$\tilde{f}(t,a)=\exp\left(\int_0^t \lambda(\tilde{t})d\tilde{t}\right)f(t,a) \tag{4.129}$$

results in the homogeneous cell population balance model

$$\frac{\partial \tilde{f}(t,a)}{\partial t}+\frac{\partial \tilde{f}(t,a)}{\partial a}=0, \quad \tilde{f}(0,a)=f_0(a), \tag{4.130}$$

which was solved as Case 1.

The case of λ being a function of a is handled similarly. Consider

$$\frac{\partial f(t,a)}{\partial t}+\frac{\partial f(t,a)}{\partial a}=-\lambda(a)f(t,a), \quad f(0,a)=f_0(a). \tag{4.131}$$

Multiply the population balance model by $\exp(\int_0^a \lambda(\tilde{a})d\tilde{a})$ to give

$$\exp\left(\int_0^a \lambda(\tilde{a})d\tilde{a}\right)\frac{\partial f(t,a)}{\partial t}+\exp\left(\int_0^a \lambda(\tilde{t})d\tilde{a}\right)\frac{\partial f(t,a)}{\partial a} = -\lambda(a)\exp\left(\int_0^a \lambda(\tilde{a})d\tilde{a}\right)f(t,a), \quad f(0,a)=f_0,$$
(4.132)

and do the replacement

$$\frac{\partial}{\partial a}\left(\exp\left(\int_0^a \lambda(\tilde{a})d\tilde{a}\right)f(t,a)\right)=\lambda(a)\exp\left(\int_0^a \lambda(\tilde{a})d\tilde{a}\right)f(t,a)+\exp\left(\int_0^a \lambda(\tilde{a})d\tilde{a}\right)\frac{\partial f(t,a)}{\partial a}$$
(4.133)

to derive

$$\frac{\partial}{\partial t}\left(\exp\left(\int_0^a \lambda(\tilde{a})d\tilde{a}\right)f(t,a)\right) + \frac{\partial}{\partial a}\left(\exp\left(\int_0^a \lambda(\tilde{a})d\tilde{a}\right)f(t,a)\right) = 0, \quad f(0,a) = f_0(a). \quad (4.134)$$

Defining

$$\tilde{f}(t,a) = \exp\left(\int_0^a \lambda(\tilde{a})d\tilde{a}\right)f(t,a) \quad (4.135)$$

results in the homogeneous cell population balance model

$$\frac{\partial \tilde{f}(t,a)}{\partial t} + \frac{\partial \tilde{f}(t,a)}{\partial a} = 0, \quad \tilde{f}(0,a) = \exp\left(\int_0^a \lambda(\tilde{a})d\tilde{a}\right)f_0(a), \quad (4.136)$$

which was solved as Case 1.

The case where λ is a function of both t and a can be handled in a similiar manner as when λ is a function only of t,

$$\frac{\partial f(t,a)}{\partial t} + \frac{\partial f(t,a)}{\partial a} = -\lambda(t,a), \quad f(0,a) = f_0(a). \quad (4.137)$$

Multiply the population balance model by $\exp\left(\int_0^t \lambda(\tilde{t},a)d\tilde{t}\right)$ to give

$$\exp\left(\int_0^t \lambda(\tilde{t},a)d\tilde{t}\right)\frac{\partial f(t,a)}{\partial t} + \exp\left(\int_0^t \lambda(\tilde{t},a)d\tilde{t}\right)\frac{\partial f(t,a)}{\partial a}$$
$$= -\lambda(t,a)\exp\left(\int_0^t \lambda(\tilde{t},a)d\tilde{t}\right)f(t,a), \quad f(0,a) = f_0, \quad (4.138)$$

and do the replacement

$$\frac{\partial}{\partial t}\left(\exp\left(\int_0^t \lambda(\tilde{t},a)d\tilde{t}\right)f(t,a)\right) = \lambda(t,a)\exp\left(\int_0^t \lambda_t(\tilde{t},a)d\tilde{t}\right)f(t,a)$$
$$+ \exp\left(\int_0^t \lambda(\tilde{t},a)d\tilde{t}\right)\frac{\partial f(t,a)}{\partial t} \quad (4.139)$$

to derive

$$\frac{\partial}{\partial t}\left(\exp\left(\int_0^t \lambda(\tilde{t},a)d\tilde{t}\right)f(t,a)\right) + \frac{\partial}{\partial a}\left(\exp\left(\int_0^t \lambda(\tilde{t},a)d\tilde{t}\right)f(t,a)\right) = 0, \quad f(0,a) = f_0(a). \quad (4.140)$$

87

Defining

$$\tilde{f}(t, a) = \exp\left(\int_0^t \lambda(\tilde{t}, a) d\tilde{t}\right) f(t, a) \tag{4.141}$$

results in the homogeneous cell population balance model

$$\frac{\partial \tilde{f}(t, a)}{\partial t} + \frac{\partial \tilde{f}(t, a)}{\partial a} = 0, \quad \tilde{f}(0, a) = f_0(a), \tag{4.142}$$

which was solved as Case 1.

The above transformation approach can be applied to the other population balance models investigated in this chapter.

The finite difference method can be shown to also have zero discretization error for population balance models with multiple internal coordinates (where a is a vector) and external coordinates (where x is the axial distance along a plug-flow vessel). Since population balance models have the same form as reaction-convection-diffusion equations, the same zero-error finite difference method also applies to those systems when the same assumptions are made.

4.3   Conclusions

In this chapter, we proposed a finite difference scheme for the solution of a general class of population balance models. The chapter pedagogically progresses through increasingly more complicated population balance models, demonstrating how the proposed finite difference method can be applied to obtain no numerical discretization error, through the use of some transformations. Further, when applied directly to more general PBEs, we have derived error expressions which show that the error is first order, transitioning to zero order as the growth rate and non-homogeneous terms become smoother functions of a.

Typically, the study of finite difference methods to solve population balance models focuses on developing inceasingly more complicated and higher order accurate finite difference methods, which can result in the numerical solution becoming increasingly more computationally expensive. Furthermore, these higher ordered methods are subject to aphysical oscillations that do not appear in first order or zero error solutions such as that proposed in

this chapter.

By specifically choosing to apply a first-order forward difference for the time derivative and a first-order backward difference for the derivative with respect to the intrinsic variable, the numerical discretization error is reduced to zero in homogeneous population balances with constant growth rate, G. In more complicated systems in which the growth rate varies with time or the intrinsic variable or a non-homogeneous forcing function is present, the error expressions developed here demonstrate how the discretization error that results from the application of the difference scheme behaves benignly. This indicates that the finite difference scheme analyzed here is applicable to a wide variety of industrially relevant problems.

Chapter 5

Analytical Solutions of Population Balance Models

Many chemical and biological processes are well-described by population balance models, in which the main state is a distribution over some property such as age, length, or mass. This chapter derives analytical solutions for some classes of population balance models, which can be applied directly in specific applications within those classes, or used as limiting cases for the validation of numerical methods applicable to more general systems. The analytical solutions are also used to prove that the finite difference method in the previous chapter gives zero error for those classes.

Population balance models are widely used for describing population dynamics, which arise in a variety of chemical and biological applications. This chapter derives analytical solutions for some classes of population balance models that commonly appears in these applications, namely, to populations of biological cells and crystals. The analytical solutions are derived in a tutorial manner, as the specific steps in the derivations are more widely applicable than the specific applications themselves. The analytical solutions are also compared with a more general analytical solution whose published theoretical derivation is more complicated than the derivations given in this chapter.

Analytical solutions are not available for all population balance models, and numerical methods remain as the only approach for those PBMs in which analytical solutions are not available. A large literature derives finite difference methods for the numerical simulation of

population balance models, as well as for more general partial differential equations, with the goal being to minimize numerical errors associated with the finite difference approximations (e.g., see [20, 22, 32–34, 39, 50, 68] and citations therein). Especially important for this class of partial differential equations is the need to reduce numerical diffusion (i.e., smearing of the numerical solution compared to the true solution) and numerical dispersion (i.e., oscillations in the numerical solution that do not arise in the true solution).

The previous chapter describes a finite difference method with no discretization error for the simulation of classes of population balance models that arise in many applications, with the proofs of zero error based on Taylor series expansions. As an alternative approach, this chapter applies the analytical solutions to prove that the finite difference method in the previous chapter produces zero discretization error. The advantages of the proofs in this chapter are that they are much shorter and require less algebra; the advantages of the proofs in the previous chapter are that they do not require knowledge of the analytical solutions and require less sophisticated mathematics.

Section 5.1 describes species and population balance models. Section 5.2 presents analytical solutions to the population balance models, which are applied in Section 5.3 to prove that the numerical method in the previous chapter has zero discretization error. Section 5.4 concludes the chapter.

5.1 Species and Population Balance Models

Species balances for spatially well-mixed systems can be written as ordinary differential equations (ODEs),

$$\frac{d\hat{f}(t)}{dt} = \hat{h}(t, \hat{f}),\tag{5.1}$$

where $\hat{f}$ is the species density, t is time, and $\hat{h}$ is a forcing function which can be a function of $\hat{f}$ and t.

When a species has an additional intrinsic variable, such as age or size, the partial

differential equation (PDE) corresponding to the ODE model is

$$\frac{\partial \hat{f}(t,a)}{\partial t} + \frac{\partial (G(t,a)\hat{f}(t,a))}{\partial a} = \hat{h}(t,a,\hat{f}), \tag{5.2}$$

which describes the time evolution of the distribution of $\hat{f}$ with respect to a, where a is the additional intrinsic variable and $G = da/dt$ is the rate of change of the intrinsic variable with respect to time. For example, for cell population balance models in which the variable a is the cell age, $G = 1$. When the intrinsic variable a is the size or mass of the cell, or the number or concentration of organelles within a cell, then G is more generally describable by a constant or a function of a and/or t. The forcing function h can also be a function of the intrinsic variable a.

In most applications, the $G(t,a)$ in the population balance model (5.2) is separable, that is, can be written as $G(t,a) = G_t(t)G_a(a)$. In this case, the PDE can be transformed by multiplication by $G_a(a)$ to give

$$G_a(a)\frac{\partial \hat{f}(t,a)}{\partial t} + G_a(a)\frac{\partial (G_t(t)G_a(a)\hat{f}(t,a))}{\partial a} = G_a(a)\hat{h}(t,a,\hat{f}), \tag{5.3}$$

which can be written as

$$\frac{\partial (G_a(a)\hat{f}(t,a))}{\partial t} + G_a(a)G_t(t)\frac{\partial (G_a(a)\hat{f}(t,a))}{\partial a} = G_a(a)\hat{h}(t,a,\hat{f}), \tag{5.4}$$

With the definitions $f(t,a) = G_a(a)\hat{f}(t,a)$ and $h(t,a) = G_a(a)\hat{h}(t,a,\hat{f})$, this equation simplifies to

$$\frac{\partial f(t,a)}{\partial t} + G_a(a)G_t(t)\frac{\partial f(t,a)}{\partial a} = h(t,a,f), \tag{5.5}$$

which has the form

$$\frac{\partial f(t,a)}{\partial t} + G(t,a)\frac{\partial f(t,a)}{\partial a} = h(t,a,f), \tag{5.6}$$

in which the growth rate is outside of the partial with respect to a. The rest of this chapter assumes that the growth rate $G(t,a)$ is separable, so the population balance model can be written as (5.5).

5.2 Analytical Solutions

Analytical solutions for special cases of the population balance model have been available for decades and new solutions continue to be derived. An example of the latter is a 2020 paper published in *Scientific Reports* which considered the population balance model

$$\frac{\partial \hat{f}(t,a)}{\partial t} + \frac{\partial (G\hat{f}(t,a))}{\partial a} = D\frac{\partial^2 \hat{f}}{\partial a^2} - ka + \hat{h}(a), \quad \hat{f}(0,a) = \hat{f}_0(a), \tag{5.7}$$

where G, D, and k are constant growth rate, diffusivity, and kinetic constant; and $\hat{h}$ is a forcing function which can be age dependent. Analytical solutions are provided for various choices of boundary conditions over finite or semi-infinite domains for a, e.g.,

$$\hat{f}(t,0) = f_t(t), \quad \lim_{t \to \infty} \frac{\partial \hat{f}}{\partial a} = 0. \tag{5.8}$$

Here we consider a population balance model with growth rate and forcing function that depend on a:

$$\frac{\partial \hat{f}(t,a)}{\partial t} + \frac{\partial (G(a)\hat{f}(t,a))}{\partial a} = \hat{h}(a), \quad \hat{f}(0,a) = \hat{f}_0(a). \tag{5.9}$$

An exact analytical solution to this population balance model is [53]

$$\hat{f}(t,a) = \frac{G[\lambda(t,a)]}{G(a)} f_0[\lambda(t,a)] + \frac{1}{G(a)} \int_{\lambda(t,a)}^{a} \hat{h}(\tilde{a})d\tilde{a}, \tag{5.10}$$

where λ and Q are defined by

$$\lambda(t,a) := z^{-1}[z(a) - t] \tag{5.11}$$

and

$$z(a) := \int \frac{1}{G(a)} da. \tag{5.12}$$

This analytical solution requires that the growth rate is positive, the system contains no aggregation or breakage, and any birth or death rates are not explicit functions of time. The analytical expression (5.10) was derived by a combination of a novel transformation and the method of characteristics (e.g., [15, 45] and citations therein).

This section applies simple variable transformations and the method of characteristics to

derive exact analytical solutions for some population balance models with time- and size-dependent growth rate. The derivations of the analytical solutions are very similar to [53], with some analytical solutions being less general in some ways and some being more general in some ways than (5.10). In particular, some of the analytical solutions are applicable to population balance models with time-dependent and negative growth rates, although with the restriction that $h(a) = 0$. In all cases, the resulting expressions are simpler than (5.10). The methods are presented in a pedigogical way, starting with a simple population balance model to clearly illustrate the approach, before moving to a more complex population balance model.

Let's first consider the homogeneous version of the population balance model (5.9):

$$\frac{\partial \hat{f}(t,a)}{\partial t} + \frac{\partial (G(a)\hat{f}(t,a))}{\partial a} = 0, \quad \hat{f}(0,a) = \hat{f}_0(a), \tag{5.13}$$

with $G(a) > 0$.[1] Multiplying by $G(a)$ and defining a new function f (e.g., [20]) by

$$f(t,a) = G(a)\hat{f}(t,a), \tag{5.14}$$

allows the PDE (5.13) to be written as

$$\frac{\partial f(t,a)}{\partial t} + G(a)\frac{\partial f(t,a)}{\partial a} = 0, \quad f_0(0,a) = G(a)\hat{f}_0(a). \tag{5.15}$$

If f is assumed to be parameterizable in terms of a single characteristic variable s, then

$$\frac{df}{ds} = \frac{\partial f}{\partial t}\frac{dt}{ds} + \frac{\partial f}{\partial a}\frac{da}{ds}. \tag{5.16}$$

Mapping the individual terms in the expressions in (5.13) and (5.16) results in the characteristic equations

$$\frac{dt}{ds} = 1, \tag{5.17}$$

$$\frac{da}{ds} = G(a), \tag{5.18}$$

---

[1]This assumption is removed later.

and

$$\frac{df}{ds} = 0. \tag{5.19}$$

Being able to find a solution to these equations would confirm the validity of the assumption that f is parameterizable in terms of a single characteristic variable. Integrating the characteristic equations gives

$$t = s + c_1 \tag{5.20}$$

$$\int_0^a \frac{1}{G(\tilde{a})} d\tilde{a} = s + c_2, \tag{5.21}$$

and

$$f = f^* \tag{5.22}$$

where f^* cannot depend on the characteristic variable s. Without loss of generality, the constant c_1 can be set to zero so that s is the same as the time variable, $t = s$. With the definition $a_0 := a|_{s=0}$, (5.51) implies that a_0 must satisfy

$$\int_0^{a_0} \frac{1}{G(\tilde{a})} d\tilde{a} = c_2, \tag{5.23}$$

which implies some relationships between a_0 and a and t:

$$\int_0^a \frac{1}{G(\tilde{a})} d\tilde{a} = t + \int_0^{a_0} \frac{1}{G(\tilde{a})} d\tilde{a}, \tag{5.24}$$

$$\int_{a_0}^a \frac{1}{G(\tilde{a})} d\tilde{a} = t. \tag{5.25}$$

Evaluating the initial condition for $f(t, a)$ in (5.15) at $t = 0$ and $a = a_0$ gives that

$$f(t, a) = f(0, a_0) = G(a_0)\hat{f}_0(a_0) \tag{5.26}$$

for any value of $a_0 > 0$.

If a_0 in (5.25) is analytically solvable in terms of a and t, then that expression for a_0 can be inserted into the right-hand side of (5.26) to produce an analytical solution for the transformed population balance model (5.15). To construct an analytical expression for a_0

in (5.26), first define a function

$$z(a) = \int_0^a \frac{1}{G(\tilde{a})} d\tilde{a}, \tag{5.27}$$

which is one-to-one for any positive function $G(a)$.[2] Then (5.25) can be written as

$$z(a) - z(a_0) = t, \tag{5.28}$$

which can be solved for a_0 as

$$a_0 = z^{-1}[z(a) - t]. \tag{5.29}$$

Insertion into (5.26) gives the analytical solution of the population balance model (5.13) as

$$f(t, a) = G(z^{-1}[z(a) - t]) \hat{f}_0(z^{-1}[z(a) - t]), \tag{5.30}$$

Inserting this expression into (5.14) results in the analytical solution to (5.13):

$$\hat{f}(t, a) = \frac{G(z^{-1}[z(a) - t])}{G(a)} \hat{f}_0(z^{-1}[z(a) - t]). \tag{5.31}$$

This analytical solution is a special case of the more general expression (5.10).

Analytical solutions for z and z^{-1} have been derived for several growth functions, including for linear, monosurface, and diffusion-limited [53]. For example, the expressions for $G(a) = a$ are

$$z(a) = \int_0^a \frac{1}{\hat{a}} d\hat{a} = \ln a, \tag{5.32}$$

$$z^{-1}(a) = e^a, \tag{5.33}$$

$$z^{-1}[z(a) - t] = \exp[\ln a - t] = ae^{-t}. \tag{5.34}$$

---

[2]This approach also works if the lower limit is replaced by a different constant, or if any indefinite integral is used.

Then the analytical solution of the population balance model (5.13) is

$$\hat{f}(t,a) = \frac{G(z^{-1}[z(a)-t])}{G(a)} \hat{f}_0(z^{-1}[z(a)-t]) \tag{5.35}$$

$$\hat{f}(t,a) = \frac{G(ae^{-t})}{G(a)} \hat{f}_0(ae^{-t}) = e^{-t}\hat{f}_0(ae^{-t}). \tag{5.36}$$

This expression satisfies the initial condition,

$$\hat{f}(0,a) = e^{-0}\hat{f}_0(ae^{-0}) = \hat{f}_0(a). \tag{5.37}$$

Insertion into the original population balance model (5.13) gives

$$\frac{\partial \hat{f}(t,a)}{\partial t} + \frac{\partial(G(a)\hat{f}(t,a))}{\partial a} = \frac{\partial \hat{f}(t,a)}{\partial t} + \frac{\partial(a\hat{f}(t,a))}{\partial a} \tag{5.38}$$

$$= \frac{\partial(e^{-t}\hat{f}_0(ae^{-t}))}{\partial t} + \frac{\partial(ae^{-t}\hat{f}_0(ae^{-t}))}{\partial a} \tag{5.39}$$

$$= e^{-t}\frac{\partial \hat{f}_0(ae^{-t})}{\partial t} + \frac{\partial e^{-t}}{\partial t}\hat{f}_0(ae^{-t}) + ae^{-t}\frac{\partial \hat{f}_0(ae^{-t})}{\partial a} + \frac{\partial(ae^{-t})}{\partial a}\hat{f}_0(ae^{-t}) \tag{5.40}$$

$$= e^{-t}\hat{f}_0'(ae^{-t})(-ae^{-t}) - e^{-t}\hat{f}_0(ae^{-t}) + ae^{-t}\hat{f}_0'(ae^{-t})e^{-t} + e^{-t}\hat{f}_0(ae^{-t}) \tag{5.41}$$

$$= 0. \tag{5.42}$$

An implicit assumption of [53] is that $G(a)$ is positive, which is required for the $z(a)$ and $z^{-1}(a)$ to be one-to-one functions, and all of the examples in that paper also satisfied $G(a) > 0$. Negative $G(a)$ is common in many applications, including in the dissolution of crystals and precipitates. The case where $G(a) < 0$ is handled in the same way, and the case in which $G(a)$ can have any sign can be handled by splitting $G(a)$ into segments in which $G(a)$ has a single sign in each segment, and adding the resulting solutions obtained for each segment.

Let's consider the population balance model with size- and time-dependent growth rate,

$$\frac{\partial \hat{f}}{\partial t} + G_t(t)\frac{\partial(G_a(a)\hat{f})}{\partial a} = 0, \quad \hat{f}(0,a) = \hat{f}_0(a), \tag{5.43}$$

where the time-dependency was moved outside of the partial derivative with respect to a.

An exact analytical solution can be generated for this case by using the method of characteristics after dividing through by $G_t(t)$, multiplying through by $G_a(a)$, and defining a new function f,

$$f(t, a) = G_a(a)\hat{f}(t, a). \tag{5.44}$$

Then the original population balance model (5.43) can be written as the transformed population balance model

$$\frac{1}{G_t(t)}\frac{\partial f}{\partial t} + G_a(a)\frac{\partial f}{\partial a} = 0, \quad f_0(0, a) = G_a(a)\hat{f}_0(a). \tag{5.45}$$

If f is assumed to be parameterizable in terms of a single characteristic variable s, then

$$\frac{df}{ds} = \frac{\partial f}{\partial t}\frac{dt}{ds} + \frac{\partial f}{\partial a}\frac{da}{ds}. \tag{5.46}$$

Mapping the individual terms in the expressions in (5.45) and (5.46) results in the characteristic equations

$$\frac{dt}{ds} = \frac{1}{G_t(t)}, \tag{5.47}$$

$$\frac{da}{ds} = G_a(a), \tag{5.48}$$

and

$$\frac{df}{ds} = 0. \tag{5.49}$$

Being able to find a solution to these equations would confirm the validity of the assumption that f is parameterizable in terms of a single characteristic variable. Integrating the characteristic equations gives

$$\int_0^t G_t(\tilde{t})d\tilde{t} = s + c_1 \tag{5.50}$$

$$\int_0^a \frac{1}{G_a(\tilde{a})}d\tilde{a} = s + c_2, \tag{5.51}$$

and

$$f = f^* \tag{5.52}$$

where f^* cannot depend on the characteristic variable s. Without loss of generality, the constant c_1 can be set to zero so that

$$\int_0^t G_t(\tilde{t})d\tilde{t} = s \tag{5.53}$$

The time dependency $G_t(t)$ is assumed to be greater than zero, which implies that w is monotonically increasing.[3] With the definition $a_0 := a|_{s=0}$, (5.51) implies that a_0 must satisfy

$$\int_0^{a_0} \frac{1}{G_a(\tilde{a})}d\tilde{a} = c_2, \tag{5.54}$$

which implies some relationships between a_0 and a and t:

$$\int_0^a \frac{1}{G_a(\tilde{a})}d\tilde{a} = \int_0^t G_t(\tilde{t})d\tilde{t} + \int_0^{a_0} \frac{1}{G_a(\tilde{a})}d\tilde{a}, \tag{5.55}$$

$$\int_{a_0}^a \frac{1}{G_a(\tilde{a})}d\tilde{a} = \int_0^t G_t(\tilde{t})d\tilde{t}. \tag{5.56}$$

Evaluating the initial condition for $f(t,a)$ in (5.45) at $t = 0$ and $a = a_0$ gives that

$$f(t,a) = f(0,a_0) = G_a(a_0)\hat{f}_0(a_0) \tag{5.57}$$

for any value of $a_0 > 0$.

If a_0 in (5.56) is analytically solvable in terms of a and t, then that expression for a_0 can be inserted into the right-hand side of (5.57) to produce an analytical solution for the transformed population balance model (5.45). To construct an analytical expression for a_0 in (5.56), first define a function

$$z(a) = \int_0^a \frac{1}{G_a(\tilde{a})}d\tilde{a}, \tag{5.58}$$

---

[3]This assumption can be removed by small revisions to the analysis.

which is one-to-one for any positive $G(a)$.[4] Then (5.55) can be written as

$$z(a) - z(a_0) = \int_0^t G_t(\tilde{t})d\tilde{t}, \tag{5.59}$$

which can be solved for a_0 as

$$a_0 = z^{-1}[z(a) - w(t)]. \tag{5.60}$$

Insertion into (5.57) gives the analytical solution of the population balance model (5.45) as

$$f(t,a) = G_a(z^{-1}[z(a) - \int_0^t G_t(\tilde{t})d\tilde{t}])\hat{f}_0(z^{-1}[z(a) - \int_0^t G_t(\tilde{t})d\tilde{t}]), \tag{5.61}$$

Inserting this expression into (5.44) results in the analytical solution to (5.43):

$$\hat{f}(t,a) = \frac{G_a(z^{-1}[z(a) - \int_0^t G_t(\tilde{t})d\tilde{t}])}{G_a(a)}\hat{f}_0(z^{-1}[z(a) - \int_0^t G_t(\tilde{t})d\tilde{t}]). \tag{5.62}$$

This analytical solution generalizes the expression (5.10) to include time-dependent growth rates, for the special case where the forcing function is zero.

As an example, consider the case where $G_t = e^{-t}$ and $G_a(a) = a$. The expression for s from (5.53) is

$$\int_0^t G_t(\tilde{t})d\tilde{t} = \int_0^t e^{-t}d\tilde{t} = 1 - e^{-t}. \tag{5.63}$$

As before, the expression for z and z^{-1} for $G(a) = a$ are

$$z(a) = \int_0^a \frac{1}{\hat{a}}d\hat{a} = \ln a, \tag{5.64}$$

and

$$z^{-1}(a) = e^a. \tag{5.65}$$

Then

$$z^{-1}[z(a) - \int_0^t G_t(\tilde{t})d\tilde{t}] = \exp[\ln a - 1 + e^{-t}] = a\exp(e^{-t} - 1) \tag{5.66}$$

---

[4]This approach also works if the lower limit is replaced by a different constant, or if any indefinite integral is used.

Then the analytical solution of the population balance model (5.43) is

$$\hat{f}(t,a) = \frac{a\exp(e^{-t}-1)}{a}\hat{f}_0(a/t) = \exp(e^{-t}-1)\hat{f}_0(a\exp(e^{-t}-1)). \qquad (5.67)$$

5.3 Numerical Analysis

Finite difference methods approximate the partial differentials on the left-hand side of (5.6). To reduce the numerical discretization error, that is, the difference between the numerical approximation described by the discretized equation and the true solution described by the PDE, the well-established strategy is to use increasingly complicated and higher order accurate finite difference expansions. While this approach reduces the number of discretization points needed to achieve a specified level of numerical accuracy, the computational cost per discretization point increases.

The previous chapter takes a different approach, which is to select particular first-order finite difference expressions for both partial derivative terms and choose the mesh size so that the sum of the two discretized expressions in the left-hand side (5.6) has zero numerical discretization error. That chapter also showed that this exact cancellation of errors could require the mesh size to be age or time dependent. The approach both results in the lowest cost per discretization point and allows the user to select the number of discretization points based on the level of detail desired in the solution rather than based on achieving a desired numerical discretization error. Specifically, a first-order forward difference was employed for the time differential and a first-order backward difference was used for the differential for the intrinsic variable a. This approach, for an appropriately chosen mesh and possibly also doing a change in variables, resulted in exact cancellation of the error introduced in the finite difference discretization of the first term in (5.6) by the error introduced in the finite difference discretization of the second term.

This section applies analytical solutions of the population balance models to provide alternative proofs of the zero error and related results in the previous chapter.

5.3.1   Case 1: Cell Population Balance Model

First the approach is illustrated for the homogeneous cell population balance model [60], that is, with growth rate G equal to 1,

$$\frac{\partial f(t,a)}{\partial t} + \frac{\partial f(t,a)}{\partial a} = 0, \quad f(0,a) = f_0(a), \tag{5.68}$$

over $a \in \mathcal{R}$ and $t \geq 0$. Applying the above finite difference scheme yields

$$\frac{f_{i+1}^j - f_i^j}{\Delta t} + \frac{f_i^j - f_i^{j-1}}{\Delta a} = 0 \tag{5.69}$$

where i is the time index, j is the index for the intrinsic variable, and Δa and Δt are real positive scalars. An exact analytical solution to the PDE (5.68) can be derived and is given by

$$f(t,a) = f_0(a - t), \tag{5.70}$$

which is proved by

$$\frac{\partial f}{\partial t} = -f_0(a - t), \tag{5.71}$$

$$\frac{\partial f}{\partial a} = f_0(a - t), \tag{5.72}$$

$$\frac{\partial f}{\partial t} + \frac{\partial f}{\partial a} = -f_0(a - t) + f_0(a - t) = 0, \tag{5.73}$$

and

$$f_0(a - t)|_{t=0} = f_0(a). \tag{5.74}$$

This exact analytical solution can then be substituted into the finite difference approximation shown in (5.69) to quantify the numerical discretization error:

$$\text{error} = \frac{f_0(a - (t + \Delta t)) - f_0(a - t)}{\Delta t} + \frac{f_0(a - t) - f_0(a - \Delta a - t)}{\Delta a} \tag{5.75}$$

By selecting the mesh sizes so that $\Delta t = \Delta a$, the discretization error satisfies

$$\text{error} = \frac{f_0(a - t - \Delta t) - f_0(a - \Delta a - t)}{\Delta t} = 0, \tag{5.76}$$

which shows that the proposed finite difference scheme and mesh selection results in no numerical discretization error.

5.3.2   Case 2: Population Balance Model with Constant Growth Rate

Next analyze the homogeneous population balance model in which $G = g$ is a non-zero constant,

$$\frac{\partial f(t,a)}{\partial t} + g\frac{\partial f(t,a)}{\partial a} = 0, \quad f(0,a) = f_0(a), \tag{5.77}$$

over $a \in \mathcal{R}$ and $t \geq 0$. Applying the aforementioned finite difference scheme yields

$$\frac{f_{i+1}^j - f_i^j}{\Delta t} + g\frac{f_i^j - f_i^{j-1}}{\Delta a} = 0 \tag{5.78}$$

An exact analytical solution to (5.77) can be derived as

$$f(t,a) = f_0(a - gt), \tag{5.79}$$

which is proved by

$$\frac{\partial f}{\partial t} = -gf_0(a - gt), \tag{5.80}$$

$$\frac{\partial f}{\partial a} = f_0(a - gt), \tag{5.81}$$

$$\frac{\partial f}{\partial t} + g\frac{\partial f}{\partial a} = -gf_0(a - gt) + gf_0(a - gt) = 0, \tag{5.82}$$

and

$$f_0(a - gt)|_{t=0} = f_0(a). \tag{5.83}$$

The exact analytical solution can then be substituted into the finite difference approximation in (5.78) to derive an expression for the numerical discretization error:

$$\text{error} = \frac{f_0(a - g(t + \Delta t)) - f_0(a - gt)}{\Delta t} + g\frac{f_0(a - gt) - f_0(a - \Delta a - gt)}{\Delta a}. \tag{5.84}$$

By selecting the mesh for t and a to satisfy $\Delta a = g\Delta t$, the error is

$$\text{error} = \frac{f_0(a - gt - g\Delta t)) - f_0(a - \Delta a - gt)}{\Delta t} = 0, \tag{5.85}$$

which shows that the finite difference scheme with the selected mesh results in no numerical discretization error.

5.3.3 Case 3: Population Balance Model for Size-dependent Growth

Next, analyze the transformed homogeneous population balance model (5.15) in which $G = G(a)$,

$$\frac{\partial f(t, a)}{\partial t} + G(a)\frac{\partial f(t, a)}{\partial a} = 0, \quad f(0, a) = f_0(a), \tag{5.86}$$

with $t \geq 0$, $G(a)$ continuous in $a \in \mathcal{R}$, and $G(a) > 0, \forall a$.[5] Applying the aforementioned finite difference scheme gives

$$\frac{f_{i+1}^j - f_i^j}{\Delta t_i} + G(a_j)\frac{f_i^j - f_i^{j-1}}{\Delta a_j} = 0. \tag{5.87}$$

Consider the transformation

$$z(a) = \int_0^a \frac{1}{G(\tilde{a})}d\tilde{a}, \tag{5.88}$$

which is one-to-one since $G(a) > 0$. Then

$$\frac{\partial z}{\partial a} = \frac{dz}{da} = \frac{1}{G(a)} \tag{5.89}$$

and

$$G(a)\frac{\partial f(t, a)}{\partial a} = G(a)\frac{\partial f(t, a)}{\partial z}\frac{dz}{da} = G(a)\frac{\partial f(t, a)}{\partial z}\frac{1}{G(a)} = \frac{\partial f(t, a)}{\partial z}. \tag{5.90}$$

Then the PDE (5.86) can be rewritten as

$$\frac{\partial \bar{f}(t, z)}{\partial t} + \frac{\partial \bar{f}(t, z)}{\partial z} = 0, \quad \bar{f}(0, z) = \bar{f}_{z0}(z), \tag{5.91}$$

---

[5]Similar results can be derived for the case where $G(a) < 0, \forall a$ by a slight tweak in the equations.

where $\bar{f}$ denotes that f has been reparameterized in terms of t and z. If the population balance model (5.91) is solved numerically or analytically, its solution can be used to construct the solution (5.86) by using (5.88) to map each value of z to a, that is, to map each triplet $(\bar{f}, t, z)$ to $(\bar{f}, t, z)$

Either analytically or numerically invert $z(a)$ to construct the mapping $z^{-1}(a)$, which can be inserted into $f_0(a)$ to construct $f_{z0}(z) = f_0(a(z))$. One way to do this inversion numerically is to plot $z(a)$ to construct pairs (z_i, a_i) and then reorder to give (a_i, z_i), aka $a(z)$.

Equation (5.91) resembles the cell population balance model where $G = 1$ and the analytical solution was $f(t, a) = f_0(a - t)$, so the analytical solution of (5.91) is

$$\hat{f}(t, z) = \hat{f}_{z0}(z - t), \tag{5.92}$$

which can be reparameterized in terms of a by replacing z with

$$z(a) = \int_0^a \frac{1}{G(\hat{a})} d\hat{a} \tag{5.93}$$

and using the initial condition parameterized in terms of a, to give

$$f(t, a) = \hat{f}_{z0}\left(\int_0^a \frac{1}{G(\hat{a})} d\hat{a} - t \right). \tag{5.94}$$

The proof that this analytical expression solves the population balance model (**??**) is by taking the appropriate partial derivatives and substitutions:

$$\frac{\partial f}{\partial t} = -\hat{f}_{z0}\left(\int_0^a \frac{1}{G(\hat{a})} d\hat{a} - t \right), \tag{5.95}$$

$$\frac{\partial f}{\partial a} = \frac{1}{G(a)} \hat{f}_{z0}\left(\int_0^a \frac{1}{G(\hat{a})} d\hat{a} - t \right), \tag{5.96}$$

$$\frac{\partial f}{\partial t} + G(a)\frac{\partial f}{\partial a} = -\hat{f}_{z0}\left(\int_0^a \frac{1}{G(\hat{a})} d\hat{a} - t \right) + \frac{G(a)}{G(a)} \hat{f}_{z0}\left(\int_0^a \frac{1}{G(\hat{a})} d\hat{a} - t \right) = 0, \tag{5.97}$$

The function $\hat{f}_{z0}(z)$ is constructed from $f_0(a)$ by construction:

$$\hat{f}_{z0}\left(\int_0^a \frac{1}{G(\hat{a})}d\hat{a} - t\right)\bigg|_{t=0} = \hat{f}_{z0}(z-t)\big|_{t=0} = \hat{f}_{z0}(z) = f_0(a). \qquad (5.98)$$

This analysis indicates that the numerical discretization method results in zero error when applied to the population balance model obtained by change of variables from a to z. The exact solution for $f(t, a)$ is directly computable from $\hat{f}(t, z)$ by the mappings in (5.93) and (5.98).

5.3.4 Case 4: Population Balance Model With Time-dependent Growth Rate

Next consider the population balance model with time-varying growth rate $G = G(t) > 0, \forall t \geq 0$,

$$\frac{\partial f(t,a)}{\partial t} + G(t)\frac{\partial f(t,a)}{\partial a} = 0, \quad f(0,a) = f_0(a). \qquad (5.99)$$

Dividing both sides by $G(t)$ and defining a new variable τ such that

$$\tau = \int_0^t G(\hat{t})\partial\hat{t} \qquad (5.100)$$

results in

$$\frac{\partial\hat{f}(\tau,a)}{\partial\tau} + \frac{\partial\hat{f}(\tau,a)}{\partial a} = 0, \quad \hat{f}(0,a) = \hat{f}_0(a) = f_0(a), \qquad (5.101)$$

which is the cell population balance model (i.e., has $da/d\tau = 1$). The exact analytical solution of this PDE is

$$\hat{f}(\tau,a) = \hat{f}_0(a-\tau) = f_0(a-\tau) \qquad (5.102)$$

and the solution to the original population balance model (5.99) is

$$f(t,a) = f_0\left(a - \int_0^t G(\hat{t})d\hat{t}\right). \qquad (5.103)$$

107

Inserting into the original PDE (5.99) verifies that this analytical solution is correct:

$$\frac{\partial f}{\partial t} = -G(t)f_0\left(a - \int_0^t G(\hat{t})d\hat{t}\right),$$ (5.104)

$$\frac{\partial f}{\partial a} = f_0\left(a - \int_0^t G(\hat{t})d\hat{t}\right),$$ (5.105)

$$\frac{\partial f}{\partial t} + G(t)\frac{\partial f}{\partial a} = -G(t)f_0\left(a - \int_0^t G(\hat{t})d\hat{t}\right) + G(t)f_0\left(a - \int_0^t G(\hat{t})d\hat{t}\right) = 0,$$ (5.106)

and

$$f_0\left(a - \int_0^t G(\hat{t})d\hat{t}\right)\Big|_{t=0} = f_0(a).$$ (5.107)

The analysis in Section 5.3.1 shows that the finite difference scheme has zero error for the population balance model written in terms of τ and a, which can be used to construct the solution to the (5.100).

Applying the finite difference scheme to the original population balance model (5.99) would have yielded

$$\frac{f_{i+1}^j - f_i^j}{\Delta t_i} + G(t_i)\frac{f_i^j - f_i^{j-1}}{\Delta a_j} = 0.$$ (5.108)

Substituting the analytical solution into this discretized PDE gives the combined discretization error of

$$\text{error} = \frac{f_0\left(a - \int_0^{t_i+\Delta t_i} G(\hat{t})d\hat{t}\right) - f_0\left(a - \int_0^{t_i} G(\hat{t})d\hat{t}\right)}{\Delta t_i} +$$
$$G(t_i)\frac{f_0\left(a - \int_0^{t_i} G(\hat{t})d\hat{t}\right) - f_0\left(a - \Delta a_j - \int_0^{t_i} G(\hat{t})d\hat{t}\right)}{\Delta a_j}.$$ (5.109)

Choosing $\Delta a_j = G(t_i)\Delta t_i$ results in

$$\text{error} = \frac{f_0\left(a - \int_0^{t+\Delta t_i} G(\hat{t})d\hat{t}\right) - f_0\left(a - G(t_i)\Delta t_i - \int_0^{t_i} G(\hat{t})d\hat{t}\right)}{\Delta t_i}.$$ (5.110)

The numerical error in the direct application of the finite difference scheme is zero for all f_0 if and only if

$$\int_0^{t_i+\Delta t_i} G(\hat{t})d\hat{t} = G(t_i)\Delta t_i + \int_0^{t_i} G(\hat{t})d\hat{t}$$ (5.111)

$$\int_{t_i}^{t_i+\Delta t_i} G(\hat{t})d\hat{t} = G(t_i)\Delta t_i \tag{5.112}$$

This condition will rarely hold in practice for non-constant $G(t)$. In contrast, the above change in variables from t to τ results in zero discretization error when applying the finite difference scheme to the population balance model for $f(\tau, a)$, which can then be used to construct $f(t, a)$ in the original population balance model (5.99).

5.3.5 Case 5: Non-Homogeneous Population Balance Model With Constant Growth Rate

Finally, consider the non-homogeneous population balance model

$$\frac{\partial f(t, a)}{\partial t} + g\frac{\partial f(t, a)}{\partial a} = h(t, a), \quad f(0, a) = f_0(a). \tag{5.113}$$

Applying the discretization scheme yields

$$\frac{f_{i+1}^j - f_i^j}{\Delta t_i} + g\frac{f_i^j - f_i^{j-1}}{\Delta a_j} = h(t_i, a_j). \tag{5.114}$$

First consider the case of constant h. Then the error is

$$\text{error} = \frac{f_{i+1}^j - f_i^j}{\Delta t} + g\frac{f_i^j - f_i^{j-1}}{\Delta a} - h. \tag{5.115}$$

In this case, the method of characteristics can be used to determine an analytical solution for f,

$$f(t, a) = ht + f_0(a - gt), \quad t \geq 0, \tag{5.116}$$

which is proved by

$$\frac{\partial f}{\partial t} = h - gf_0(a - gt), \tag{5.117}$$

$$\frac{\partial f}{\partial a} = f_0(a - gt), \tag{5.118}$$

$$\frac{\partial f}{\partial t} + g\frac{\partial f}{\partial a} = h - gf_0(a - gt) + gf_0(a - gt) = h, \tag{5.119}$$

109

and

$$[ht + f_0(a - gt)]|_{t=0} = f_0(a). \tag{5.120}$$

The exact analytical solution can then be substituted into the finite difference approximation in (5.114) to quantify the numerical discretization error:

$$\text{error} = \frac{ht_i + h\Delta t_i + f_0(a_j - gt_i - g\Delta t_i) - ht_i - f_0(a_j - gt_i)}{\Delta t_i}$$
$$+ g\frac{ht_i + f_0(a_j - gt_i) - ht_i - f_0(a_j - \Delta a_j - gt_i)}{\Delta a_j} - h. \tag{5.121}$$

Selecting $\Delta a_j = g\Delta t_i$ results in

$$\text{error} = \frac{f_0(a_j - gt_i - g\Delta t_i) - f_0(a_j - \Delta a_j - gt_i)}{\Delta t_i} = 0, \tag{5.122}$$

which shows that the finite difference approximation results in no numerical discretization error.

Let's consider the case in which $h = h(t)$. A similar analytical solution can be generated through the method of characteristics, which is given by

$$f(t, a) = \int_0^t h(\hat{t})d\hat{t} + f_0(a - gt), \quad t \geq 0, \tag{5.123}$$

which is proved by taking the appropriate derivatives:

$$\frac{\partial f}{\partial t} = h(t) - gf_0(a - gt), \tag{5.124}$$

$$\frac{\partial f}{\partial a} = f_0(a - gt), \tag{5.125}$$

$$\frac{\partial f}{\partial t} + g\frac{\partial f}{\partial a} = h(t) - gf_0(a - gt) + gf_0(a - gt) = h(t), \tag{5.126}$$

and

$$f(0, a) = \left[\int_0^t h(\hat{t})d\hat{t} + f_0(a - gt)\right]\bigg|_{t=0} = f_0(a). \tag{5.127}$$

Substituting the exact analytical solution into the finite difference approximation in (5.114)

gives

$$\text{error} = \frac{\int_0^{t_i+\Delta t_i} h(\hat{t})d\hat{t} + f_0(a_j - gt_i - g\Delta t_i) - \int_0^{t_i} h(\hat{t})d\hat{t} - f_0(a_j - gt_i)}{\Delta t_i} +$$

$$g\frac{\int_0^{t_i} h(\hat{t})d\hat{t} + f_0(a_j - gt_i) - \int_0^{t_i} h(\hat{t})d\hat{t} - f_0(a_j - \Delta a_j - t_i)}{\Delta a_j} - h(t_i). \quad (5.128)$$

Selecting $\Delta a_j = g\Delta t_i$ results in the simplified error expression

$$\text{error} = \frac{\int_0^{t_i+\Delta t_i} h(\hat{t})d\hat{t} - \int_0^{t_i} h(\hat{t})d\hat{t} - h(t_i)\Delta t_i}{\Delta t_i}. \quad (5.129)$$

The error is zero if

$$\int_{t_i}^{t_i+\Delta t_i} h(\hat{t})d\hat{t} = h(t_i)\Delta t_i, \quad (5.130)$$

which occurs for very few choices of $h(t)$, e.g., when $h(t)$ is constant or is a staircase function. The analysis of this section shows the zero error obtained by the finite difference scheme in Cases 1 to 4 applies only to nonhomogeneous population balance equations where the forcing function h is a constant. In contrast, transforming the population balance models first and then applying the finite difference equation results in zero discretization error.

5.4 Conclusions

This chapter derives analytical solutions to several classes of population balance models using the method of characteristics, and applies the analytical solutions to provide alternative proofs that the finite difference method in the previous chapter has zero discretization error. Additional results are derived that include (1) the analytical solution for the population balance model with general time-dependent forcing function, and (2) conditions for zero error when the finite difference method is applied directly to some population balance models without first performing a transformation of variables.

The results in this and the previous chapter show that a finite difference method that combines first-order discretizations with transformations and certain mesh sizes is able to derive exact solutions for several classes of population balance models. In some sense, these exact solutions – although obtained by numerical methods – are also a type of analytical

solution to the population balance models.

Even for classes of population balance models in which the finite difference method does not produce zero error, the method is shown to have benign behavior more generally. An advantage of the proposed method is that the number of flops for each mesh calculation is very low, and the use of first-order methods imply that the proposed method will also be much more accurate in regions of high derivatives (e.g., as discussed in detail in the textbooks by Randall Leveque [32, 33]) and will not introduce the aphysical oscillations that can occur with higher order methods. While most of the population balance modelling community has moved away from first-order first difference methods due to concerns about numerical diffusion (e.g., [20]), these chapters show that first-order first difference methods, when applied a very specific way, can provide numerical solutions that are both highly accurate and have low computational cost. In particular, these solutions are well suited for calculations in which the PBM must be solved a large number of times, such as in parameter estimation and Markov Chain Monte Carlo analysis (e.g., [21, 52]) and in nonlinear model predictive control (e.g., [30, 42]).

Chapter 6

Concluding Remarks

6.1 Importance/Motivation

Vaccines are some of the most valuable drugs we are able to produce due to their widespread applicability in staving off viral infections, some of which can be lethal. Being able to produce these drugs quickly while maintaining their efficacy is of the utmost importance, and to ensure this is possible, we must turn to continuous viral vaccine production. While some viral vaccine platforms can be upgraded to produce continuously using designer cell lines, certain cell-virus combinations exhibit oscillatory behavior that can cause many production issues. My research has focused on various ways to approach the mitigation of this oscillatory behavior including applying feedback control and designing new reactor types. Additionally, using population balance models, we can track the age distributions of cells in a continuous reactor and potentially design capture methods to remove older, less productive cells from vaccine production processes.

6.2 CSTR Stabilization

While reducing or eliminating oscillatory behavior in bioreactors can be approached in a multitude of ways, the method I chose through the course of my research was to start simple. Continuous stirred tank reactors are well-known and well-understood pieces of equipment in the biomanufacturing industry that are nearly ubiquitous across companies. That said, the

simplest approach to stabilization is adapting equipment that is already in place. Using the Frensing Influenza model, I explored how this could be done by applying ideas from optimal design. Beginning with open loop testing, I was quickly able to determine **open loop step test result**. Furthermore, these results suggested that oscillatory behavior can be reduced or eliminated using feedback control. Even the most basic PID controller - a P-only controller - showed an exceptional ability to dampen the oscillatory nature of the Frensing system and stabilize the relevant states around their steady state values over a short window of time **get this time value**. While a P-only controller was sufficient to stabilize the system, more complex controller setups will likely be more efficient in doing so. One relevant example would be a model predictive controller with a time-based proportional gain. Alternative to the control-based approaches, connecting multiple CSTRs in series is yet another method for reducing oscillatory behavior. By placing the tanks in series, the first and middle tanks serve to stabilize the oscillations in relevant states such that the output of the final tank is stable and predictable. The number of tanks needed is around 5 for the Frensing system, but will likely vary across other cell-virus systems.

6.3 Alternative Hollow Fiber Reactor

Hollow fiber bioreactors provide a narrow residence time distribution for cell-virus cultures, thus curtailing the creation of late-forming defective viruses in the case of the AGE1.CR.pIX/influenza virus system. Because DIPs cannot accumulate periodically in an alternative HFBR, the oscillatory behavior that occurs in certain cell/virus systems is eliminated. To obtain a sufficient output of standard virus that is not diluted with DIPs, the alternative HFBR model using model parameters fit to data by Frensing et al.6 indicates that the average residence time of cells should set to about 12 hours. This value can likely be optimized to further improve STV to DIP collection ratio, or similar productivity metrics. The results presented here indicate an upper limit of 250 microns on the radius of the hollow fiber lumen is necessary to ensure adequate cell densities throughout the bioreactor to maintain a high volumetric production of standard virus. This maximum radius is primarily set by the low diffusivities of cells. For larger lumen radii, the target and standard-virus-infected cells are

depleted in the outer regions of the lumen, which leads to lower production of standard virus per unit volume of hollow fiber. Using hollow fibers with smaller radii might improve performance, but potential plugging is a concern, depending on choice of cell line and typical cell diameters. The diffusivities of the metabolites are sufficiently high to keep their radial profiles relatively uniform in the alternative HFBR. By using high perfusion rates of medium through the ECS, sufficient nutrients can be supplied, and the effluent nutrient stream can be recycled. Recycling of cells after a single pass through the hollow fiber is not advisable as 80% are incapable of producing standard virus; i.e., they are DIP- and co-infected cells. This depletion of useful cells is due to the cell-virus kinetics revealed by Frensing's experiments. The alternative HFBR enables the disposal of the spent cells, as does a harvested well-stirred bioreactor. A conventional HFBR, with cells anchored in the extra-capillary space, would eventually suffer the same problem, so the spent cells would have to be removed and the ECS re-cultured.

6.4   PBE

In this chapter, we proposed a finite difference scheme for the solution of a general class of population balance models. The chapter pedagogically progresses through increasingly more complicated population balance models, demonstrating how the proposed finite difference method can be applied to obtain no numerical discretization error, through the use of some transformations. Further, when applied directly to more general PBEs, we have derived error expressions which show that the error is first order, transitioning to zeroth order as the growth rate and non-homogeneous terms become smoother functions of a.

Typically, the study of finite difference methods to solve population balance models focuses on developing increasingly more complicated and higher order accurate finite difference methods, which can result in the numerical solution becoming increasingly more computationally expensive. Furthermore, these higher ordered methods are subject to aphysical oscillations that do not appear in first order or zero error solutions such as that proposed in this chapter.

By specifically choosing to apply a first-order forward difference for the time derivative

and a first-order backward difference for the derivative with respect to the intrinsic variable, the numerical discretization error is reduced to zero in homogeneous population balances with constant growth rate, G. In more complicated systems in which the growth rate varies with time or the intrinsic variable or a non-homogeneous forcing function is present, the error expressions developed here demonstrate how the discretization error that results from the application of the difference scheme behaves benignly. This indicates that the finite difference scheme analyzed here is applicable to a wide variety of industrially relevant problems.

Additionally, I derived analytical solutions to several classes of population balance models using the method of characteristics, and applied the analytical solutions to provide alternative proofs that the finite difference method in the previous chapter has zero discretization error. Additional results are derived that include (1) the analytical solution for the population balance model with general time-dependent forcing function, and (2) conditions for zero error when the finite difference method is applied directly to some population balance models without first performing a transformation of variables.

The results in this and the previous chapter show that a finite difference method that combines first-order discretizations with transformations and certain mesh sizes is able to derive exact solutions for several classes of population balance models. In some sense, these exact solutions – although obtained by numerical methods – are also a type of analytical solution to the population balance models.

Even for classes of population balance models in which the finite difference method does not produce zero error, the method is shown to have benign behavior more generally. An advantage of the proposed method is that the number of flops for each mesh calculation is very low, and the use of first-order methods imply that the proposed method will also be much more accurate in regions of high derivatives (e.g., as discussed in detail in the textbooks by Randall Leveque [32, 33]) and will not introduce the aphysical oscillations that can occur with higher order methods. While most of the population balance modelling community has moved away from first-order first difference methods due to concerns about numerical diffusion (e.g., [20]), these chapters show that first-order first difference methods, when applied a very specific way, can provide numerical solutions that are both highly accurate and have low computational cost. In particular, these solutions are well suited for

calculations in which the PBM must be solved a large number of times, such as in parameter estimation and Markov Chain Monte Carlo analysis (e.g., [21, 52]) and in nonlinear model predictive control (e.g., [30, 42]).

6.5   Future Directions

My work has covered quite a few areas of continuous viral vaccine production, and I look forward to where future students might take some of these ideas. For instance, the utility of the population balance model approach to age tracking can be extended to other intrinsic variables like cell size or mass or any of a number of other viable choices. In doing this, future researchers will be able to determine how these variables might impact the productivity of viral production platforms. The hollow fiber reactor design itself was always meant to be plug and play for different cell lines and virus types, which allows plenty of opportunity to expand on the reactor and its uses. Many of my conclusions are stepping stones, and the possibilities of where they can lead are very exciting.

Bibliography

[1] E. Aamir, Z. K. Nagy, C. D. Rielly, T. Kleinert, and B. Judat. Combined quadrature method of moments and method of characteristics approach for efficient solution of population balance models for dynamic modeling and crystal size distribution control. *Industrial and Engineering Chemistry Research*, 48(18):8575–8584, 2009.

[2] C. F. Abegg, J. D. Stevens, and M. A. Larson. Crystal size distributions in continuous crystallizers when growth rate is size dependent. *AIChE Journal*, 14(1):118–122, 1968.

[3] P. S. Chow, X Y Liu, and RBH Zhang, J; Tan. Spherulitic growth kinetics of protein crystals. *Applied Physics Letters*, 81(11):1975–1977, 2002.

[4] D. Colucci, D. Fissore, A. A. Barresi, and R. D. Braatz. A new mathematical model for monitoring the temporal evolution of the ice crystal size distribution during freezing in pharmaceutical solutions. *European Journal of Pharmaceutics and Biopharmaceutics*, 148:148–159, 2020.

[5] R. Courant, K. Friedrichs, and H. Lewy. Uber die partiellen differenzengleichungen der mathematischen physik. *Mathematische Annalen (in German)*, 100(1):32–74, 1928.

[6] E. Dalas, J. K. Kallitsis, and P. G. Koutsoutkos. Crystallization of hydroxyapatite on polymers. *Langmuir*, 7(8):1822–1826, 1991.

[7] C. D. De Gooijer, R. H. Koken, F. L. Van Lier, M. Kool, J. M. Vlak, and J. Tramper. A structured dynamic model for the baculovirus infection process in insect cell reactor configurations. *Biotechnol. Bioeng.*, 40(4):537–548, 1992.

[8] C.D. De Gooijer, F.L.J. Van Lier, E.J. Van den End, J.M. Vlak, and J. Tramper. A model for baculovirus production with continuous insect cell cultures. *Appl. Microbiol. Biotechnol.*, 30(5):497–501, 1989.

[9] E.C. Eckstein, D.G. Bailey, and A.H. Shapiro. Self-diffusion of particles in shear flow of a suspension. *J. of Fluid Mech.*, 79(1):191–208, 1977.

[10] A. Einstein. *Investigations in the Theory of the Brownian Movement.* Dover, NY, 1956.

[11] G. Evans, J. Blackledge, and P. Yardley. *Numerical Methods for Partial Differential Equations.* Springer-Verlag, 2000.

[12] M.C. Flickinger. *Upstream Industrial Biotechnology, Volume 2.* John Wiley & Sons Inc., Hoboken, NJ, 2013.

[13] T. Frensing, F.S. Heldt, A. Pflugmacher, I. Behrendt, I. Jordan, D. Flockerzi, Y. Genzel, and U. Reichl. Continuous influenza virus production in cell culture shows a periodic accumulations of defective interfering particles. *PLoS One*, 8(9), 2013.

[14] T. Frensing, S.Y. Kupke, M. Bachmann, S. Fritzsche, L.E. Gallo-Ramirez, and U. Reichl. Influenza virus intracellular replication dynamics, release kinetics, and particle morphology during propagation in mdck cells. *Appl. Microbiol. Biotechnol.*, 100(16):7181–7192, 2016.

[15] F. Févotte and G. Févotte. A method of characteristics for solving population balance equations (PBE) describing the adsorption of impurities during crystallization processes. *Chemical Engineering Science*, 65(10):3191–3198, 2010.

[16] Y. Genzel, T. Vogel, J. Buck, I. Behrent, D.V. Ramirez, G. Schiedner, I. Jordan, and U. Reichl. High cell density cultivations by alternating tangential flow (atf) perfusion for influenza a virus production using suspension cells. *Vaccine*, 32:2770–2781, 2014.

[17] M.W. Glacken, Fleischaker R.J., and A.J. Sinskey. Reduction of waste product excretion via nutrient control: possible strategies for maximizing product and cell yields on serum in cultures of mammalian cells. *Biotech. and Bioeng.*, 28(9):1376–1389, 1986.

[18] G.B. Gori. Continuous cultivation of virus in cell suspensions by use of the lysostat. *Appl. Microbiol.*, 13(6):909–917, 1965.

[19] H. Gron, A. Borissova, and K. J. Roberts. In-process ATR-FTIR spectroscopy for closed-loop supersaturation control of a batch crystallizer in producing monosodium glutamate crystals of defined size. *Industrial and Engineering Chemistry Research*, 42(1):198–206, 2003.

[20] R. Gunawan, I. Fusman, and R. D. Braatz. High resolution algorithms for multidimensional population balance equations. *AIChE Journal*, 50(11):2738–2749, 2004.

[21] Martin W. Hermanto, Nicholas C. Kee, Reginald B.H. Tan, Min-Sen Chiu, and Richard D. Braatz. Robust Bayesian estimation of kinetics for the polymorphic transformation of L-glutamic acid crystals. *AIChE Journal*, 54(12):3248–3259, 2008.

[22] Michael J. Hounslow. A discretized population balance for continuous systems at steady state. *AIChE Journal*, 36(1):106–116, 1990.

[23] Martin Iggland and Marco Mazzotti. Population balance modeling with size-dependent solubility. *Crystal Growth & Design*, 12(3):1489–1500, 2012.

[24] H. Jacobson and L.S. Jacobson. Virustat, a device for continuous production of viruses. *Appl. Microbiol.*, 14(6):940–952, 1966.

[25] I. Jordan, A. Vos, S. Beilfuss, A. Neubert, S. Breul, and V. Sandig. An avian cell line designed for production of highly attenuated viruses. *Vaccine.*, 27(5):748–756, 2009.

[26] R. Kompier, J. Tramper, and J. Vlak. A continuous process for the production of baculovirus using insect-cell cultures. *Biotechnol. Lett.*, 10(12):849–854, 1988.

[27] K.B. Konstantinov and C.L. Cooney. White paper on continuous bioprocessing. *J. Pharm. Sci.*, 104(3):813–820, 2014.

[28] M. J. Kurtz, G. Y. Zhu, A. Zamamiri, M. A. Henson, and M. A. Hjortso. Control of oscillating microbial cultures described by population balance models. *Industrial and Engineering Chemistry Research*, 37(10):4059–4070, 1998.

[29] Leon Lapidus and George F. Pinder. *Numerical Solution of Partial Differential Equations in Science and Engineering.* John Wiley & Sons, Inc., 1999.

[30] P. A. Larsen, D. B. Patience, and J. B. Rawlings. Industrial crystallization process control. *IEEE Control Systems Magazine*, 26(4):70–80, 2006.

[31] Stigg Larsson and Vidar Thomée. *Partial Differential Equations with Numerical Methods.* Springer-Verlag, 2003.

[32] Randall J. Leveque. *Numerical Methods for Conservation Laws.* SIAM, New York, 1990.

[33] Randall J. Leveque. *Finite Volume Methods for Hyperbolic Problems.* SIAM, New York, 2002.

[34] Randall J. Leveque. *Finite Difference Methods for Ordinary and Partial Differential Equations - Steady-State and Time-Dependent Problems.* SIAM, New York, 2007.

[35] Z. Liao, E. Klein, C.K. Poh, Z. Huang, J. Lua, P.A. Hardy, and D. Gao. Measurement of hollow fiber membrane transport properties in hemodialyzers. *J. of Membrane Science*, 256:176–183, 2005.

[36] V. Lohr, O. Hädicke, Y. Genzel, I. Jordan, H. Büntemeyer, S. Klamt, and U. Reichl. The avian cell line age1.cr.pix characterized by metabolic flux analysis. *BMC Biotechnology*, 14(72), 2014.

[37] V. Lohr, A. Ratha, Y. Genzel, I. Jordan, V. Sandig, and U. Reichl. New avian suspension cell lines provide production of influenza virus and mva in serum-free media: Studies on growth, metabolism and virus propagation. *Vaccine*, 27(36):4975–4982, 2009.

[38] Daniele L. Marchisio and Rodney O. Fox. *Computational Models for Polydisperse Particulate and Multiphase Systems.* Cambridge University Press, 2013.

[39] Ali Mesbah, Herman J. M. Kramer, Adrie E. M. Huesman, and Paul M. J. Van den Hof. A control oriented study on the numerical solution of the population balance equation for crystallization processes. *Chemical Engineering Science*, 60(20):4262–4277, 2009.

[40] J.W. Möller. Determination of diffusion coefficients and molecular weights of ribonucleic acids and viruses. *Biochemistry*, 51(3):501–509, 1964.

[41] Z. K. Nagy and E. Aamir. Systematic design of supersaturation controlled crystallization processes for shaping the crystal size distribution using an analytical estimator. *Chemical Engineering Science*, 84:656–670, 2012.

[42] Zoltan K. Nagy and Richard D. Braatz. Robust nonlinear model predictive control of batch processes. *AIChE Journal*, 49(7):1776–1786, 2004.

[43] A. Novick and L. Szilard. Science. *Description of the chemostat*, 112(2920):715–716, 1950.

[44] S.S. Osturk and B.O. Palsson. Growth, metabolic, and antibody production kinetics of hybridoma cell culture: 1. analysis of data from controlled batch reactors. *Biotechnol. Prog.*, 7:471–480, 1991.

[45] Y. Peng, Z. Zhu, R. D. Braatz, and A. S. Myerson. Gypsum crystallization during phosphoric acid production: Modeling and experiments using the mixed-solvent-electrolyte thermodynamic model. *Industrial & Engineering Chemistry Research*, 54(32):7914–7924, 2015.

[46] E. Petiot, D. Jacob, S. Lanthier, V. Lohr, S. Ansorge, and A.A. Kamen. Metabolic and kinetic analyses of influenza production in perfusion hek293 cell culture. *BMC Biotechnology*, 11(84), 2011.

[47] J.M. Piret and C.L. Cooney. Mammalian cell and protein distributions in ultrafiltration hollow fiber bioreactors. *Biotech. and Bioeng.*, 36:902–910, 1990.

[48] J.M. Piret and C.L. Cooney. Model of oxygen transport limitations in hollow fiber bioreactors. *Biotech. and Bioeng.*, 37:80–92, 1991.

[49] William H. Press, Brian P. Flannery, Saul A. Teukolsky, and William T. Vetterling. *Numerical Recipes in C: The Art of Scientific Computing*. Cambridge University Press, second edition, 1992.

[50] S. Qamar, M. P. Elsner, I. A. Angelov, G. Warnecke, and A. Seidel-Morgenstern. A comparative study of high resolution schemes for solving population balances in crystallizations. *Computers & Chemical Engineering*, 30(6–7):1119–1131, 2006.

[51] Vincent Quedeville, Hicham Ouazaite, Bastien Polizzi, Rodney O. Fox, Philippe Villedieu, Pascal Fede, Fabien Létisse, and Jérôme Morchain. A two-dimensional population balance model for cell growth including multiple uptake systems. *Chemical Engineering Research and Design*, 132:966–981, 2018.

[52] James B. Rawlings, Stephen M. Miller, and Walter R. Witkowski. Model identification and control of solution crystallization processes: A review. *Industrial and Engineering Chemistry Research*, 32(7):1275–1296, 1993.

[53] Tony Saad, Alex W. Abboud, Sean T. Smith, and Terry A. Ring. A class of exact solutions for population balances with arbitrary internal coordinates. *AIChE Journal*, 61(5):1691–1698, 2015.

[54] C. A. Schall, J. S. Riley, E. Li, E. Arnold, and J. M. Wiencek. Application of temperature control strategies to the growth of hen egg-white lysozyme crystals. *Journal of Crystal Growth*, 165(3):299–307, 1996.

[55] F. Tapia, Y. Genzel, I. Jordan, V. Sandig, and U. Reichl. Continuous production of viral vaccines with a two-stage bioreactor system. *ECI Digital Archives*, 2015.

[56] F. Tapia, T. Laske, M. Wasik, M. Rammhold, Y. Genzel, and U. Reichl. Production of defective interfering particles of influenza a virus in parallel continuous cultures at two residence times – insights from qpcr measurements and viral dynamics modeling. *Frontiers of Bioeng. and Biotech.*, 7(275):1–15, 2019.

[57] F. Tapia, D. Vazquez-Ramirez, Y. Genzel, and U. Reichl. Bioreactors for high cell density and continuous multi-stage cultivations: options for process intensification in cull culture-based viral vaccine production. *Appl. Microbiol. Biotechnol.*, 100(5):2121–2132, 2016.

[58] F. Tapia, T. Vogel, Y. Genzel, I. Behrendt, M. Hirschel, J.D. Gangemi, and U. Reichl. Production of high-titer human influenza a virus with adherent and suspension mdck cells cultured in a single-use hollow fiber bioreactor. *Vaccine*, 32:1003–1011, 2014.

[59] F. Tapia, D. Wohlfarth, V. Sandig, I. Jordan, Y. Genzel, and U. Reichl. Continuous influenza virus production in a tubular bioreactor system provides stable titers and avoids the 'von magnus effect'. *PLOS ONE*, 14(11):1–21, 2019.

[60] E. Trucco. Mathematical models for cellular systems the Von Foerster equation, Part 1. *Bulletin of Mathematical Biophysics*, 27:285–304, 1965.

[61] F.L. van Lier, E.J. van den End, C.D. de Gooijer, J.M. Vlak, and J. Tramper. Continuous production of baculovirus in a cascade of insect-cell reactors. *Appl. Microbiol. Biotechnol.*, 33(1):43–47, 1990.

[62] F.L. van Lier, W.C. van der Meijs, N.G. Grobben, R.A. Olie, J.M. Vlak, and Tramper J. Continuous beta-galactosidase production with a recombinant baculovirus insect-cell system in bioreactors. *J. Biotechnol.*, 22(3):291–298, 1992.

[63] F.L. van Lier, G.C. van Duijnhoven, M.M. de Vaan, J.M. Vlak, and Tramper J. Continuous beta-galactosidase production in insect cells with a p10 gene based baculvirus vector in a two-stage bioreactor system. *Biotechnol. Prog.*, 10(1):60–64, 1994.

[64] P. von Magnus. Incomplete forms of influenza virus. *Science Direct*, 2(3527), 1954.

[65] Jeffrey D. Ward, Duncan A. Mellichamp, and Michael F. Doherty. Choosing an operating policy for seeded batch crystallization. *AIChE Journal*, 52(6):2046–2054, 2006.

[66] K. Westin and A. C. Rasmuson. Crystal growth of aragonite and calcite in presence of citric acid, DTPA, EDTA and pyromellitic acid. *Journal of Colloid and Interface Science*, 282(2):359–369, 2005.

[67] X. Y. Woo, R. B. H. Tan, and R. D. Braatz. Precise tailoring of the crystal size distribution by controlled growth and continuous seeding from impinging jet crystallizers. *CrystEngComm*, 13:2006–2014, 2011.

[68] Xing Yi Woo, Reginald B. H. Tan, Pui Shan Chow, and Richard D. Braatz. Simulation of mixing effects in antisolvent crystallization using a coupled CFD-PDF-PBE approach. *Crystal Growth & Design*, 6(6):1291–1303, 2006.

[69] M. Woolhouse, F. Scott, Z. Hudson, R. Howey, and M. Chase. Human viruses: discovery and emergence. *Philos Trans R Soc Lond B Biol Sci*, 367(1604), 2012.

[70] G. Y. Zhu, A. Zamamiri, M. A. Henson, and M. A. Hjortso. Model predictive control of continuous yeast bioreactors using cell population balance models. *Chemical Engineering Science*, 55(24):6155–6167, 2000.